



UNIVERSITY OF LJUBLJANA
FACULTY OF MATHEMATICS AND PHYSICS
DEPARTMENT OF MATHEMATICS
Mathematics - 3rd Cycle Degree

Tadej Kanduč

**APPROXIMATION AND
INTERPOLATION SPLINES
ON TRIANGULATIONS**

Doctoral thesis

ADVISER: Assoc. Prof. Dr. Gašper Jaklič

Ljubljana, 2013

UNIVERZA V LJUBLJANI
FAKULTETA ZA MATEMATIKO IN FIZIKO
ODDELEK ZA MATEMATIKO
Modul matematika - 3. stopnja

Tadej Kanduč

**APROKSIMACIJSKI IN
INTERPOLACIJSKI ZLEPKI
NAD TRIANGULACIJAMI**
Doktorska disertacija

MENTOR: izr. prof. dr. Gašper Jaklič

Ljubljana, 2013

Podpisani Tadej Kanduč izjavljam:

- da sem doktorsko disertacijo z naslovom "*Aproksimacijski in interpolacijski zlepki nad triangulacijami*" (angl. "*Approximation and interpolation splines on triangulations*") izdelal samostojno pod mentorstvom izr. prof. dr. Gašperja Jakliča in
- da Fakulteti za matematiko in fiziko Univerze v Ljubljani dovoljujem objavo elektronske oblike svojega dela na spletnih straneh.

Ljubljana, 22. 5. 2013

Podpis:

Zahvala

Iskreno se zahvaljujem svojemu mentorju izr. prof. dr. Gašperju Jakliču, ki mi je tekom doktorskega študija predal veliko neprecenljivega znanja in nasvetov ter me neprestano spodbujal. Pri raziskovalnem delu me je usmerjal, ko je bilo to potrebno, ter me po drugi strani naučil samostojnosti in ustvarjalnosti.

Zahvaliti se želim podjetju Turboinštitut d.d., še posebej dr. Andreju Lipeju, ter dr. Alenu Orbaniću s Fakultete za matematiko in fiziko, ki so mi omogočili mesto mladega raziskovalca v gospodarstvu. Na delovnem mestu sem si pridobil veliko dragocenega praktičnega znanja.

Zahvaljujem se tudi svojim staršem za vso podporo, ki so mi jo nudili tekom študija.

Abstract

In the thesis, some new results on correctness of polynomial Lagrange interpolation problem on triangles are presented. The results are based on positivity of principal minors of Bézier collocation matrices for non-parametric patches. L. L. Schumaker stated the conjecture, that for uniformly distributed domain points on triangle the corresponding collocation matrix has positive principal minors. The conjecture on the minors for polynomial total degree ≤ 17 and for some particular configurations of domain points is confirmed. By stating the exact lower bound for the principal minors, the main conjecture is extended. A generalisation of domain points' positions imposing correctness of the interpolation problem is analysed for polynomial degree ≤ 4 .

In the parametric case, two novel constructions solving Hermite interpolation problem (interpolation of points and tangent planes) are proposed. In the first one, a construction of good boundary curves of cubic triangular patches is analysed. The curves minimise an approximate strain energy functional. It is shown that the curves are regular and without shape defects. The shape of the curves is analysed with respect to a given shape parameter. The remaining free parameters of the spline surface are set in such a way that the patches have small Willmore energy. It is shown that a unique interpolant exists at mild presumptions.

Next, a generalisation of macro-elements to the parametric case is considered. Hermite interpolation by two types of parametric C^1 macro-elements on triangulations is presented in detail. Cubic triangular splines interpolate points and the corresponding tangent planes at domain vertices and approximate tangent planes at midpoints of domain edges. Quintic splines additionally interpolate normal curvature forms at the vertices. Control points of the interpolants are constructed in two steps. In the first one, uniformly distributed control points of a linear spline interpolant are projected to the interpolation planes. To ensure the smoothness conditions between patches, a correction of control points is obtained as the solution of a least square minimisation. The interpolation schemes inherit many desired properties from the functional case such as local and simple geometric construction and linear complexity.

At the end, the interpolation schemes are tested in numerical examples and practical applications.

Math. Subj. Class. (2010): 65D07, 65D05, 65D17, 65F40.

Keywords: Bernstein polynomial, Bézier surface, spline surface, parametric surface, cubic spline, triangular patch, triangulation, Lagrange interpolation, Hermite interpolation, collocation matrix, principal minor, strain energy, Willmore energy, energy minimisation, macro-element.

Povzetek

V disertaciji predstavimo nekaj novih rezultatov s področja korektnosti polinomske Lagrangeeve interpolacije nad trikotniki. Rezultati slonijo na pozitivnosti glavnih minorjev Bézierovih kolokacijskih matrik za neparametrične krpe. L. L. Schumaker je postavil naslednjo domnevo. Če izberemo enakomerno razporejene interpolacijske točke na trikotniku, potem so glavni minorji pripadajoče kolokacijske matrike pozitivni. V disertaciji pokažemo, da trditev velja za vse glavne minorje, če je totalna stopnja polinomov ≤ 17 , in za nekatere posebne razporeditve interpolacijskih točk. Omenjeno domnevo razširimo s postavitvijo natančne spodnje meje za vrednosti glavnih minorjev. Na koncu analiziramo korektnost interpolacijskega problema za splošnejšo lego točk in totalno stopnjo ≤ 4 .

V parametričnem okolju predstavimo dve novi shemi, ki rešita Hermiteov interpolacijski problem (interpolacija točk in tangentnih ravnin). V prvi podrobno analiziramo konstrukcijo primernih robnih krivulj kubične trikotne krpe. Optimalne krivulje minimizirajo funkcional približne napetostne energije. Krivulje so regularne in brez zank ter osti. Kakovost krivulje študiramo v odvisnosti od danega parametra oblike. Preostale parametre kubičnega zleпка določimo tako, da imajo krpe majhno Willmorejevo energijo. Enolična rešitev interpolacijskega problema obstaja pri šibkih predpostavkah.

Drugo shemo dobimo s posplošitvijo makro-elementov na parametričen primer. Podrobneje predstavimo dva tipa parametričnih C^1 makro-elementov na triangulacijah, ki rešita Hermiteov interpolacijski problem. Kubični trikotni zleпки interpolirajo točke in pripadajoče tangentne ravnine v vozliščih triangulacije ter aproksimirajo tangentne ravnine na sredini povezav triangulacije. Zleпки stopnje pet v vozliščih dodatno interpolirajo forme normalnih ukrivljenosti. Kontrolne točke zlepkov konstruiramo v dveh korakih. V prvem, enakomerno razporejene kontrolne točke linearnega interpolanta projiciramo na interpolacijske ravnine. Da zadostimo pogojem gladkosti med trikotnimi krpami, popravke kontrolnih točk izračunamo kot rešitev po metodi najmanjših kvadratov. Interpolacijski shemi posedujeta veliko zaželenih lastnosti iz funkcijskega primera kot so lokalna in geometrijska konstrukcija ter linearna časovna zahtevnost.

Na koncu interpolacijski shemi testiramo na različnih numeričnih primerih in v praktičnih aplikacijah.

Math. Subj. Class. (2010): 65D05, 65D07, 65D17.

Ključne besede: Bernsteinov polinom, Bézierova ploskev, dvorazsežen zlepek, parametrična ploskev, kubičen zlepek, trikotna krpa, triangulacija, Lagrangeeva interpolacija, Hermiteova interpolacija, kolokacijska matrika, glavni minor, napetostna energija, Willmorejeva energija, minimizacija energije, makro-element.

Contents

Zahvala	vii
Abstract	ix
Povzetek	xi
1 Introduction	1
1.1 Lagrange Interpolation	2
1.2 Hermite Interpolation	4
1.2.1 Boundary Curves	5
1.2.2 Energy Minimising Hermite Scheme	6
1.3 Parametric Macro-Elements	7
2 Preliminaries	11
2.1 Bernstein Polynomials and Splines	11
2.2 de Casteljau Algorithm and Continuity Conditions	12
3 Constrained Lagrange Interpolation Problem on Triangle	15
3.1 On Positivity of Principle Minors of Bézier Collocation Matrix	16
3.2 New Conjectures	22
3.3 Application: Lagrange Interpolation on Triangulations	23
3.4 On Constrained Interpolation at Generalised Domain Points	25
4 Hermite Interpolation by Cubic Curves with Small Strain Energy	29
4.1 Interpolation Problem	29
4.2 Hermite Interpolation Scheme	30
4.3 Choosing Parameter ω	33
4.4 Numerical Examples	35
5 Hermite Interpolation by Cubic Patches with Small Willmore Energy	37
5.1 Interpolation Problem and PN Triangles	37
5.2 Boundary Curves	38
5.3 Interior Control Point and Approximate Willmore Energy	42
5.4 Algorithm	46
6 Geometric Interpolation by Bivariate Parametric Macro-Elements	47
6.1 Motivation: Non-Parametric Macro-Elements	47
6.2 Interpolation Conditions and Minimising Cells	48
6.2.1 Tangent Plane Interpolation and Minimising Cell for $\mathcal{R}_1(v)$	49

6.2.2	Normal Curvature Interpolation and Minimising Cell for $\mathcal{R}_2(v)$. . .	53
6.2.3	Tangent Plane Approximation at Midpoint of an Edge	56
6.2.4	Algorithms	57
6.3	Macro-Elements	59
6.3.1	Polynomial Macro-Element in $\mathcal{S}_5^{1,2}(\Delta)$	59
6.3.2	Clough–Tocher Macro-Element in $\mathcal{S}_3^{1,1}(\Delta_{CT})$	60
6.4	Remarks	62
7	Numerical Examples	63
7.1	Surface Approximation	63
7.1.1	Sphere Approximation	63
7.1.2	Torus Approximation	66
7.1.3	Free-Form Surface Approximation	69
7.1.4	Comparison of Parametric and Non-Parametric Macro-Elements	70
7.2	Surface Reconstruction	71
7.3	Hole Filling Problem	75
8	Conclusions	79
	Bibliography	83
	Index	89
	Razširjeni povzetek	91

Chapter 1

Introduction

Approximation, interpolation and representation of (real-life) objects are the basic problems in numerical mathematics, especially in the field of Computer-Aided Geometric Design (CAGD). Good approximation scheme should satisfy various criteria. First of all, the approximant should closely resemble the original object. This is measured by different types of errors, shape preserving property (the shape of the approximation object should closely follow the original one and should not contain any additional oscillations) and approximation order containing information on how quickly the error fades, when approximation data are denser and denser. The scheme should be robust, therefore a unique solution of the approximation problem should exist at mild presumptions. To reduce time and space complexity of the problem and to be able to provide an in-depth analysis of the algorithm, local construction of the approximant is essential. Insensitive and stable construction are also important properties since in practice we deal with input data that already contain some error.

Splines are recognised as highly effective tools which are commonly used in practical applications: modelling various types of objects in different branches of industry (car industry, aeronautics, movie and computer game industry, etc.), image analysis, solving (partial) differential equations. They possess many desired characteristics such as basis with local support, fast, stable and simple construction, shape preserving property, good convergence properties, a direct connection of the spline shape with its control mesh, etc. In contrast to the theory of uniform splines which is a well understood topic, many basic questions on bivariate (multivariate) splines remain open. These include the dimension of spline spaces, basis construction, interpolation correctness, geometric continuity and the problem how to determine remaining free parameters of a spline.

Tensor product Bézier surfaces are a straightforward generalisation of Bézier curves and are therefore often used in practice. In recent years, theory of Bézier surfaces on triangulations has developed considerably. Splines of triangular patches offer more shape flexibility than rectangular ones and can consequently form more general surfaces. Most of the theory focuses on non-parametric splines (surfaces defined by functions $s : \Omega \subset \mathbb{R}^2 \rightarrow \mathbb{R}$). The drawback of the latter is that they cannot approximate complex 3D objects since they do not have enough degrees of freedom. To overcome the problem, parametric spline surfaces (surfaces embedded in \mathbb{R}^3 , parametrised by domain $\Omega \subset \mathbb{R}^2$) are used in those cases. More on splines can be found in [22, 28] and references therein.

Most of the interpolation problems can be roughly classified into two main groups: Lagrange and Hermite interpolation. In the first one, the interpolation data in non-parametric setting consist only of function values, whereas in the Hermite case the data

1 Introduction

include function derivatives also.

Problem 1.1. For distinct interpolation points $\{\zeta_\ell\}_{\ell=1}^n \subset \Omega \subset \mathbb{R}^2$, values $\{z_\ell \in \mathbb{R}\}_{\ell=1}^n$ and spline space \mathcal{S} , find a spline $s \in \mathcal{S}$ that solves Lagrange interpolation problem

$$s(\zeta_\ell) = z_\ell, \quad \ell = 1, 2, \dots, n.$$

Problem 1.2. For distinct interpolation points $\{\zeta_\ell\}_{\ell=1}^n \subset \Omega \subset \mathbb{R}^2$, values $\{z_\ell \in \mathbb{R}\}_{\ell=1}^n$, $\{k_\ell\}_{\ell=1}^n$, $k_\ell \in \{0, 1, \dots, d\}$, and spline space \mathcal{S} , find a spline $s \in \mathcal{S}$ that solves Hermite interpolation problem

$$s^{(k_\ell)}(\zeta_\ell) = z_\ell, \quad \ell = 1, 2, \dots, n.$$

Note that the number of interpolation data n depends on the dimension of the spline space \mathcal{S} . In the parametric case, function values and derivatives in the interpolation data are usually replaced by spatial points, tangent planes, curvature forms, etc. The problem of existence and uniqueness of the interpolant s can be transformed to the study of non-singularity of the corresponding collocation (interpolation) matrix. We say that the problem is *correct* if a unique solution exists. If the interpolant is not uniquely defined, the remaining free parameters can be used to interpolate additional data or to improve the quality of the shape of the interpolant by satisfying various criteria.

The Lagrange problems are usually more difficult since the interpolation in the interior of triangles is also considered. Although some results on Lagrange problem in the parametric settings are known (see [40], e.g.), most of the research have been focused on non-parametric case which is easier to tackle.

1.1 Lagrange Interpolation

It is well known that in the univariate case, a unique solution of the polynomial Lagrange interpolation problem exists if the interpolation points are distinct. The solution can be written in the Lagrange basis in a closed and compact form [22].

In the multivariate setting, the Lagrange interpolation problem is significantly more complex and solution of the problem depends on explicit positions of interpolation points. Among rich number of papers dedicated to this research area let us mention just a few [33, 15, 31, 14, 7]. Here, we will focus on bivariate polynomials of total degree $\leq d$. From known properties of polynomials it follows that the interpolation problem at $\binom{d+2}{2}$ interpolation points is correct iff the points do not lie on an algebraic curve of degree $\leq d$. Unfortunately, the property is difficult to verify in practical applications.

In recent years, several sufficient configurations of interpolation points yielding a unique solution were studied. In some cases, constructions of interpolation points that are optimal based on different criteria were considered. For example, the so-called Padua points have minimal order of growth of Lebesgue constants [7, 8] and Fekete points yield the maximal absolute value of the Vandermonde determinant [9]. One of the most commonly used constructive configurations are *lattices* (principal lattices, natural lattices, $(d+1)$ -pencil lattices), i.e., a configuration of interpolation points obtained by intersection of hyperplanes [15, 52, 39, 11].

Let $\mathcal{I}_d := \{\mathbf{i} := (i, j, k) : i + j + k = d, i, j, k \in \mathbb{Z}_+\}$. It is a well-known fact that bivariate Bernstein basis polynomials of degree d , $\{B_{\mathbf{i}}^d\}_{\mathbf{i} \in \mathcal{I}_d}$, form a basis of the space of bivariate polynomials of degree $\leq d$. The polynomial interpolation problem is correct for *domain points*

$$\mathcal{D}_{d,\tau} := \{(i/d, j/d, k/d) : (i, j, k) \in \mathcal{I}_d\},$$

expressed in barycentric coordinates with respect to a given triangle τ . Thus the corresponding *collocation matrix* $M := [B_{\eta}^d(\xi)]_{\xi \in \mathcal{D}_{d,\tau}, \eta \in \mathcal{I}_d}$ is nonsingular.

In [57], an interesting conjecture was stated that by removing some of the basis polynomials and the corresponding interpolation points, the problem remains correct. More precisely, by choosing an arbitrary nonempty subset $\mathcal{J} \subset \mathcal{D}_{d,\tau}$ and the corresponding set of indices Γ , the submatrix $M_{\Gamma} := [B_{\eta}^d(\xi)]_{\xi \in \mathcal{J}, \eta \in \Gamma}$ is nonsingular, and furthermore, $\det M_{\Gamma} > 0$. The authors of [57] verified the conjecture by computer for all $d \leq 7$ and provided a proof of nonsingularity of principal matrices for some special configurations of domain points for arbitrary d . For more details see [51].

Positivity of determinants (or minors) of collocation matrices is an important property in approximation theory. Nonsingularity of such a matrix implies correctness of the associated interpolation problem. Positivity of principal minors or even total positivity is used in the proofs of some well-known results, see [22, 30, 32], e.g. Matrices with positive principal minors are known as *P-matrices*. Much on them is known, see [56, 20], e.g. Unfortunately, those tools could not be applied for the study of the problem at hand, so a different approach will be used.

In the univariate case, a stronger property on the minors is confirmed. For every nonempty subset of the collection of the univariate Bernstein basis polynomials $\{B_{\ell}^d\}_{\ell=0}^d$ and the corresponding subset of interpolation data $\mathcal{J} = \{x_{\ell}\}_{\ell=0}^d, 0 = x_0 < x_1 < \dots < x_d = 1$, the collocation matrix has a positive determinant. The result follows from the fact that the collocation matrix $[B_{\ell}^d(x)]_{\ell=0, x \in \mathcal{J}}^d$ is totally non-negative with positive principal minors (see [23, 30], e.g.).

In the bivariate case, the collocation matrices are not totally non-negative and similar techniques as in the proofs for the univariate case cannot be applied. Also, a straightforward way of verifying the conjecture by computing principal minors of M is time consuming due to the exponential growth of the number of subsets that need to be analysed, and for $d > 7$ exceeds current computational facilities. For example, for $d = 10$ one would need to verify all of the $2^{\binom{10+2}{2}} - 1 \approx 7.4 \cdot 10^{19}$ minors.

Nonsingularity of the minors is in close connection to *constrained Lagrange interpolation* problem, i.e. the problem of constructing a Lagrange interpolation polynomial with some predetermined control coefficients. The conjecture provides an important property for constructing Lagrange interpolation splines on triangulations [57, 58]. The spline is obtained by locally solving constrained interpolation problems on certain triangles. An example is shown in Fig. 1.1.

In the thesis, the conjecture on positivity of determinant of the bivariate Bézier collocation matrix M is confirmed. Furthermore, the result is proven for an arbitrary $\Gamma \subset \mathcal{I}_d$ for $d \leq 17$. Thus the constrained Lagrange interpolation problem has a unique solution. This covers all the cases useful in practice since it is well known that Lagrange polynomial interpolants of high degrees have undesired properties. Some particular configurations of domain points are analysed. A conjecture on exact lower bound of $\det M_{\Gamma}$ is stated.

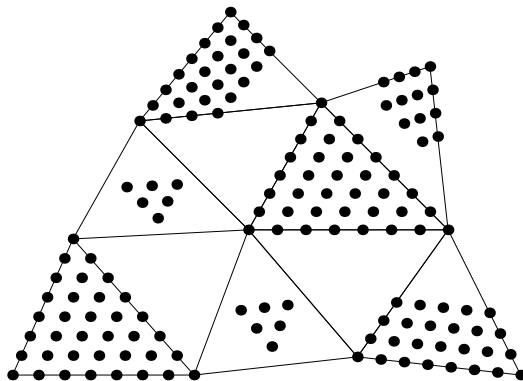


Figure 1.1: Interpolation points (black dots) for a spline $s \in \mathcal{S}_7^{2,3}(\Delta)$ (i.e., a spline of polynomial degree 7, C^2 global smoothness and C^3 smoothness at the vertices).

1.2 Hermite Interpolation

Hermite interpolation problems are usually less complex to tackle since the interpolation data are commonly prescribed only on the boundaries of the triangular patches. In non-parametric setting, one of the most recognised tools are *macro-elements* [51]. The terminology used by M. J. Lai and L. L. Schumaker shows a connection to the finite-element theory. Macro-elements are a special type of C^r smooth interpolation splines, defined on triangulated domains [51, 50, 1, 73, 16]. Their main advantage is the structure avoiding the curse of dimension, i.e., the dimension of the space of bivariate splines of low degrees is still unknown [38, 2]. The shape of the spline depends only on local data. The approximants are obtained in a closed form and have the optimal approximation order. Since they have many desired properties, they are an important and a well established tool in approximation theory and in solving PDEs [51]. The methods can also be applied effectively in other research branches, such as terrain reconstruction and optimal route planning [49].

Parametric schemes are of great importance in free-form shape modelling. The most straightforward connections between patches can be described by standard C^r smoothness conditions that have a direct connection to the domain parametrisation. The drawback of C^r splines is that they cannot form surfaces of arbitrary topology [36]. The problem can be solved by relaxing the smoothness conditions to *geometric* or *visual continuity* (denoted by G^r or VC^r), that does not depend on the parametrisation. For instance, G^0 conditions are the same as C^0 and G^1 smooth splines have continuously varying tangent planes. Since the geometric continuity conditions are nonlinear, a common approach is to study simplified sufficient conditions [25, 28]. The complexity of the problem increases at interior vertices where the smoothness conditions interlace (the vertex enclosure or the twist compatibility problem). A standard approach is to impose G^1 smoothness conditions between adjacent triangular patches (see [26, 67, 35, 27, 28, 53] and references therein). Most interpolating schemes of this type are local and can form surfaces of arbitrary topology.

The schemes that solve the interpolation problem have considerably more degrees of freedom than their non-parametric counterparts. How to determine them in order to obtain surfaces with good approximation properties and simple constructions, remains

a challenge. Algorithms usually consist of two steps: construction of a wireframe of interpolation boundary curves and computation of the remaining interior control points of the patches [26, 35, 70]. The schemes are generally fairly complex, usually involving additional subdivision processes, degree raising or blending techniques. In [54], it was pointed out that many algorithms produce surfaces with unpleasant shapes, e.g. surfaces with poor curvature distribution or shape defects. Undesirable shapes are mostly a result of inappropriate boundary curves of the patches.

1.2.1 Boundary Curves

Construction of good boundary curves is essential to overcome aforementioned problems. It is related to the construction of parametric spline curves that interpolate a given set of data points. The curve has to interpolate the points in the prescribed order and it should be shape-preserving, i.e., if the data are sampled from an analytical curve, the interpolant should closely follow its shape (see [17, 19, 21, 34], e.g.). The most common are cubic splines since they are of low degree and they possess enough flexibility to accurately approximate free-form curves. One of the standard approaches is to use a cubic C^2 interpolating spline [22, 28], which minimises the strain energy for each component of the curve. Its construction, however, is global since it involves solving a large (fortunately banded) system of equations.

A notable improvement on geometric interpolation was made recently (see [24, 37, 41, 63, 55] and references therein). The geometric schemes have a high order asymptotic accuracy by using polynomials of lower degrees. However, the interpolation problems become nonlinear and are much harder to tackle than in standard parametric approaches.

In recent years, several local methods for constructing geometric cubic G^1 interpolating splines were suggested, particularly for planar data [71, 44, 43]. For spatial data see [42] and the references therein. The methods are based on the polynomial Hermite geometric interpolation of order 1, i.e., local interpolation of two data points and the corresponding tangent directions. The tangent lengths are left as unknowns and are computed as a result of minimisation of a particular energy functional, usually based on the curvature [71, 44, 42] or the curvature deviation [43]. More on energy functionals can be found in [69, 65, 22, 28] and references therein.

In [71], cubic G^1 Hermite interpolation was studied. The optimal curve minimises the approximate strain energy. In the interpolation scheme, the prescribed tangent directions need to satisfy particular requirements. If the conditions are not fulfilled, additional (artificial) data points and tangent directions need to be inserted. In [44, 42] these disadvantages were overcome by a careful approximation of the energy functional. This has increased the admissible set of tangent directions and no additional data were needed.

In the thesis, a novel geometric Hermite interpolation scheme in \mathbb{R}^3 , based on approximate strain energy minimisation, is presented. The results of [71, 44, 42] are its particular sub-cases. The minimising curves are regular, locally without loops, cusps or folds. Admissible tangent directions and the shape of the curve is analysed with respect to the shape parameter.

1.2.2 Energy Minimising Hermite Scheme

Since the proposed Hermite interpolation scheme for curves has many desired properties, we extend it to the one for surfaces. The given data are spatial points and the corresponding normals of tangent planes. Our cubic Hermite Bézier spline surface is constructed in two steps. In the first, construction of energy minimising boundary curves of a triangular patch is analysed. This is an established approach in parametric spline surface construction [26, 70, 35, 67]. In contrast to the standard Hermite problem for curves, here the tangent directions are not prescribed but they only need to lie in the corresponding tangent planes.

We show that the optimal approximate strain energy minimising boundary curves for a particular shape parameter value are boundary curves of *PN (Point-Normal) triangles*. The latter are a special type of cubic triangular Bézier surfaces that solve the Hermite problem [68]. (Curved) PN triangles are an important yet inexpensive improvement of flat triangles since they produce smoother surfaces with much smaller number of patches and they can be efficiently rendered with GPU [66].

The parameters that remain undefined after all the interpolation conditions are satisfied can be used to impose various conditions. The parameters can be chosen in such a way to satisfy G^1 smoothness conditions between adjacent patches (see [70, 26], e.g.), to solve a partial differential equation (see [3] and references therein) or to minimise a given functional [4, 29]. We consider the latter case.

We would like to construct a spline with small variation of normal curvature of the surface, an important geometric property from the visual aspect and for the rendering. Therefore the remaining free parameters are set in such a way that the *Willmore energy* of the surface is minimal. The energy is a quantity that measures how much a surface deviates from a sphere. For an arbitrary surface \mathbf{s} it is defined by

$$\mathcal{W}(\mathbf{s}) = \frac{1}{4} \int_{\mathbf{s}} (\kappa_1 - \kappa_2)^2 dA,$$

where κ_1, κ_2 are the principal curvatures of \mathbf{s} at each surface point and dA is the surface area element. If \mathbf{s} is a part of a sphere, its energy is equal to zero.

In general, Willmore energy of a surface cannot be computed analytically. Many simplifications of the energy integral were proposed (see [6] and references therein). A common approach is a triangular discretisation of the domain of integration. For some other discretisations that ensure the Willmore energy integrand is invariant under translations, rotations, etc., see [6], e.g. The problem of finding a surface with the smallest energy is usually solved by constructing an appropriate gradient flow, the so-called Willmore flow. Usually the flow is discretised by a finite element approach (see [5, 62, 61], e.g.). Often, minimisations of energy functionals are done by an iterative numerical method.

Since the minimisation of Willmore energy functional over all free parameters of a patch is a very hard problem, we simplify it. A solution of the simplified problem can then be used as a good starting point for an iterative solver for the original problem. As an example, we approximate a function with two interpolating splines with small energy (see Fig. 1.2). The first one is a solution of the original problem and the second is our interpolant that solves the simplified problem. Although the second spline has a larger energy than the first, the shape of the spline closely resembles the original surface.

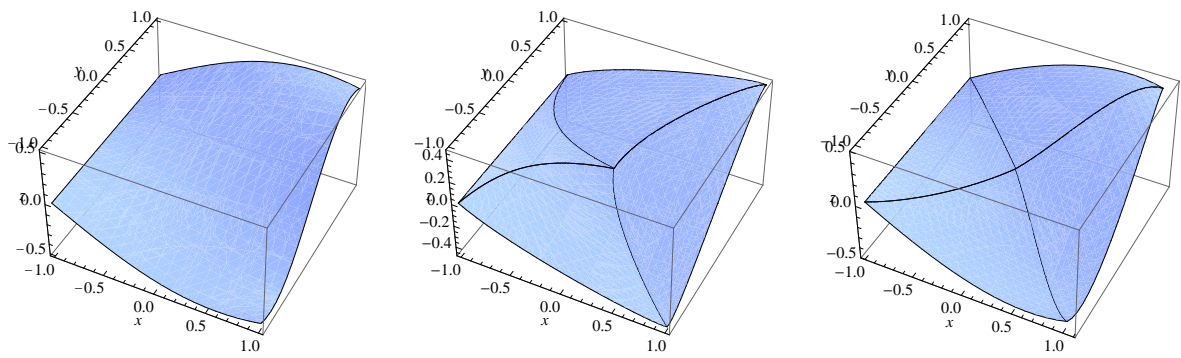


Figure 1.2: The function $g(x, y) = \sin((x+1)y)$ (left) is approximated with two Willmore minimising interpolation splines. The solution of the original problem with 36 degrees of freedom has energy $\mathcal{W} = 0.287$ (middle). Our interpolation spline solves the simplified problem with four degrees of freedom and has energy $\mathcal{W} = 0.587$ (right).

Furthermore, the construction of the second spline is local and much faster than in the first case.

1.3 Parametric Macro-Elements

An alternative to determine the free parameters of a parametric spline surface is to try to set them in similar way as they are defined in algorithms for (non-parametric) macro-elements. The latter have many good properties and it would be desirable to include them in a parametric scheme. An example of both interpolation splines is shown in Fig. 1.3.

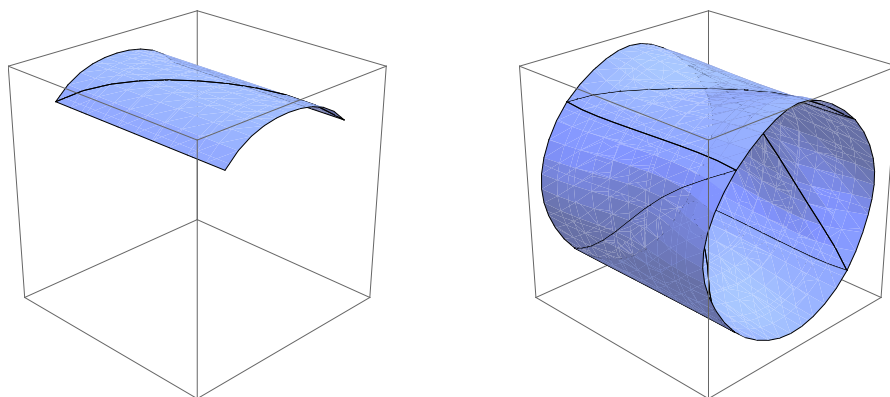


Figure 1.3: Non-parametric macro-element can only represent a part of a cylinder-like object (left). The parametric counterpart can on the other hand represent the whole surface (right).

The drawback of the Willmore energy minimising scheme is that the spline surface is neither parametrically nor visually smooth. Although many different techniques to subsequently smoothen out the joints between patches exists (subdivision, blending, corrections of control points), they require additional post-processing and complexity to

describe the final surface increases considerably. To construct a smooth spline, more degrees of freedom are needed. This can be achieved by increasing the number of the polynomial total degree or the number of patches. Instead of studying G^r smoothness conditions, an alternative is to construct splines satisfying stricter C^r continuity conditions [29, 28, 72, 4]. The advantage of this approach is that the smoothness conditions are linear and they imply a simple geometric construction of control points. The main drawback is that the schemes cannot approximate a surface of arbitrary topology [36]. Therefore, in order to approximate a complex manifold, these schemes should be combined with the aforementioned geometric continuity methods or some relaxations on C^r continuity at certain points or curves of the surface should be applied.

In thesis, we propose an extension of macro-elements from the standard functional to the parametric case. We focus on two special types, the quintic polynomial [51, 73] and the cubic Clough–Tocher [51, 50, 16] macro-element spaces, although the presented generalisations could also be applied to other types of spaces. Cubic triangular splines interpolate points and the corresponding tangent planes at domain vertices and approximate tangent planes at midpoints of domain edges. Quintic splines additionally interpolate normal curvature forms at the vertices. Most of the theory is easily transferred to the parametric setting so we can apply well-known constructions to approximate more complex parametric surfaces. Since the interpolation conditions do not completely determine the shape of the spline, the remaining free shape parameters influence the locations of control points. To achieve the desired positions, uniformly distributed control points of a linear spline interpolant are projected to the corresponding interpolation planes. A correction of points is needed to satisfy smoothness conditions between the patches. It is obtained as the solution of a least square minimisation.

Our interpolation scheme inherits many desired properties from the functional case such as local and geometric construction and linear complexity. The construction does not involve subdivision or degree raising. Therefore the number of control points remains unchanged and the user can easily modify the shape of the interpolant if necessary. If the interpolation data are taken from a non-parametric surface, our approximant resembles the standard functional macro-element.

The structure of the thesis is as follows.

Chapter 2: Some basic notations and well-known properties of spline spaces that are important in further chapters are presented.

Chapter 3: The conjecture on positivity of principal minors of the bivariate Bézier collocation matrix is confirmed for total polynomial degree $d \leq 17$ and for some particular configurations of domain points. The conjecture is extended by stating the lower bound for the minors. Some results on positivity of the minors for generalised domain points are presented.

Chapter 4: Hermite interpolation scheme for cubic curves is analysed. The curves minimise approximate strain energy functional. Geometric conditions for the existence of the interpolant and the shape of the curve are studied with respect to shape parameter. The

chapter is concluded by some numerical examples.

Chapter 5: Construction of cubic triangular patches with small Willmore energy is considered. The interpolation problem is outlined and PN triangles are recalled. The construction of strain energy minimising boundary curves is presented. Next, an approximate Willmore energy functional is studied. It is shown that the minimisation problem has a unique solution at mild presumptions.

Chapter 6: Hermite interpolation schemes for two non-parametric macro-element spaces are recalled. Construction of control points imposed by three types of geometric interpolation conditions is analysed afterwards. The algorithms are applied to two well-known macro-element spaces in parametric setting, to the polynomial and the Clough–Tocher one.

Chapter 7: The Hermite schemes are tested in numerical examples, such as surface approximation, surface reconstruction and hole filling problem.

Chapter 8: Conclusions and important properties of the derived methods are emphasised.

Contents of the following papers are included in the thesis: [45, 46, 48, 47]. Figures and numerical tests were constructed by software package Wolfram Mathematica.

Chapter 2

Preliminaries

In this short chapter some basic notations for triangulations, Bernstein polynomials and splines, and definitions of \bullet^\triangleright , $\langle \bullet, \bullet \rangle$ are presented. C^r smoothness conditions between the triangular patches are recalled.

Let Δ be a (regular) *triangulation* of a given domain $\Omega \subset \mathbb{R}^2$. Every edge e and triangle τ of Δ will be described as a list of vertices: $e = (v_0, v_1)$ and $\tau = (v_0, v_1, v_2)$, respectively. Let a set of all vertices and edges be denoted by \mathcal{V} and \mathcal{E} , respectively. Let Δ_{CT} be the *Clough–Tocher refinement* of Δ , i.e., every triangle of Δ is split at its barycenter into three sub-triangles. Triangles of original triangulation Δ are called *macro-triangles* and triangles of refined triangulation Δ_{CT} are *micro-triangles*.

We will use lightface and boldface characters to distinguish between non-parametric and parametric objects. For instance, a problem of constructing a Lagrange non-parametric spline $s : \Omega \rightarrow \mathbb{R}$ will be presented in the next chapter. On the other hand, finding a parametric spline surface $\mathbf{s} : \Omega \rightarrow \mathbb{R}^3$ that solves a Hermite problem will be dealt later on.

2.1 Bernstein Polynomials and Splines

Let \mathbf{i} be a weak 3–composition of an integer d , i.e., $\mathbf{i} = (i, j, k)$, such that $|\mathbf{i}| := i + j + k = d$ and $i, j, k \in \mathbb{Z}_+$. Let $\mathcal{I}_d := \{\mathbf{i} \mid |\mathbf{i}| = d\}$ be a set of all weak 3–compositions of the integer d . The set \mathcal{I}_d consists of $\binom{d+2}{2}$ compositions.

Let τ be a triangle in \mathbb{R}^2 . Every point $v \in \mathbb{R}^2$ can be written in barycentric coordinates $v = v(\tau) = (\alpha, \beta, \gamma)$, $\alpha + \beta + \gamma = 1$, with respect to τ . The *Bernstein basis polynomials* of total degree d in barycentric coordinates are defined as

$$B_{\mathbf{i}}^d(v) := B_{ijk}^d(\alpha, \beta, \gamma) := \binom{d}{\mathbf{i}} v^{\mathbf{i}} := \frac{d!}{i!j!k!} \alpha^i \beta^j \gamma^k, \quad |\mathbf{i}| = d.$$

Here the standard multi-index notation and a convention $0^0 = 1$ are used. It is a well-known fact that the Bernstein polynomials are a basis of the space of bivariate polynomials of total degree $\leq d$, $\mathcal{P}_d := \mathcal{L}\{x^{\ell_1} y^{\ell_2} : \ell_1, \ell_2 \in \mathbb{Z}_+, \ell_1 + \ell_2 \leq d\}$. Hence, for every non-parametric $p \in \mathcal{P}_d$ and parametric polynomial (also a *Bézier patch*) $\mathbf{p} \in \mathcal{P}_d^3$ there exist a unique *Bézier representation*,

$$p =: \sum_{|\mathbf{i}|=d} c_{\mathbf{i}} B_{\mathbf{i}}^d, \quad \mathbf{p} =: \sum_{|\mathbf{i}|=d} \mathbf{c}_{\mathbf{i}} B_{\mathbf{i}}^d.$$

2 Preliminaries

Here, $c_i \in \mathbb{R}$ and $\mathbf{c}_i \in \mathbb{R}^3$ are called *control coefficients* and *control points*, respectively.

Let the *space of polynomial splines* of total degree $\leq d$ with C^r global smoothness and C^ρ , $\rho \geq r$, smoothness at vertices $v \in \mathcal{V}$ be denoted by

$$\begin{aligned}\mathcal{S}_d^{r,\rho}(\Delta) &:= \{s \in C^r(\Omega) \cap C^\rho(\mathcal{V}) : s|_\tau \in \mathcal{P}_d, \tau \in \Delta\}, \\ \mathbf{S}_d^{r,\rho}(\Delta) &:= \{\mathbf{s} \in C^r(\Omega) \cap C^\rho(\mathcal{V}) : \mathbf{s}|_\tau \in \mathcal{P}_d^3, \tau \in \Delta\}.\end{aligned}$$

A *spline* $s \in \mathcal{S}_d^{r,\rho}(\Delta)$ consist of patches $p^{[\tau]}$, $s|_\tau =: p^{[\tau]} = \sum c_i^{[\tau]} B_i^d$, for $\tau \in \Delta$. Similarly, $\mathbf{s}|_\tau =: \mathbf{p}^{[\tau]} = \sum \mathbf{c}_i^{[\tau]} B_i^d$, for $\tau \in \Delta$.

We will often use the following two notations. Let $\mathbf{a} = (a_\ell)_{\ell=1}^r$ be a vector of scalars and let $\mathbf{b} = (b_\ell)_{\ell=1}^r$ be a vector, consisting of scalars or points. Then their formal scalar product is

$$\langle \mathbf{a}, \mathbf{b} \rangle := \sum_{\ell=1}^r a_\ell b_\ell.$$

The product on the right-hand side is a standard scalar multiplication. If \mathbf{a} and \mathbf{b} are standard vectors (in \mathbb{R}^3), then $\langle \bullet, \bullet \rangle$ is the standard dot product.

Linear interpolation spline surface $\mathbf{s}^\triangleright$ will be used as a reference before constructing the parametric surface. We will use the symbol \bullet^\triangleright to indicate different objects (patches, control points, sets, e.g.) that correspond to the linear spline interpolant $\mathbf{s}^\triangleright$. Namely, let a triangle $(v_0, v_1, v_2) \in \Delta$ and the associated interpolation points $\mathbf{P}_0, \mathbf{P}_1, \mathbf{P}_2$ in \mathbb{R}^3 be given. The corresponding linear spline patch $\mathbf{p}^\triangleright$ of polynomial degree d is defined as

$$\mathbf{p}^\triangleright := \sum_{|\mathbf{i}|=d} \mathbf{c}_i^\triangleright B_i^d,$$

with uniformly distributed control points

$$\mathbf{c}_i^\triangleright := \langle \mathbf{i}/d, (\mathbf{P}_0, \mathbf{P}_1, \mathbf{P}_2) \rangle.$$

Note that the points $\{\mathbf{c}_i^\triangleright\}_{|\mathbf{i}|=d}$ of the patch $\mathbf{p}^\triangleright$ lie on the same plane.

2.2 de Casteljau Algorithm and Continuity Conditions

Let $\mathbf{e}_1, \mathbf{e}_2, \mathbf{e}_3, \mathbf{0}$ be $(1, 0, 0)$, $(0, 1, 0)$, $(0, 0, 1)$ and $(0, 0, 0)$, respectively. The *intermediate de Casteljau points* for parameter $v = (\alpha, \beta, \gamma)$ are defined as

$$\mathbf{c}_i^{(k)} := \mathbf{c}_i^{(k)}(v) := \left\langle v, \left(\mathbf{c}_{\mathbf{i}+\mathbf{e}_1}^{(k-1)}, \mathbf{c}_{\mathbf{i}+\mathbf{e}_2}^{(k-1)}, \mathbf{c}_{\mathbf{i}+\mathbf{e}_3}^{(k-1)} \right) \right\rangle, \quad |\mathbf{i}| = d - k,$$

and $\mathbf{c}_i^{(0)} := \mathbf{c}_i$ are control points of a patch. The presented sequence of nested computations is called *de Casteljau algorithm*. The algorithm is used to stably compute points on the surface from control points. For instance, the point $\mathbf{c}_0^{(d)}(v)$ is a point on the patch at domain parameter v .

The following two well-known theorems state the C^r *continuity conditions* across an adjoining edge and at a vertex.

Theorem 2.1. Let $\mathbf{p}^{[\tau_1]}$ and $\mathbf{p}^{[\tau_2]}$ be adjacent patches, defined on triangles $\tau_1 = (v_0, v_1, v_2)$ and $\tau_2 = (v_0, v_2, v_3)$, respectively (see Fig. 2.1, left). For $0 \leq r \leq d$, the patches join with C^r continuity across the edge $e = (v_0, v_2)$ if

$$\mathbf{c}_{ijk}^{[\tau_2]} = \left(\mathbf{c}_{i0j}^{[\tau_1]} \right)^{(k)} (v_3(\tau_1)), \quad k \leq r, \quad |\mathbf{i}| = d.$$

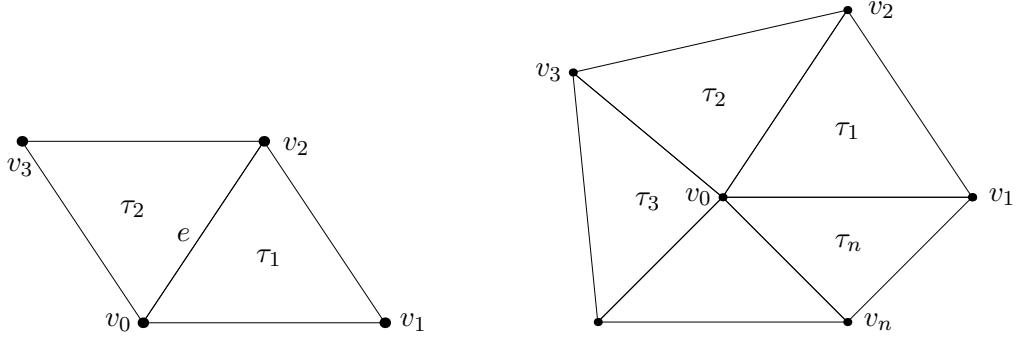


Figure 2.1: Adjacent triangles (left) and a cell with center v_0 (right).

Theorem 2.2. Let Δ be a triangulation with triangles $\{\tau_\ell = (v_0, v_\ell, v_{\ell+1})\}_{\ell=1}^n$ (Fig. 2.1, right). If v_0 is interior vertex, $v_{n+1} \equiv v_1$. For $0 \leq r \leq d$, the patches $\mathbf{p}^{[\tau_\ell]}$ join with C^r continuity at the vertex v_0 if

$$\mathbf{c}_{ijk}^{[\tau_{\ell+1}]} = \left(\mathbf{c}_{i0j}^{[\tau_\ell]} \right)^{(k)} (v_{\ell+2}(\tau_\ell)), \quad j + k \leq r, \quad |\mathbf{i}| = d, \quad 1 \leq \ell \leq n - 1.$$

We call a set of triangles in Thm. 2.2 a *cell*. The smoothness conditions in Thm. 2.1 and Thm. 2.2 can be interpreted as an extrapolation of control points from one patch to another. Note that the conditions do not involve absolute positions of vertices but only their barycentric coordinates. Hence, if we would apply an affine transformation to whole Δ , the smoothness conditions would not change.

For simplicity we will identify boundary control points of adjacent patches and therefore presume C^0 continuity of the spline. Therefore, if $\mathbf{p}^{[\tau_1]}$ and $\mathbf{p}^{[\tau_2]}$ are adjacent as in Thm. 2.1,

$$\mathbf{c}_{ij0}^{[\tau_2]} \equiv \mathbf{c}_{i0j}^{[\tau_1]}, \quad |\mathbf{i}| = d.$$

Chapter 3

Constrained Lagrange Interpolation Problem on Triangle

In this chapter, we show that for any subset of uniformly distributed domain points on triangle and $d \leq 17$, the constrained Lagrange interpolation problem is correct. Results for some special configurations of points are also given. Next, we briefly present application of this result in Lagrange interpolation problem on triangulations. In the last part, we present some results on generalised interpolation points.

Necessary and sufficient conditions on interpolation points that yield a unique solution of the Lagrange problem on triangle remains an open problem. Configurations of points that yield an incorrectness have measure zero and therefore very rarely occur if a random configuration is chosen. In spite of this fact, such configurations are important to detect and avoid configurations that are close to inadmissible ones. Collocation matrix of the latter configuration would be close to singular and a poor approximation of the interpolant is expected.

Most constructions of interpolation points are based on sufficient conditions, e.g. lattices. A more general constructive configuration is described by the following theorem.

Theorem 3.1 ([14, 51]). *Let $n = \binom{d+2}{2}$. Suppose $\{v_\ell\}_{\ell_1=1}^n := \bigcup_{\ell_1=1}^{d+1} \{v_{\ell_1 \ell_2}\}_{\ell_2=1}^{\ell_1}$ is a set of distinct points in the plane such that for a collection $\{L_{\ell_1}\}_{\ell_1=1}^{d+1}$ of distinct lines in the plane, for each $\ell_1 = 1, 2, \dots, d+1$ the points $\{v_{\ell_1 \ell_2}\}_{\ell_2=1}^{\ell_1}$ lie on L_{ℓ_1} but not on $\bigcup_{\ell_3=\ell_1+1}^{d+1} L_{\ell_3}$. Then the interpolation problem at the points $\{v_\ell\}_{\ell_1=1}^n$ is correct.*

An example of points satisfying the presumptions of Thm. 3.1 is shown in Fig. 3.1. A special case of the configuration in Thm. 3.1 is the following set of uniformly distributed domain points

$$\mathcal{D}_{d,\tau} := \{\xi_{\mathbf{i}} : \mathbf{i} \in \mathcal{I}_d\},$$

where points $\xi_{\mathbf{i}} := \xi_{ijk} := \mathbf{i}/d$ are expressed in barycentric coordinates with respect to a given triangle τ . Let us denote the subset of all compositions with ℓ zeros by $\mathcal{I}_d^{(\ell)} \subset \mathcal{I}_d$, $\ell = 0, 1, 2$. A domain point $\xi_{\mathbf{i}}$ is boundary if at least one of its barycentric coordinates is zero, i.e., $\mathbf{i} \in \mathcal{I}_d^{(1)} \cup \mathcal{I}_d^{(2)}$.

Many powerful properties of the standard Lagrange interpolation rely on the characteristics of the space \mathcal{P}_d . Those properties usually cannot be applied in the case of the constrained interpolation since the interpolation space is a strict subspace of \mathcal{P}_d . The problem is tackled in the following section by directly analysing the collocation matrices.

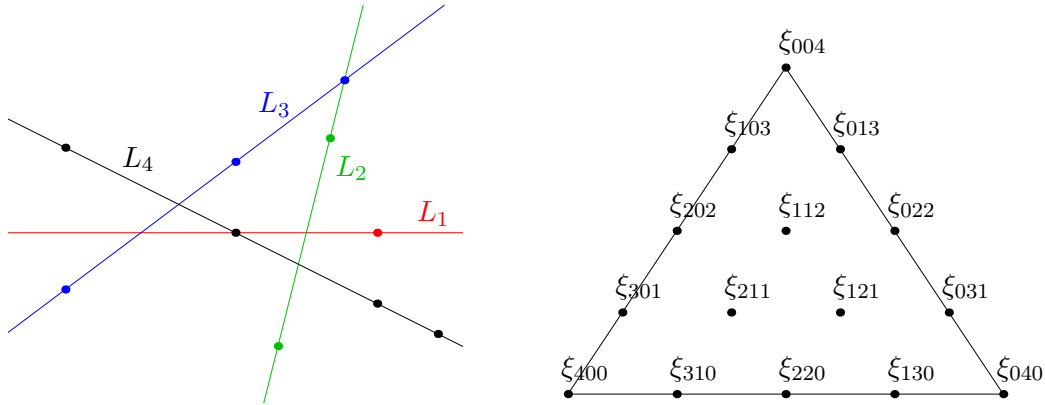


Figure 3.1: A set of admissible interpolation points obtained by Thm. 3.1 for $d = 3$ (left) and domain points $\mathcal{D}_{4,\tau}$ on triangle (right).

3.1 On Positivity of Principle Minors of Bézier Collocation Matrix

The following conjecture will be tackled in this section.

Conjecture 3.2 ([51]). *For a given triangle τ and nonempty set $\Gamma = \{\mathbf{i}_1, \mathbf{i}_2, \dots, \mathbf{i}_n\} \subset \mathcal{I}_d$, the collocation matrix*

$$M_\Gamma := [B_j^d(\xi_i)]_{i,j \in \Gamma} = \begin{bmatrix} B_{i_1}^d(\xi_{i_1}) & B_{i_2}^d(\xi_{i_1}) & \dots & B_{i_n}^d(\xi_{i_1}) \\ B_{i_1}^d(\xi_{i_2}) & B_{i_2}^d(\xi_{i_2}) & \dots & B_{i_n}^d(\xi_{i_2}) \\ \vdots & \vdots & \ddots & \vdots \\ B_{i_1}^d(\xi_{i_n}) & B_{i_2}^d(\xi_{i_n}) & \dots & B_{i_n}^d(\xi_{i_n}) \end{bmatrix}$$

is nonsingular. Furthermore, $\det M_\Gamma > 0$.

If $\Gamma = \mathcal{I}_d$, then M_Γ is the collocation matrix for the standard interpolation problem and is nonsingular by Thm. 3.1.

A confirmation of Conjecture 3.2 would imply the following. Let $\Gamma \subset \mathcal{I}_d$ and let $\mathcal{L}(\{B_i^d\}_{i \in \Gamma})$ be the given interpolation space. Then the interpolation problem for the points $\{\xi_i\}_{i \in \Gamma}$ in the domain would be correct. An example is shown in Fig. 3.2. The conjecture is an important property to solve interpolation problems by spline functions, since some control coefficients of the sought spline are determined by the smoothness and the rest by the interpolation conditions (see [57, 58, 51], e.g.).

Note that the matrix M_Γ is not symmetric. Determinant of M_Γ is independent of the ordering of elements of Γ as long as the same ordering for rows and columns is used. It is common to use the counter-lexicographical ordering $\prec_{c\text{-lex}}$,

$$(d, 0, 0), (d - 1, 1, 0), (d - 1, 0, 1), (d - 2, 2, 0), \dots, (0, 0, d),$$

but a particular ordering of elements in \mathcal{I}_d , which yields a block lower triangular matrix $M_{\mathcal{I}_d}$ (see [10]), will be more convenient. The linear ordering \prec_b is defined as: $\mathbf{i} \prec_b \mathbf{j}$ if one of the following holds true:

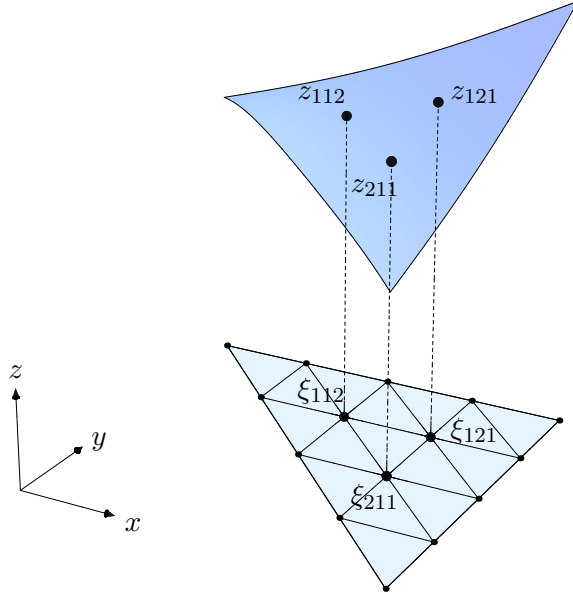


Figure 3.2: Let boundary control coefficients $\{c_i \in \mathbb{R} : \mathbf{i} \in \mathcal{I}_4^{(1)} \cup \mathcal{I}_4^{(2)}\}$ of a Bézier surface p and real values $z_{211}, z_{121}, z_{112}$ be fixed. Conjecture 3.2 ensures that interior control coefficients $\{c_i \in \mathbb{R} : \mathbf{i} \in \mathcal{I}_4^{(0)}\}$ can be set in such a way that $p(\xi_i) = z_i, \mathbf{i} \in \mathcal{I}_4^{(0)}$.

1. $\mathbf{i} \in \mathcal{I}_d^{(\ell_1)}$ and $\mathbf{j} \in \mathcal{I}_d^{(\ell_2)}$ for $0 \leq \ell_2 < \ell_1 \leq 2$,
2. $\mathbf{i}, \mathbf{j} \in \mathcal{I}_d^{(\ell)}$ for $\ell \in \{0, 1, 2\}$ and $\text{sgn}(\mathbf{i}) \prec_{\text{c-lex}} \text{sgn}(\mathbf{j})$,
3. $\mathbf{i}, \mathbf{j} \in \mathcal{I}_d^{(\ell)}$ for $\ell \in \{0, 1, 2\}$ and $\text{sgn}(\mathbf{i}) = \text{sgn}(\mathbf{j})$ and $\mathbf{i} \prec_{\text{c-lex}} \mathbf{j}$.

Here $\text{sgn}(\mathbf{i}) = \text{sgn}(i, j, k) := (\text{sgn}(i), \text{sgn}(j), \text{sgn}(k))$. The ordering \prec_{b} implies that the matrix $M_{\mathcal{I}_d}$ has a structure

$$M_{\mathcal{I}_d} = \begin{bmatrix} M_{\mathcal{I}_d^{(2)}} & & \\ * & M_{\mathcal{I}_d^{(1)}} & \\ * & * & M_{\mathcal{I}_d^{(0)}} \end{bmatrix},$$

where

$$M_{\mathcal{I}_d^{(2)}} = \begin{bmatrix} M_{\{(d,0,0)\}} & & \\ & M_{\{(0,d,0)\}} & \\ & & M_{\{(0,0,d)\}} \end{bmatrix}, \quad M_{\mathcal{I}_d^{(1)}} = \begin{bmatrix} M_{\Gamma_e} & & \\ & M_{\Gamma_e} & \\ & & M_{\Gamma_e} \end{bmatrix},$$

and $\Gamma_e := \{(i, j, 0) \in \mathcal{I}_d : i, j \geq 1\}$. An example, the matrix $M_{\mathcal{I}_4}$, is shown in Fig. 3.3.

The problem of verifying the positivity of principal minors of the matrix $M_{\mathcal{I}_d}$ is reduced to each diagonal block matrix separately. The matrix M_{Γ_e} is a univariate Bézier collocation matrix and by [23] it is totally non-negative with positive principal minors. Therefore, the problem reduces to the study of a $\binom{d-1}{2} \times \binom{d-1}{2}$ matrix $M_{\mathcal{I}_d^{(0)}}$, which, unfortunately, represents a very large part of the matrix $M_{\mathcal{I}_d}$ for a large d .

3 Constrained Lagrange Interpolation Problem on Triangle

$$M_{\mathcal{I}_4} = \frac{1}{256} \begin{bmatrix} 256 & 0 & 0 & 0 & 0 & 0 & 0 & 0 & 0 & 0 & 0 & 0 & 0 & 0 & 0 \\ 0 & 256 & 0 & 0 & 0 & 0 & 0 & 0 & 0 & 0 & 0 & 0 & 0 & 0 & 0 \\ 0 & 0 & 256 & 0 & 0 & 0 & 0 & 0 & 0 & 0 & 0 & 0 & 0 & 0 & 0 \\ 81 & 1 & 0 & 108 & 54 & 12 & 0 & 0 & 0 & 0 & 0 & 0 & 0 & 0 & 0 \\ 16 & 16 & 0 & 64 & 96 & 64 & 0 & 0 & 0 & 0 & 0 & 0 & 0 & 0 & 0 \\ 1 & 81 & 0 & 12 & 54 & 108 & 0 & 0 & 0 & 0 & 0 & 0 & 0 & 0 & 0 \\ 81 & 0 & 1 & 0 & 0 & 0 & 108 & 54 & 12 & 0 & 0 & 0 & 0 & 0 & 0 \\ 16 & 0 & 16 & 0 & 0 & 0 & 64 & 96 & 64 & 0 & 0 & 0 & 0 & 0 & 0 \\ 1 & 0 & 81 & 0 & 0 & 0 & 12 & 54 & 108 & 0 & 0 & 0 & 0 & 0 & 0 \\ 0 & 81 & 1 & 0 & 0 & 0 & 0 & 0 & 0 & 108 & 54 & 12 & 0 & 0 & 0 \\ 0 & 16 & 16 & 0 & 0 & 0 & 0 & 0 & 0 & 64 & 96 & 64 & 0 & 0 & 0 \\ 0 & 1 & 81 & 0 & 0 & 0 & 0 & 0 & 0 & 12 & 54 & 108 & 0 & 0 & 0 \\ 16 & 1 & 1 & 32 & 24 & 8 & 32 & 24 & 8 & 4 & 6 & 4 & 48 & 24 & 24 \\ 1 & 16 & 1 & 8 & 24 & 32 & 4 & 6 & 4 & 32 & 24 & 8 & 24 & 48 & 24 \\ 1 & 1 & 16 & 4 & 6 & 4 & 8 & 24 & 32 & 8 & 24 & 32 & 24 & 24 & 48 \end{bmatrix}$$

Figure 3.3: Matrix $M_{\mathcal{I}_4}$ with the linear ordering \prec_b .

Let us simplify the considered matrix. Let us construct a matrix N_Γ from M_Γ in the following way:

- for every column, divide each element, that corresponds to polynomial B_i^d , by $\binom{d}{i}$,
- multiply the obtained matrix by d^d .

Thus an entry $B_j^d(\xi_i)$ is transformed into i^j and

$$\det N_\Gamma = \frac{d^{d \cdot |\Gamma|}}{\prod_{i \in \Gamma} \binom{d}{i}} \det M_\Gamma. \quad (3.1)$$

Clearly, the matrix N_Γ is a principal submatrix of $N_{\mathcal{I}_d}$. Since $\text{sgn} \det M_\Gamma = \text{sgn} \det N_\Gamma$, Conjecture 3.2 holds true for M_Γ iff it holds true for N_Γ .

The matrix $N_{\mathcal{I}_d}$ has some nice properties. It consists only of non-negative integers. The matrix has a simpler structure than $M_{\mathcal{I}_d}$ and is closely related to combinatorial objects. Note that some of the properties are not preserved by the transformation $M_\Gamma \rightarrow N_\Gamma$ (for example, the largest element in a row of N_Γ is not necessarily on the diagonal). As an example, the matrix $N_{\mathcal{I}_4}$ is shown in Fig. 3.4.

We are now ready to present one of the main results of this chapter.

Theorem 3.3. *Let $d \leq 17$. Then Conjecture 3.2 holds true, i.e., $\det M_\Gamma > 0$ for every nonempty subset $\Gamma \subset \mathcal{I}_d$.*

Proof. Fix d , $1 \leq d \leq 16$. The matrix $M_{\mathcal{I}_d} + M_{\mathcal{I}_d}^T$ is symmetric and positive definite since its Cholesky decomposition exists. Therefore the matrix $M_{\mathcal{I}_d}$ is positive definite, i.e., $\mathbf{x}^T M_{\mathcal{I}_d} \mathbf{x} > 0$ for every $\mathbf{0} \neq \mathbf{x} \in \mathbb{R}^n$, $n = \binom{d+2}{2}$. Thus all principal submatrices of $M_{\mathcal{I}_d}$ are positive definite too and all principal minors are positive.

$$N_{\mathcal{I}_4} = \begin{bmatrix} 256 & 0 & 0 & 0 & 0 & 0 & 0 & 0 & 0 & 0 & 0 & 0 & 0 & 0 & 0 & 0 & 0 & 0 \\ 0 & 256 & 0 & 0 & 0 & 0 & 0 & 0 & 0 & 0 & 0 & 0 & 0 & 0 & 0 & 0 & 0 & 0 \\ 0 & 0 & 256 & 0 & 0 & 0 & 0 & 0 & 0 & 0 & 0 & 0 & 0 & 0 & 0 & 0 & 0 & 0 \\ 81 & 1 & 0 & 27 & 9 & 3 & 0 & 0 & 0 & 0 & 0 & 0 & 0 & 0 & 0 & 0 & 0 & 0 \\ 16 & 16 & 0 & 16 & 16 & 16 & 0 & 0 & 0 & 0 & 0 & 0 & 0 & 0 & 0 & 0 & 0 & 0 \\ 1 & 81 & 0 & 3 & 9 & 27 & 0 & 0 & 0 & 0 & 0 & 0 & 0 & 0 & 0 & 0 & 0 & 0 \\ 81 & 0 & 1 & 0 & 0 & 0 & 27 & 9 & 3 & 0 & 0 & 0 & 0 & 0 & 0 & 0 & 0 & 0 \\ 16 & 0 & 16 & 0 & 0 & 0 & 16 & 16 & 16 & 0 & 0 & 0 & 0 & 0 & 0 & 0 & 0 & 0 \\ 1 & 0 & 81 & 0 & 0 & 0 & 3 & 9 & 27 & 0 & 0 & 0 & 0 & 0 & 0 & 0 & 0 & 0 \\ 0 & 81 & 1 & 0 & 0 & 0 & 0 & 0 & 0 & 27 & 9 & 3 & 0 & 0 & 0 & 0 & 0 & 0 \\ 0 & 16 & 16 & 0 & 0 & 0 & 0 & 0 & 0 & 16 & 16 & 16 & 0 & 0 & 0 & 0 & 0 & 0 \\ 0 & 1 & 81 & 0 & 0 & 0 & 0 & 0 & 0 & 3 & 9 & 27 & 0 & 0 & 0 & 0 & 0 & 0 \\ 16 & 1 & 1 & 8 & 4 & 2 & 8 & 4 & 2 & 1 & 1 & 1 & 4 & 2 & 2 & 2 & 2 & 2 \\ 1 & 16 & 1 & 2 & 4 & 8 & 1 & 1 & 1 & 8 & 4 & 2 & 2 & 4 & 2 & 2 & 2 & 2 \\ 1 & 1 & 16 & 1 & 1 & 1 & 2 & 4 & 8 & 2 & 4 & 8 & 2 & 4 & 8 & 2 & 2 & 4 \end{bmatrix}$$

 Figure 3.4: Matrix $N_{\mathcal{I}_4}$ with the linear ordering \prec_b .

For $d = 17$, the matrix $M_{\mathcal{I}_d} + M_{\mathcal{I}_d}^T$ has three negative eigenvalues. The matrices $M_{\mathcal{I}_d^{(2)}}$ and $M_{\mathcal{I}_d^{(1)}}$ are P-matrices, thus the problem reduces to the study of the matrix $M_{\mathcal{I}_d^{(0)}}$. Since the Cholesky decomposition of the matrix $M_{\mathcal{I}_d^{(0)}} + M_{\mathcal{I}_d^{(0)}}^T$ exists, the rest of the proof is similar to the first part. \square

For $d = 18$, the smallest eigenvalue of $M_{\mathcal{I}_d} + M_{\mathcal{I}_d}^T$ is approximately $-1.1 \cdot 10^{-7}$. For $d \geq 18$, the number of negative eigenvalues of the matrix $M_{\mathcal{I}_d} + M_{\mathcal{I}_d}^T$ increases with d . Therefore, this approach cannot be used to prove the conjecture in general. However, our result covers all the cases important in practice, since polynomial interpolants of high degrees have undesirable properties.

Eigenvalues of $M_{\mathcal{I}_d}$ are derived in a closed form in [18],

$$\lambda_\ell := \frac{d!}{(d-\ell)!d^\ell}, \quad \ell = 1, 2, \dots, d,$$

with multiplicities $3, 3, 4, 5, \dots, d+1$. Unfortunately, the result cannot be applied for the matrix $M_{\mathcal{I}_d} + M_{\mathcal{I}_d}^T$. As an example, the spectrum of $M_{\mathcal{I}_{10}} + M_{\mathcal{I}_{10}}^T$ is shown in Tab. 3.1.

Remark 3.4. *The matrix $N_{\mathcal{I}_d}$ is positive definite only for $d \leq 4$.*

Remark 3.5. *Entries in the matrix $M_{\mathcal{I}_d} + M_{\mathcal{I}_d}^T$ are rational numbers, hence the Cholesky decomposition can be carried out in exact arithmetics and no numerical error can influence the computation.*

The approach for proving Theorem 3.3 can also be used to prove a similar result for the trivariate case: the trivariate Bézier collocation matrix for $d \leq 15$ is positive definite and thus the constrained polynomial Lagrange interpolation problem is correct. And in univariate case, the matrix is positive definite for $d \leq 18$.

3 Constrained Lagrange Interpolation Problem on Triangle

eigenvalue	mult.	eigenvalue	mult.	eigenvalue	mult.
2.341	1	0.2854	1	$7.224 \cdot 10^{-3}$	1
2.308	2	0.2675	1	$7.038 \cdot 10^{-3}$	2
1.856	2	0.2585	1	$6.565 \cdot 10^{-3}$	1
1.841	1	0.2568	2	$6.560 \cdot 10^{-3}$	1
1.475	1	0.1225	1	$6.399 \cdot 10^{-3}$	2
1.412	2	0.1179	2	$6.220 \cdot 10^{-3}$	2
1.303	1	0.1076	2	$6.209 \cdot 10^{-3}$	1
1.001	2	0.1033	2	$6.752 \cdot 10^{-4}$	2
0.9377	1	0.1028	1	$6.600 \cdot 10^{-4}$	2
0.8855	2	0.03647	2	$6.574 \cdot 10^{-4}$	1
0.6082	1	0.03531	1	$6.160 \cdot 10^{-4}$	2
0.5742	2	0.03253	2	$6.079 \cdot 10^{-4}$	1
0.5221	2	0.03241	1	$5.951 \cdot 10^{-4}$	2
0.5180	1	0.03126	1	$5.923 \cdot 10^{-4}$	1
0.2995	2	0.03115	2		

Table 3.1: Spectrum of the matrix $M_{\mathcal{I}_{10}} + M_{\mathcal{I}_{10}}^T$ together with eigenvalue multiplicities.

Theorem 3.3 implies the following result.

Theorem 3.6. *Let $\Gamma \subset \mathcal{I}_d$ and let $d \leq 17$. Then for any $\{z_i\}_{i \in \Gamma}$, there is a unique polynomial of the form*

$$p := \sum_{i \in \Gamma} c_i B_i^d$$

such that

$$p(\xi_i) = z_i, \quad i \in \Gamma.$$

Remark 3.7. *Theorem 3.6 generalises [57, Thm. 3]. Its proof avoids computation of all sub-determinants, as was the case in [57].*

Now let us consider some particular configurations of domain points (and the corresponding choices of Γ) for arbitrary d .

Theorem 3.8. *Let d be arbitrary and let Γ satisfy one of the following assumptions:*

- (a) $|\Gamma| \leq 2$,
- (b) *let one of the components of (i, j, k) be fixed for all elements in Γ ,*
- (c) $\Gamma = \mathcal{I}_d$,
- (d) $\Gamma = \{(i, j, k) \in \mathcal{I}_d : i \geq i_0, j \geq j_0, k \geq k_0\}$ *for fixed non-negative integers i_0, j_0, k_0 ,*
- (e) $\Gamma \subset \mathcal{I}_d^{(2)} \cup \mathcal{I}_d^{(1)}$,

(f) $\Gamma = \Gamma_1 \cup \Gamma_2$, where Γ_1 is one of the sets, defined in (a), (b) or (d), and Γ_2 is a set in (e).

Then $\det M_\Gamma > 0$.

Proof. (a) For $|\Gamma| = 1$, the matrix M_Γ is a positive number. Now let $\Gamma = \{\mathbf{i}_1, \mathbf{i}_2\}$. Since the largest element of every column in M_Γ is on the diagonal of M_Γ ,

$$\det M_\Gamma = \begin{vmatrix} B_{\mathbf{i}_1}^d(\xi_{\mathbf{i}_1}) & B_{\mathbf{i}_2}^d(\xi_{\mathbf{i}_1}) \\ B_{\mathbf{i}_1}^d(\xi_{\mathbf{i}_2}) & B_{\mathbf{i}_2}^d(\xi_{\mathbf{i}_2}) \end{vmatrix} > 0.$$

(b) Let one of the components of (i, j, k) be fixed. Without loss of generality we may assume that $\mathbf{i}_\ell = (i_\ell, j_\ell, k)$, $i_\ell + j_\ell + k = d$, $\ell \in \{1, 2, \dots, |\Gamma|\}$. By dividing each element of N_Γ by k^k and multiplying each column by a proper constant, the matrix N_Γ transforms to a univariate Bézier collocation matrix, which is a P-matrix by [23].

(c) From [10] and (3.1) it follows that

$$\det M_{\mathcal{I}_d} = d^{-d \binom{d+2}{2}} \prod_{\mathbf{i} \in \mathcal{I}_d} \binom{d}{\mathbf{i}} \prod_{\ell_1=1}^{\min\{d,3\}} \left(d^{\binom{d-1}{\ell_1}} \prod_{\ell_2=1}^{d-\ell_1+1} \ell_2^{\binom{d-\ell_2+1}{\ell_1-2}} \right)^{\binom{3}{\ell_1}} > 0. \quad (3.2)$$

(d) First, let us revise the proof of nonsingularity of M_Γ (see [51]). By appropriately multiplying rows and columns of M_Γ , we obtain a collocation matrix \tilde{M}_Γ consisting of all polynomials of total degree $\leq d_0 := d - i_0 - j_0 - k_0$ and domain points that correspond to Γ . Recall that the interpolation problem remains correct if the domain points $\mathcal{D}_{d,\tau}$ are translated and scaled by a positive factor since the presumptions on interpolation points in Thm. 3.1 are preserved. Let $M(\lambda)$, $\lambda \in [0, 1]$, denote a homotopy that changes the domain points by such transformation and $M(0) = M_{\mathcal{I}_{d_0}}$, $M(1) = \tilde{M}_\Gamma$. Since $\det M_{\mathcal{I}_{d_0}} > 0$ (see Thm. 3.8 (c)) and the matrix $M(\lambda)$ is nonsingular for every $\lambda \in [0, 1]$, it follows that $\det \tilde{M}_\Gamma > 0$.

(e), (f) For $\Gamma \subset \mathcal{I}_d^{(2)} \cup \mathcal{I}_d^{(1)}$ and $\Gamma = \Gamma_1 \cup \Gamma_2$, the result follows straightforwardly from the block structure of the matrix M_Γ . \square

Remark 3.9. The set Γ in Thm. 3.8 (b) corresponds to domain points in the triangle τ , lying on a line parallel to some edge of τ (see interior points in Fig. 3.5, right).

The nonsingularity of the matrix $M_{\mathcal{I}_d}$ follows from Thm. 3.1. To prove $\det M_{\mathcal{I}_d} > 0$, most of the paper [10] is dedicated to the derivation of determinant formula in a closed form (3.2).

In Thm. 3.8 (d), the set Γ corresponds to domain points that form a scaled triangle of triangle τ (see Fig. 3.5, left).

The subset of compositions Γ in Thm. 3.8 (e) corresponds to the interpolation problem at boundary domain points of the triangle τ .

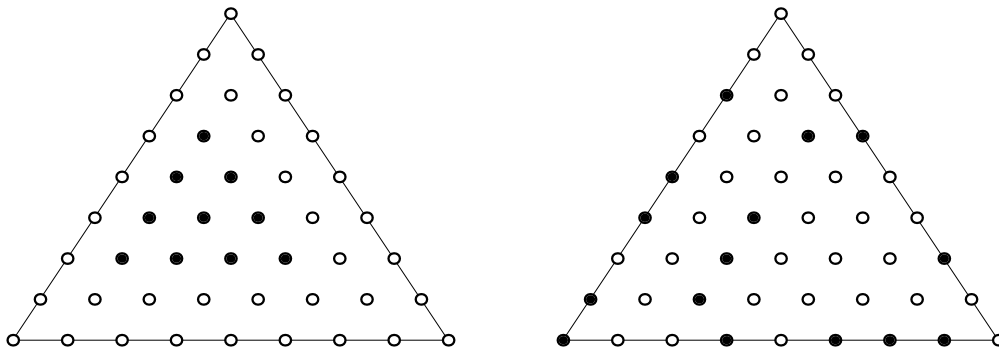


Figure 3.5: Sets of domain points (represented by black dots), satisfying presumptions in Thm. 3.8 (d) (left figure) and (f) (right figure).

3.2 New Conjectures

The following two conjectures give lower bounds on the determinants and expand the Conjecture 3.2.

Conjecture 3.10. For d fixed,

$$\min_{\substack{\Gamma \subset \mathcal{I}_d \\ \Gamma \neq \emptyset}} \det M_\Gamma = \det M_{\mathcal{I}_d}$$

and $\det M_{\mathcal{I}_d}$ is given in (3.2).

Conjecture 3.11. For $\ell \in \mathbb{N}$ let

$$n_d := \begin{cases} \ell^{3\ell}, & d = 3\ell \\ (\ell + 1)^{\ell+1} \ell^{2\ell}, & d = 3\ell + 1 \\ (\ell + 1)^{2\ell+2} \ell^\ell, & d = 3\ell + 2 \end{cases} .$$

Then

$$\min_{\substack{\Gamma \subset \mathcal{I}_d \\ \Gamma \neq \emptyset}} \det N_\Gamma = n_d.$$

Conjectures 3.10 and 3.11 were verified by a computer for $d \leq 7$. Let us prove the latter conjecture for $|\Gamma| \leq 2$ and arbitrary d . We will need the following lemma.

Lemma 3.12. Let $\mathbf{x} = (x, y, z) \in \mathbb{R}^3$ and fix $\mathbf{i} = (i, j, k) \in \mathcal{I}_d$. Let the function $f(\mathbf{x}) := \mathbf{x}^{\mathbf{i}}$ be defined on

$$\Omega = \{(x, y, z) : x + y + z = d, 0 \leq x \leq d, 0 \leq y \leq d - x\}. \quad (3.3)$$

Then f has a unique maximum at \mathbf{i} and

$$\max_{\mathbf{x} \in \Omega} f(\mathbf{x}) = \mathbf{i}^{\mathbf{i}}.$$

Proof. Let $\tau = ((0, 0), (d, 0), (0, d))$ be a triangle in the domain and let us define Bernstein polynomial $B_{\mathbf{i}}^d$ on τ . By interpreting barycentric coordinates of $B_{\mathbf{i}}^d$ as points in \mathbb{R}^3 , $B_{\mathbf{i}}^d(\mathbf{x}) = \binom{d}{\mathbf{i}} / d^d f(d \cdot \mathbf{x})$. Since $B_{\mathbf{i}}^d$ has a unique maximum at $\xi_{\mathbf{i}}$, the proof is complete. \square

Proposition 3.13. *Conjecture 3.11 holds true for $|\Gamma| \leq 2$.*

Proof. Let $|\Gamma| = 1$ and let $g(\mathbf{x}) := g(x, y, z) := \mathbf{x}^{\mathbf{x}}$ be a function, defined on the domain Ω as in (3.3). We are looking for

$$\mu := \min_{\mathbf{x} \in \Omega \cap \mathbb{Z}^3} g(\mathbf{x}).$$

A unique local minimum of g in the interior of Ω is obtained as a solution of the normal system $\partial g / \partial x = 0$, $\partial g / \partial y = 0$, and it is reached at $(d/3, d/3, d/3)$. This is a global minimum since $g(d/3, d/3, d/3) < g(\mathbf{x})$ for all \mathbf{x} at the boundary of Ω .

If $d \equiv 0 \pmod{3}$, then $\mu = (d/3)^d$.

Let us examine the case $d \equiv 1 \pmod{3}$. Then $d = (\ell + 1) + \ell + \ell$ for $\ell \in \mathbb{Z}_+$. By the symmetry of the function g and since at least one component of $\mathbf{x} \in \Omega \cap \mathbb{Z}^3$ is greater or equal to $\ell + 1$, it is enough to consider the case $\ell + 1 \leq x$ only.

Let us define

$$\Omega_x := \{\mathbf{x} = (x, y, z) \in \Omega : \ell + 1 \leq x\}.$$

Since g has no extreme point in Ω_x , the minimum value is reached at the boundary of Ω_x . Then the minimum is $\mu = (\ell + 1)^{\ell+1} \ell^{2\ell}$ and it is achieved at $(\ell + 1, \ell, \ell)$. For $\ell + 1 \leq y$ and $\ell + 1 \leq z$, the derivation is analogous.

The case $d \equiv 2 \pmod{3}$ is similar to the previous one. Since $N_{\{\mathbf{i}\}} = g(\mathbf{i})$, $\mathbf{i} \in \mathcal{I}_d$, and $n_d = \mu$, the conjecture for $|\Gamma| = 1$ is proven.

Now let us consider the case $|\Gamma| = 2$. Let us show that

$$\mathbf{i}_1^{\mathbf{i}_1} = \det N_{\{\mathbf{i}_1\}} \leq \det N_{\{\mathbf{i}_1, \mathbf{i}_2\}} = \mathbf{i}_1^{\mathbf{i}_1} \mathbf{i}_2^{\mathbf{i}_2} - \mathbf{i}_2^{\mathbf{i}_1} \mathbf{i}_1^{\mathbf{i}_2}$$

for every $\mathbf{i}_1, \mathbf{i}_2 \in \mathcal{I}_d$, $\mathbf{i}_1 \neq \mathbf{i}_2$. By Lemma 3.12 it follows that $\mathbf{i}_2^{\mathbf{i}_1} < \mathbf{i}_1^{\mathbf{i}_1}$ and $\mathbf{i}_1^{\mathbf{i}_2} \leq \mathbf{i}_2^{\mathbf{i}_2} - 1$, thus

$$\det N_{\{\mathbf{i}_1, \mathbf{i}_2\}} - \det N_{\{\mathbf{i}_1\}} = \mathbf{i}_1^{\mathbf{i}_1} (\mathbf{i}_2^{\mathbf{i}_2} - 1) - \mathbf{i}_2^{\mathbf{i}_1} \mathbf{i}_1^{\mathbf{i}_2} \geq 0.$$

Since $n_d \leq N_{\{\mathbf{i}_1, \mathbf{i}_2\}}$ holds true for every $\mathbf{i}_1, \mathbf{i}_2 \in \mathcal{I}_d$, the proof of the proposition is complete. \square

3.3 Application: Lagrange Interpolation on Triangulations

Nonsingularity of principal minors of the collocation matrix is an important property when constructing a smooth spline that interpolates scattered data. Since some degrees of freedom of the spline are determined by smoothness conditions, only the remaining control coefficients can be used for interpolation. The problem was studied in [57, 58, 60] and references therein. Here, we only mention some basic ideas for constructing the interpolant. The interpolation problem is roughly presented by the following problem.

3 Constrained Lagrange Interpolation Problem on Triangle

Problem 3.14. Let $\mathcal{V} =: \{\zeta_\ell\}_{\ell=1}^n$ be a set of points in the plane and let Δ be a triangulation (sometimes a quadrangulation or a triangulation with some restrictions) with vertices at the points of \mathcal{V} . Let d, r, ρ be appropriate integers indicating the total polynomial degree and smoothness of the spline space. Find a refinement Δ_R of Δ , a set of additional points $\{\zeta_\ell\}_{\ell=n+1}^{n'}$ and a subspace $\mathcal{S} \subset \mathcal{S}_d^{r,\rho}(\Delta_R)$ such that for every choice of data values $\{z_\ell\}_{\ell=1}^{n'}$, there exists a unique spline $s \in \mathcal{S}$ satisfying

$$s(\xi_\ell) = z_\ell, \quad \ell = 1, 2, \dots, n'.$$

The subspace \mathcal{S} usually satisfies additional smoothness conditions (e.g., higher smoothness at certain points) to overcome dimension problems of the spline space. The construction of interpolation spline $s \in \mathcal{S}$ is presented by the following steps:

- construct a triangulation Δ (or some other required decomposition of the polygonal domain Ω) with vertices at points of \mathcal{V} ,
- define the triangulation Δ_R by applying appropriate refinements on certain elements (triangles) of Δ ,
- define a space $\mathcal{S} \subset \mathcal{S}_d^{r,\rho}(\Delta_R)$ on triangulation Δ_R ,
- insert additional interpolation points at certain triangles in an appropriate way and
- show that smoothness conditions of the spline space \mathcal{S} uniquely determine all of the remaining control coefficients of the spline s once the interpolation conditions are applied.

The refinement Δ_R and interpolation points $\{\zeta_\ell\}_{\ell=n+1}^{n'}$ need to be carefully chosen in order to obtain a local and stable construction that possesses linear complexity in terms of number of triangles and that the interpolant has a full approximation power. To remain concise, details of the constructions will be skipped here (see [57, 58, 60] and references therein for further information). Let us present a simple example of Lagrange interpolation on small number of triangles instead.

Example 3.15. Let f be a Franke's test function,

$$f(x, y) := \frac{3}{4}e^{-\frac{1}{4}((9x-2)^2+(9y-2)^2)} + \frac{3}{4}e^{-\left(\frac{1}{49}(9x+1)^2+\frac{1}{10}(9y+1)\right)} \\ + \frac{1}{2}e^{-\frac{1}{4}((9x-7)^2+(9y-3)^2)} - \frac{1}{5}e^{-((9x-4)^2+(9y-7)^2)},$$

defined on a square domain $\Omega = [0, 1]^2$ (Fig. 3.6, top left). Let $\Delta = \{\tau_\ell\}_{\ell=1}^6$ be a triangulation obtained by splitting Ω into six triangles. We would like to construct an interpolation spline $s \in \mathcal{S}_{10}^{1,1}(\Delta)$. Interpolation points are chosen in such a way that at every step ℓ , $\ell = 1, 2, \dots, 6$, the patch $s|_{\tau_\ell}$ is uniquely constructed. Thm. 3.6 insures that the interpolation problem is correct. Plot of s is shown in Fig. 3.6, bottom left. Error function $|s - f|$ (Fig. 3.6, right) reveals a significant error on τ_3 and τ_4 . Considerable oscillations of s are located near the edges of Δ . The largest error is $\|s - f\|_\infty = 0.0810$.

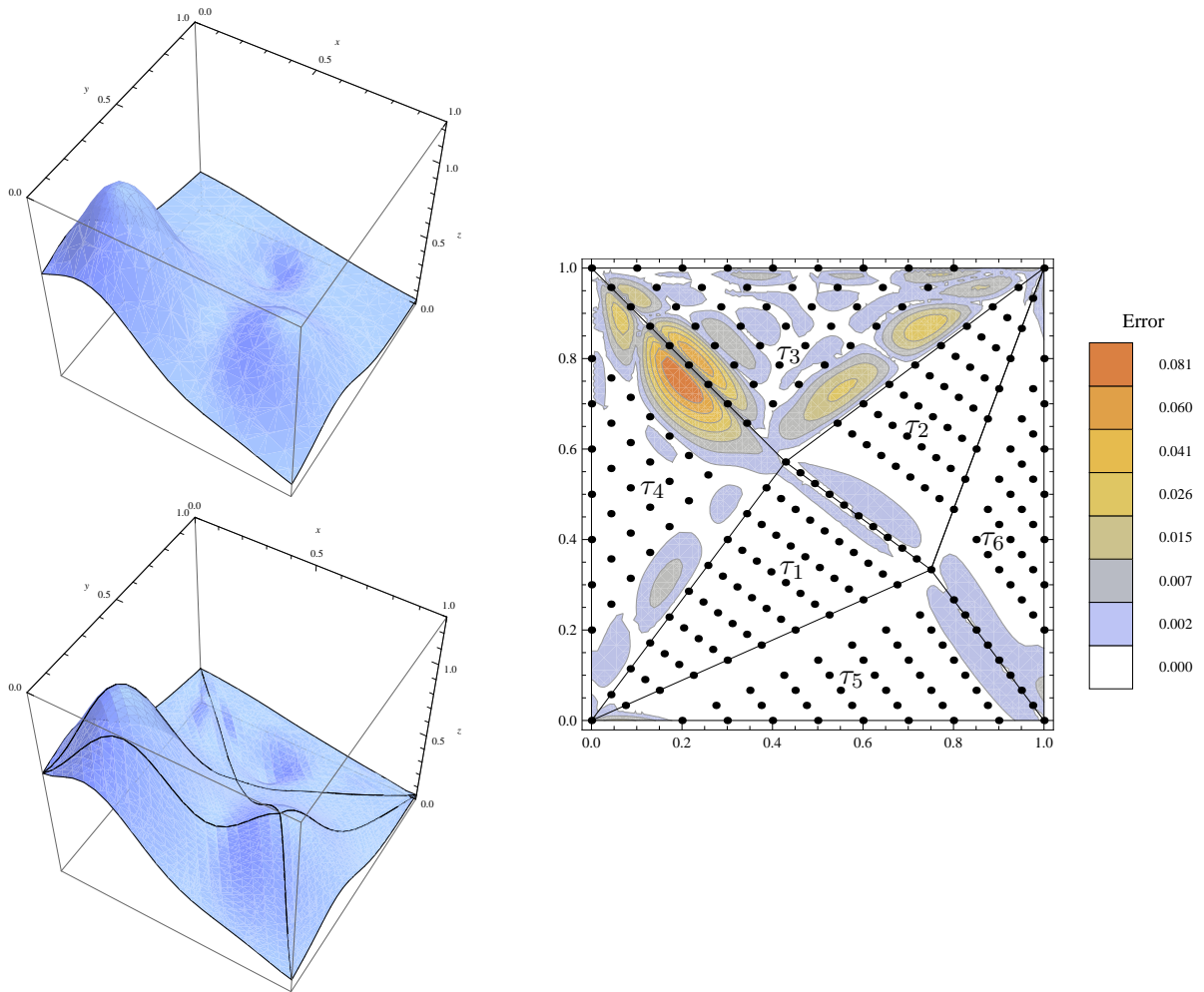


Figure 3.6: Franke's function f (top left) is approximated by spline s (bottom left). Triangulation, interpolation points and error $|s - f|$ are shown in right figure. To show the error distribution better, a nonlinear scale for colour palette is chosen.

3.4 On Constrained Interpolation at Generalised Domain Points

Till now we only considered a constrained interpolation on triangle τ at uniformly distributed domain points $\mathcal{D}_{d,\tau}$. A natural question arises on how general can configurations of interpolation points be so that the corresponding Lagrange problem remains correct.

Problem 3.16. Fix d and let $\Gamma \subset \mathcal{I}_d$. Determine necessary and sufficient conditions for a set of distinct domain points $\{\zeta_i \in \tau\}_{i \in \Gamma}$ that yield a unique polynomial of the form

$$p := \sum_{i \in \Gamma} c_i B_i^d$$

and

$$p(\zeta_i) = z_i, \quad i \in \Gamma,$$

for any values $\{z_i\}_{i \in \Gamma}$.

3 Constrained Lagrange Interpolation Problem on Triangle

Generalised domain points $\zeta_{\mathbf{i}} =: (\alpha_{\mathbf{i}}, \beta_{\mathbf{i}}, \gamma_{\mathbf{i}})$, $\mathbf{i} \in \mathcal{I}_d$, lie in τ , hence $\alpha_{\mathbf{i}}, \beta_{\mathbf{i}}, \gamma_{\mathbf{i}} \geq 0$. A case $\Gamma = \mathcal{I}_d$ is the standard Lagrange interpolation problem and it has been extensively studied (see beginning of the chapter and § 1.1). On the other hand, very little is known for a case $\emptyset \neq \Gamma \subsetneq \mathcal{I}_d$. Let us present some sufficient conditions for correctness of this problem and positivity of the determinant.

Since basis polynomials $B_{\mathbf{i}}^d$, $\mathbf{i} \in \mathcal{I}_d^{(0)}$, vanish on the edges of τ , they cannot interpolate points on the edges. Let us presume a natural restriction $\text{sgn}(\mathbf{i}) = \text{sgn}(\zeta_{\mathbf{i}})$. Therefore, an interpolation point $\zeta_{\mathbf{i}}$ lies on an edge of τ iff $\mathbf{i} \notin \mathcal{I}_d^{(0)}$. Hence, Lagrange interpolation problem at boundary and interior points is separated. Firstly, let us examine boundary interpolation points. Fix $\Gamma \subset \mathcal{I}_d$ and let $\Gamma_b := \Gamma \setminus \mathcal{I}_d^{(0)}$. Let v_ℓ , $\ell = 1, 2, 3$, be vertices of τ and let us presume the corresponding points $\{\zeta_{\mathbf{i}}\}_{\mathbf{i} \in \Gamma_b}$ are linearly ordered on every edge of the domain triangle. More precisely, for the first edge let

$$\zeta_{ij0} = (1 - \lambda_j) v_1 + \lambda_j v_2, \quad (i, j, 0) \in \Gamma_b, \quad (3.4)$$

with properties

$$\lambda_0 = 0, \lambda_d = 1 \quad \text{and} \quad \lambda_{j_1} < \lambda_{j_2} \text{ iff } j_1 < j_2.$$

Let similar conditions apply for points on the other two edges. The interpolation problem for $\{\zeta_{\mathbf{i}}\}_{\mathbf{i} \in \Gamma_b}$ is correct since the corresponding univariate collocation matrices are P-matrices [23]. Hence, the interpolation problem in Problem 3.16 for Γ is correct iff it is correct for $\Gamma \setminus \mathcal{I}_d^{(0)}$.

For interior points let us consider a case $d \leq 4$ only. Hence, the set $\Gamma_i := \Gamma \cap \mathcal{I}_d^{(0)}$ consist of at most three indices and only three non-symmetric cases need to be analysed:

- A case $|\Gamma_i| = 1$ ($d = 3, 4$) is trivial since from the positivity of Bernstein polynomials it follows that the corresponding collocation submatrix is a positive number and the problem is correct.
- Let $|\Gamma_i| = 2$ ($d = 4$) and w.l.o.g. let $\Gamma_i =: \{(2, 1, 1), (1, 2, 1)\}$ and $\zeta_{211} =: (\alpha_1, \beta_1, \gamma_1)$, $\zeta_{121} =: (\alpha_2, \beta_2, \gamma_2)$. The determinant of the corresponding submatrix is

$$D = \begin{vmatrix} 12 \alpha_1^2 \beta_1 \gamma_1 & 12 \alpha_1 \beta_1^2 \gamma_1 \\ 12 \alpha_2^2 \beta_2 \gamma_2 & 12 \alpha_2 \beta_2^2 \gamma_2 \end{vmatrix} = 144 \prod_{\ell=1}^2 \alpha_\ell \beta_\ell \gamma_\ell \cdot \begin{vmatrix} \alpha_1 & \beta_1 \\ \alpha_2 & \beta_2 \end{vmatrix}.$$

If we interpret barycentric points $\xi_{211}, \xi_{121}, v_3$ as vectors in \mathbb{R}^3 written in Cartesian coordinates, then the determinant on the right-hand side is

$$\begin{vmatrix} \alpha_1 & \beta_1 \\ \alpha_2 & \beta_2 \end{vmatrix} = \begin{vmatrix} \alpha_1 & \beta_1 & \gamma_1 \\ \alpha_2 & \beta_2 & \gamma_2 \\ 0 & 0 & 1 \end{vmatrix} = \langle \xi_{211} \times \xi_{121}, v_3 \rangle.$$

From geometric properties of coordinates it follows straightforwardly that $D = 0$ iff points $\zeta_{211}, \zeta_{121}, v_3$ are collinear and $D > 0$ iff triangle $(\zeta_{211}, \zeta_{121}, v_3)$ is positively oriented. Similar conditions are obtained for other two cases.

- The interpolation problem for the case $|\Gamma_i| = 3$ (and $d = 4$) is correct iff all three points are distinct (Thm. 3.1). Let the domain points be denoted as $\zeta_{211} =: (\alpha_1, \beta_1, \gamma_1)$, $\zeta_{121} =: (\alpha_2, \beta_2, \gamma_2)$, $\zeta_{112} =: (\alpha_3, \beta_3, \gamma_3)$. Determinant of the collocation matrix is

$$D = 1728 \begin{vmatrix} \alpha_1^2 \beta_1 \gamma_1 & \alpha_1 \beta_1^2 \gamma_1 & \alpha_1 \beta_1 \gamma_1^2 \\ \alpha_2^2 \beta_2 \gamma_2 & \alpha_2 \beta_2^2 \gamma_2 & \alpha_2 \beta_2 \gamma_2^2 \\ \alpha_3^2 \beta_3 \gamma_3 & \alpha_3 \beta_3^2 \gamma_3 & \alpha_3 \beta_3 \gamma_3^2 \end{vmatrix} = 1728 \prod_{\ell=1}^3 \alpha_\ell \beta_\ell \gamma_\ell \cdot \begin{vmatrix} \alpha_1 & \beta_1 & \gamma_1 \\ \alpha_2 & \beta_2 & \gamma_2 \\ \alpha_3 & \beta_3 & \gamma_3 \end{vmatrix}.$$

Similarly as in the previous case, from the geometric properties of domain points it follows that $D > 0$ iff triangle $(\zeta_{211}, \zeta_{121}, \zeta_{112})$ is positively oriented.

For higher degrees d the analysis of the matrices is considerably more complex and the number of non-symmetric configurations of points that need to be studied is much higher than for the case $d \leq 4$ (e.g., for $d = 5$ one would need to examine more than 20 non-symmetric configurations of interior points). An example of generalised interpolation points for $d = 4$ is shown in Fig. 3.7.

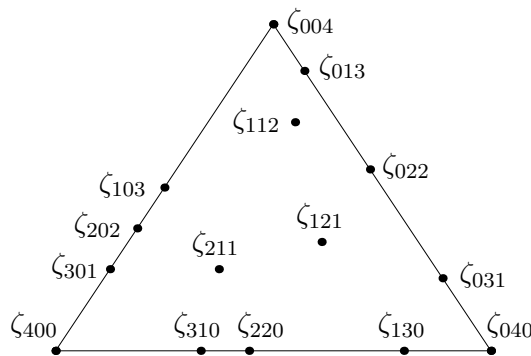


Figure 3.7: A set of generalised interpolation points $\{\zeta_i\}_{i \in \mathcal{I}_4}$ is represented by black dots. The corresponding constrained interpolation problem is correct for every $\{\zeta_i\}_{i \in \Gamma}$, $\emptyset \neq \Gamma \subset \mathcal{I}_4$.

The presented generalised domain points can easily be applied to extend some existing Lagrange interpolation schemes. In [59, 60, 13] and references therein, a set of interpolation points is a subset of evenly distributed domain points $\bigcup_{\tau \in \Delta} \mathcal{D}_{d,\tau}$. For $d \leq 4$, the configurations of points can be generalised as shown in this section. In [39], a construction of a C^0 Lagrange interpolation spline on three-pencil lattices is analysed. The continuity conditions between patches restrict positions of centers that form lattices on triangles. These restrictions can be removed by allowing the interpolation points on triangle edges not to lie on the prescribed lattices as the rest of interior interpolation points but only satisfy conditions similar to (3.4).

Chapter 4

Hermite Interpolation by Cubic Curves with Small Strain Energy

Hermite interpolation problem by cubic Bézier curves with small strain energy in \mathbb{R}^3 is considered. A parametric interpolation scheme is introduced. It is based on minimisation of approximate strain energy. As its particular cases, it reproduces three known planar methods and one spatial. The resulting interpolants are shape preserving, without loops, cusps or folds. Area of admissible tangent directions and the shape of the curve is investigated with respect to a given shape parameter.

The results of the Hermite scheme are applied to construct Hermite interpolating cubic spline surface in the next chapter. The scheme for curves can be straightforwardly generalised to construct G^1 smooth spline curves in \mathbb{R}^d [46]. By constructing optimal tangent directions, an iterative algorithm for solving the Lagrange interpolation problem is also given.

4.1 Interpolation Problem

We will study the following problem. Let endpoints $\mathbf{P}_0, \mathbf{P}_1$ and the corresponding normalised tangent directions $\mathbf{d}_0, \mathbf{d}_1$ in \mathbb{R}^3 be given and let $\Delta\mathbf{P} := \mathbf{P}_1 - \mathbf{P}_0$. We would like to construct a cubic polynomial curve $\mathbf{b} : [0, 1] \rightarrow \mathbb{R}^3$ that solves the Hermite interpolation problem

$$\begin{aligned} \mathbf{b}(0) &= \mathbf{P}_0, & \dot{\mathbf{b}}(0) &= \alpha_0 \mathbf{d}_0, \\ \mathbf{b}(1) &= \mathbf{P}_1, & \dot{\mathbf{b}}(1) &= \alpha_1 \mathbf{d}_1, \end{aligned}$$

where $\alpha_\ell \in \mathbb{R}$ are some positive parameters.

Among all feasible curves we would like to choose one with small curvature. It would be reasonable to minimise *strain energy* of the curve,

$$\int_0^1 \kappa^2(t) dt = \int_0^1 \frac{\|\dot{\mathbf{b}}(t)\|^2 \|\ddot{\mathbf{b}}(t)\|^2 - \langle \dot{\mathbf{b}}(t), \ddot{\mathbf{b}}(t) \rangle^2}{\|\dot{\mathbf{b}}(t)\|^6} dt, \quad (4.1)$$

where κ is the curvature of \mathbf{b} (see [22, 65]). In practice, the computation of the energy is too difficult. Thus, the *approximate strain energy* [69, 65, 28]

$$\varphi(\boldsymbol{\alpha}) := \int_0^1 \|\ddot{\mathbf{b}}(t)\|^2 dt \quad (4.2)$$

is used instead, where $\boldsymbol{\alpha} := (\alpha_0, \alpha_1)$, $\alpha_\ell > 0$. Note that if the curve is parametrised by the arc length, $\kappa^2(t) = \|\ddot{\mathbf{b}}(t)\|^2$.

4.2 Hermite Interpolation Scheme

Usually it is difficult to establish the existence of the minimum of φ and to obtain it in a closed form. Especially, since the minimum is sought in an open set $\{\boldsymbol{\alpha} \in \mathbb{R}^2 : \alpha_\ell > 0\}$. A natural approach is to apply a carefully chosen quadrature and minimise the obtained approximation.

Let us introduce a 3-point quadrature rule for an approximation of the integral φ , that depends on a parameter $\omega \in [0, \infty)$,

$$\psi_\omega(\boldsymbol{\alpha}) := \frac{1}{\omega + 2} \left(\|\ddot{\mathbf{b}}(0)\|^2 + \omega \left\| \ddot{\mathbf{b}}\left(\frac{1}{2}\right) \right\|^2 + \|\ddot{\mathbf{b}}(1)\|^2 \right). \quad (4.3)$$

Note that for $\omega = 0, 2, 4$ we obtain the trapezoidal, the composite trapezoidal and the Simpson's quadrature rule for φ , respectively.

By using properties of derivatives of Bézier curves, the second derivative of \mathbf{b} at particular parameter values is expressed with the interpolation data,

$$\begin{aligned} \ddot{\mathbf{b}}(0) &= 6 \Delta \mathbf{P} - (4\alpha_0 \mathbf{d}_0 + 2\alpha_1 \mathbf{d}_1), \\ \ddot{\mathbf{b}}\left(\frac{1}{2}\right) &= -\alpha_0 \mathbf{d}_0 + \alpha_1 \mathbf{d}_1, \\ \ddot{\mathbf{b}}(1) &= -6 \Delta \mathbf{P} + 2\alpha_0 \mathbf{d}_0 + 4\alpha_1 \mathbf{d}_1. \end{aligned} \quad (4.4)$$

In the spatial case, let $\vartheta_\ell := \angle(\Delta \mathbf{P}, \mathbf{d}_\ell) \in [0, \pi]$, $\ell = 0, 1$, and $\vartheta := \angle(\mathbf{d}_0, \mathbf{d}_1) \in [0, \pi]$ denote unsigned angles. In the planar case, it is more convenient to use oriented angles $\theta_\ell := \angle(\Delta \mathbf{P}, \mathbf{d}_\ell) \in (-\pi, \pi]$.

It turns out that a unique optimal interpolant exists if certain geometric conditions are satisfied.

Theorem 4.1. *The functional ψ_ω has a unique minimum at*

$$\alpha_\ell = \frac{36 [(\omega + 20)\langle \Delta \mathbf{P}, \mathbf{d}_\ell \rangle + (\omega - 16)\langle \Delta \mathbf{P}, \mathbf{d}_{1-\ell} \rangle \langle \mathbf{d}_0, \mathbf{d}_1 \rangle]}{(\omega + 20)^2 - (\omega - 16)^2 \langle \mathbf{d}_0, \mathbf{d}_1 \rangle^2}, \quad \ell = 0, 1. \quad (4.5)$$

If the angles ϑ_0, ϑ_1 and ϑ satisfy $\vartheta_0, \vartheta_1 \in [0, \pi/2)$ and the relations

$$0 < (\omega + 20) \cos(\vartheta_\ell) + (\omega - 16) \cos(\vartheta_{1-\ell}) \cos(\vartheta), \quad \ell = 0, 1, \quad (4.6)$$

then the parameters α_ℓ in (4.5) are positive and the interpolant is regular. Furthermore, the curve is loop-, cusp- and fold-free.

Proof. By using the expressions (4.4) in the functional (4.3), we obtain

$$\begin{aligned} \psi_\omega(\boldsymbol{\alpha}) &= \frac{72 [\|\Delta \mathbf{P}\|^2 - \langle \Delta \mathbf{P}, \mathbf{d}_0 \rangle \alpha_0 - \langle \Delta \mathbf{P}, \mathbf{d}_1 \rangle \alpha_1]}{(\omega + 2)} \\ &+ \frac{(\omega + 20)(\alpha_0^2 + \alpha_1^2) - 2(\omega - 16)\langle \mathbf{d}_0, \mathbf{d}_1 \rangle \alpha_0 \alpha_1}{(\omega + 2)}. \end{aligned} \quad (4.7)$$

The minimum of (4.7) is obtained by solving the normal system $\partial\psi_\omega/\partial\alpha_0 = \partial\psi_\omega/\partial\alpha_1 = 0$:

$$\begin{aligned} (\omega + 20) \alpha_0 - (\omega - 16) \langle \mathbf{d}_0, \mathbf{d}_1 \rangle \alpha_1 &= 36 \langle \Delta \mathbf{P}, \mathbf{d}_0 \rangle, \\ (\omega + 20) \alpha_1 - (\omega - 16) \langle \mathbf{d}_0, \mathbf{d}_1 \rangle \alpha_0 &= 36 \langle \Delta \mathbf{P}, \mathbf{d}_1 \rangle. \end{aligned}$$

It can easily be verified that (4.5) is the solution of the obtained linear system.

The optimal parameters $\alpha_{i,k}$ should be nonnegative. Clearly, the denominator of (4.5) is positive, since $|\langle \mathbf{d}_0, \mathbf{d}_1 \rangle| \leq 1$. The requirement on the positivity of the numerator yields relations (4.6).

We are left to show that the curve is regular and shape preserving. Let the angles $\vartheta_0, \vartheta_1, \vartheta$ satisfy admissibility conditions in the presumptions of the theorem. The curve \mathbf{b} can be written in the Bézier form as

$$\mathbf{b} = \mathbf{P}_0 B_0^3 + \left(\mathbf{P}_0 + \frac{1}{3} \alpha_0 \mathbf{d}_0 \right) B_1^3 + \left(\mathbf{P}_1 - \frac{1}{3} \alpha_1 \mathbf{d}_1 \right) B_2^3 + \mathbf{P}_1 B_3^3, \quad (4.8)$$

where $B_j^m : [0, 1] \rightarrow \mathbb{R}$, $j = 0, 1, \dots, m$, are the univariate Bernstein basis polynomials of degree m . Its derivative $\dot{\mathbf{b}}$ can be expressed as a quadratic Bézier curve,

$$\dot{\mathbf{b}} = (\alpha_0 \mathbf{d}_0) B_0^2 + (3\Delta \mathbf{P} - \alpha_0 \mathbf{d}_0 - \alpha_1 \mathbf{d}_1) B_1^2 + (\alpha_1 \mathbf{d}_1) B_2^2.$$

By using appropriate rotation and translation we can w.l.o.g. presume that

$$\begin{aligned} \mathbf{P}_0 &= (0, 0, 0), & \mathbf{d}_0 &= (\cos(\theta_0), \sin(\theta_0), 0), \\ \mathbf{P}_1 &= (\|\Delta \mathbf{P}\|, 0, 0), & \mathbf{d}_1 &= (\cos(\theta_1), \sin(\theta_1) \cos(\theta_1^{(2)}), \dots). \end{aligned}$$

Here the vectors \mathbf{d}_ℓ are written in spherical coordinates.

To prove that \mathbf{b} is regular and loop-, cusp- and fold-free, it is enough to show that the first component of $\dot{\mathbf{b}}$ is strictly positive. The first component of the first and the last control point of $\dot{\mathbf{b}}$ are positive since $\alpha_0, \alpha_1 > 0$ and $\vartheta_0, \vartheta_1 \in [0, \pi/2)$. To prove that the middle control point of $\dot{\mathbf{b}}$ has a positive first component is a harder task.

By inserting the coefficients (4.5) into the expression for the middle control point, its first component simplifies to

$$\|\Delta \mathbf{P}\| (3 - a),$$

where

$$\begin{aligned} a &:= \frac{36(\omega + 20)(c_0^2 + c_1^2) + 72(\omega - 16)c_0 c_1 b}{(\omega + 20)^2 - (\omega - 16)^2 b^2}, & c_0 &:= \cos(\theta_0), \\ b &:= \langle \mathbf{d}_0, \mathbf{d}_1 \rangle = c_0 c_1 + \sin(\theta_0) \sin(\theta_1) \cos(\theta_1^{(2)}), & c_1 &:= \cos(\theta_1). \end{aligned}$$

We would like to obtain an upper bound on the function a . It can be verified that a is monotone in ω . Therefore its maximum is reached at $\omega = 0$. Nonzero solutions of $\partial a / \partial \theta_1^{(2)} = 0$ imply $a \leq 9/5 < 3$. By inserting the solution $\theta_1^{(2)} = 0$ into a , it simplifies into

$$\frac{9(6 + \cos(2\theta_0) - 4\cos(2(\theta_0 - \theta_1)) + \cos(2\theta_1))}{34 - 16\cos(2(\theta_0 - \theta_1))}.$$

In this case, it is easy to obtain an upper bound

$$a \leq \frac{54}{25} < 3.$$

Thus the first component of the derivative $\dot{\mathbf{b}}$ is positive by the convex hull property of Bézier curves. This completes the proof. \square

Note that when the conditions (4.6) are not fulfilled, the optimal solution does not exist. One or both of the parameters α_ℓ in (4.5) are negative and the obtained result yields an undesirable shape of the interpolant.

The introduced interpolation scheme yields some existing schemes as its special cases.

Remark 4.2. Note that $\|\ddot{\mathbf{b}}\|^2$ is a quadratic function in t . Since the Simpson's rule is exact for quadratic polynomials, it follows that $\psi_4 = \varphi$. Thus, for the planar case, the curve that minimises the functional ψ_4 is the optimal curve presented in [71].

Remark 4.3. Even though the approach in [44, 42] is to apply a trapezoidal approximation of the integral and to approximate second derivatives by first ones, our method reproduces the schemes for $\omega = 16$. The optimal parameters

$$\alpha_\ell = \langle \Delta \mathbf{P}, \mathbf{d}_\ell \rangle, \quad \ell = 0, 1, \quad (4.9)$$

are easily obtained by using $\omega = 16$ in (4.5).

Remark 4.4. Although we analyse the case $\omega \geq 0$ only, similar conditions can be obtained for negative parameters. Quite surprisingly, in the planar case, the curve that minimises a non-normalised functional

$$\|\ddot{\mathbf{b}}(0)\|^2 + \omega \left\| \ddot{\mathbf{b}} \left(\frac{1}{2} \right) \right\|^2 + \|\ddot{\mathbf{b}}(1)\|^2$$

for $\omega = -2$ is the optimal curve for a curvature deviation functional (see [43])

$$\int_0^1 \|\dot{\mathbf{b}}(t) \times \ddot{\mathbf{b}}(t)\|^2 dt.$$

Here \times denotes the planar vector product. The optimal parameters can be expressed as

$$\alpha_\ell = 2(-1)^\ell \frac{c_\ell}{c}, \quad \ell = 0, 1,$$

where

$$c_\ell := \Delta \mathbf{P} \times \mathbf{d}_{1-\ell}, \quad c := \mathbf{d}_0 \times \mathbf{d}_1.$$

Plot of admissible angles such that $\alpha_\ell > 0$ for some choices of ω is presented as Fig. 4.1. In the planar case, the inequalities (4.6) can be simplified since $\vartheta = |\theta_0 - \theta_1|$. Plot of admissible angles (θ_0, θ_1) is presented as Fig. 4.2.

Every region of admissible angles θ_ℓ has an inscribed open square $(-a_\omega, a_\omega)^2$, where

$$a_\omega := \arccos \left(\frac{z(\omega - 16)}{3(\omega + 8)} \right), \quad z := \begin{cases} -1, & \text{if } \omega \leq 16, \\ 1, & \text{if } \omega > 16. \end{cases} \quad (4.10)$$

For a large ω , the curves that minimise the strain energy functional tend to a linear curve.

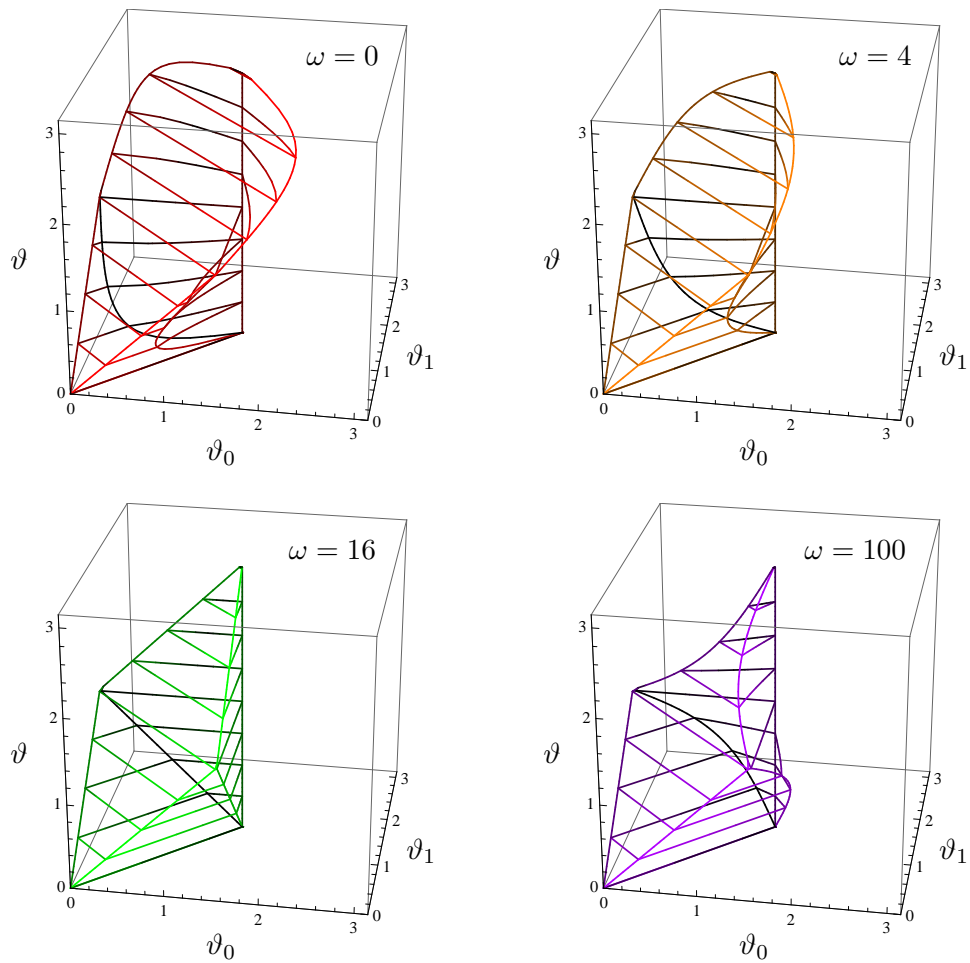


Figure 4.1: Admissible angles $(\vartheta_0, \vartheta_1, \vartheta)$ such that $\alpha_\ell > 0$. Boundaries of the regions for $\omega = 0, 4, 16, 100$ are represented with red, orange, green and purple lines, respectively.

Proposition 4.5. *If $\mathbf{d}_0 \neq \mathbf{d}_1$, the optimal parameters α_ℓ in (4.5) satisfy the relation*

$$\lim_{\omega \rightarrow \infty} \alpha_\ell = 0, \quad \ell = 0, 1.$$

If $\mathbf{d}_0 = \mathbf{d}_1$, the optimal parameters are

$$\alpha_\ell = \langle \Delta \mathbf{P}, \mathbf{d}_0 \rangle, \quad \ell = 0, 1. \quad (4.11)$$

Proof. If $\mathbf{d}_0 \neq \mathbf{d}_1$, the linear asymptote of the rational function $\alpha_\ell = \alpha_\ell(\omega)$ is the abscissa. The expression (4.11) clearly holds true if $\mathbf{d}_0 = \mathbf{d}_1$. \square

From Proposition 4.5 and the numerical experience it seems reasonable to use $\omega \in [0, 30]$ in practical applications.

4.3 Choosing Parameter ω

In this section we examine how to choose appropriate parameters ω with respect to the interpolation data. By not predetermining the parameter ω , this results in a larger area of admissible tangent directions and more control on the shape of the curve is obtained.

4 Hermite Interpolation by Cubic Curves with Small Strain Energy

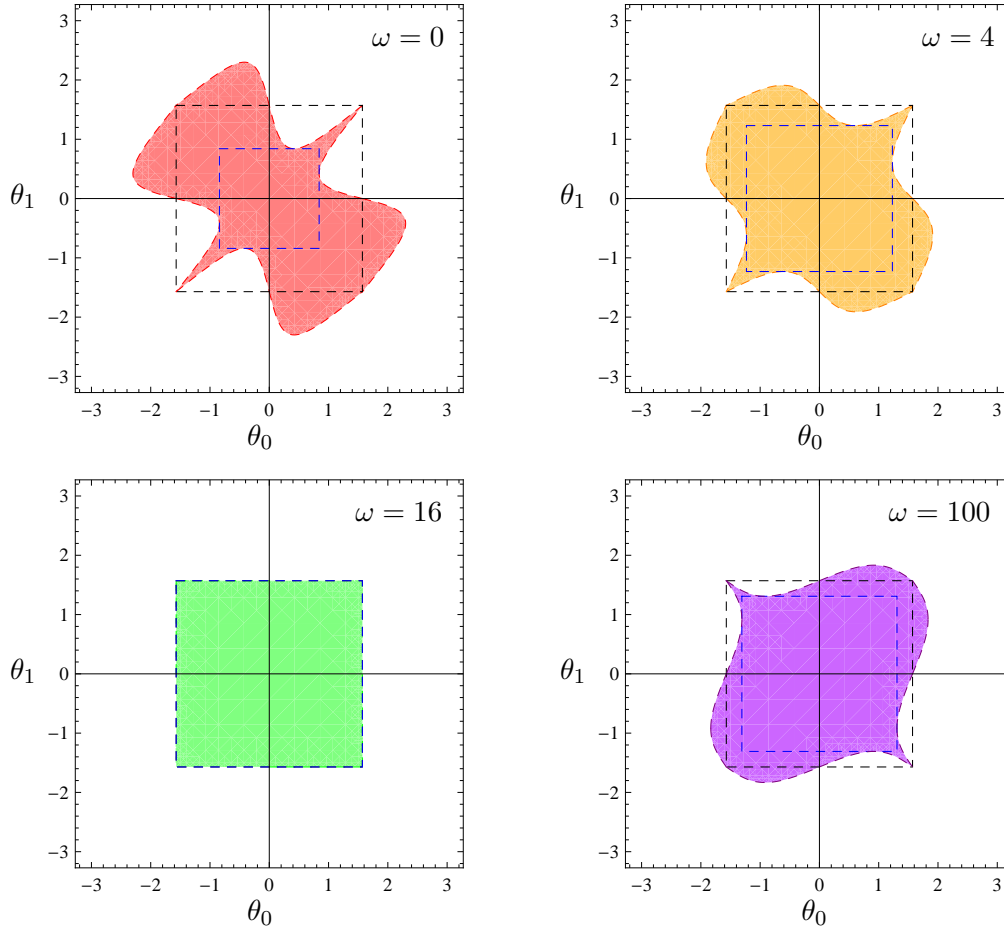


Figure 4.2: Admissible angles (θ_0, θ_1) such that $\alpha_\ell > 0$. The regions for $\omega = 0, 4, 16, 100$ are presented by red, orange, green and purple colour, respectively. An additional sufficient requirement for the regularity of the curve, $\theta_\ell \in (-\pi/2, \pi/2)$, is represented by the black square. The inscribed square $(-a_\omega, a_\omega)^2$ (see (4.10)) is represented with blue colour.

As an illustration, plots of Hermite interpolants for different tangent directions and parameters ω are presented in Fig. 4.3. The curves for $\omega = 0$ have a nice shape in top plots, whereas in the bottom right the curve is inadmissible. In contrast, the curves for $\omega = 16, 30$ are inadmissible in the first plot but perform better in bottom cases.

From inequalities (4.6) we obtain bounds on admissible parameters ω that yield positive α_ℓ . Let

$$\begin{aligned} p_\ell &:= 16 \cos(\theta_{1-\ell}) \cos(\theta) - 20 \cos(\theta_\ell), \\ r_\ell &:= \cos(\theta_\ell) + \cos(\theta_{1-\ell}) \cos(\theta). \end{aligned}$$

Then ω must fulfil conditions

$$\omega \in \mathcal{I} := \mathcal{I}_0 \cap \mathcal{I}_1,$$

where

$$\mathcal{I}_\ell = \begin{cases} [p_\ell/r_\ell + \delta, \infty), & r_\ell > 0 \\ [0, p_\ell/r_\ell - \delta], & r_\ell < 0 \end{cases}, \quad \ell = 0, 1,$$

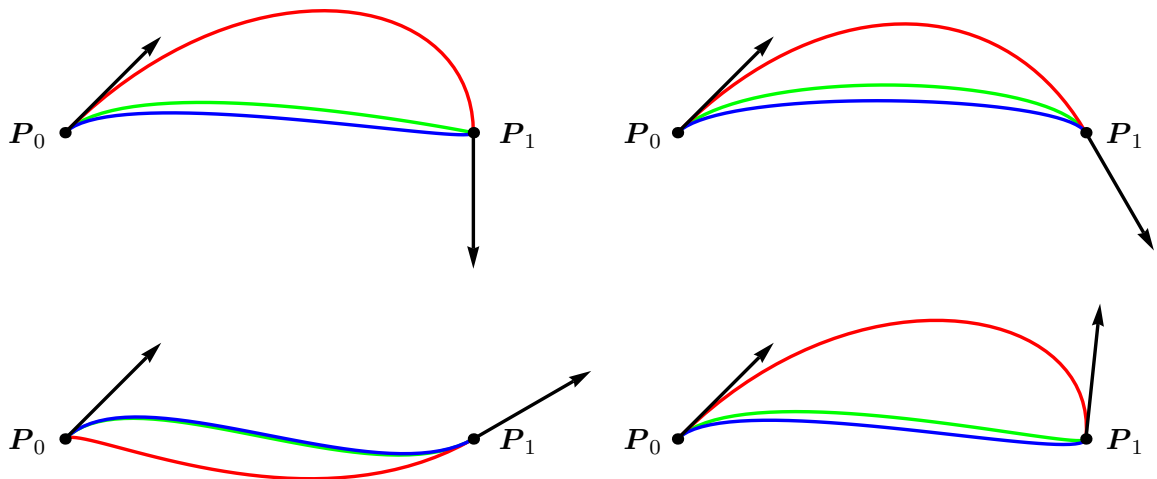


Figure 4.3: Hermite interpolants for different tangent directions. The curves for $\omega = 0, 16, 30$ are presented by red, green and blue colour, respectively.

and $\delta > 0$ is a shift that ensures that the corresponding α_ℓ are not too close to 0. Next, we propose a simple heuristic approach on how to choose the most suitable $\omega \in \mathcal{I}$ based on geometric observation. If the relation

$$\|\Delta\mathbf{P}\| \langle \mathbf{d}_0, \mathbf{d}_1 \rangle \leq \min\{\langle \Delta\mathbf{P}, \mathbf{d}_0 \rangle, \langle \Delta\mathbf{P}, \mathbf{d}_1 \rangle\} \quad (4.12)$$

holds true, the resulting curve segment has a U-shape and choosing smaller parameters ω results in a more pleasant shape. If (4.12) does not hold true, we obtain an S-shaped curve and it is better to take larger ω (see Fig. 4.3).

Therefore, let the optimal parameter be $\omega^* = \min \mathcal{I}$ if (4.12) holds true and $\omega^* = \min\{\max \mathcal{I}, 30\}$, otherwise. Note that it is better that ω^* are not too close to the boundary values p_ℓ/r_ℓ . Hence, a moderate shift δ should be taken, $\delta = 4$, e.g.

4.4 Numerical Examples

Let us conclude the chapter by numerical tests. We approximate a planar curve \mathbf{f}_1 and a spatial curve \mathbf{f}_2 ,

$$\begin{aligned} \mathbf{f}_1(t) &:= (-\sin(t) \log^2(t), \cos(8/5t)), & t \in [0, 2\pi], \\ \mathbf{f}_2(t) &:= (4t - 18t^2 + 28t^3 - 14t^4, -2t + 3/2t^4, 6t^2 - 12t^3 + 6t^4), & t \in [0, 1], \end{aligned} \quad (4.13)$$

by interpolation splines for parameter values $\omega \in \{0, 16, 30\}$. The splines are constructed as a sequence of Hermite Bézier curves, presented in 4.2. The original and the approximation curves are presented in Fig. 4.4. Interpolants resemble the shape of the original curve. The schemes for $\omega = 0$ produce round shapes that are in average the closest to the original curves. For the planar case, Hausdorff distance errors for $\omega = 0, 16, 30$ are 0.166, 0.123 and 0.215, respectively, and 0.0236, 0.0390, 0.0510 for the spatial one.

Strain energy (4.1) of \mathbf{f}_1 is 45.6 and for $\omega = 0, 16, 30$ the interpolation splines have the energy equal to 163, 222 and 350, respectively. For the spatial case, \mathbf{f}_2 has strain energy

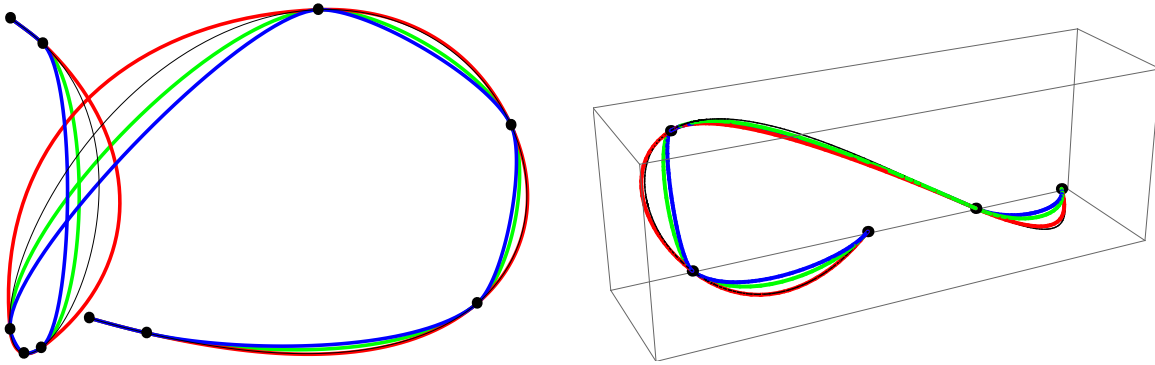


Figure 4.4: Approximation of the planar f_1 (left) and spatial curve f_2 (right) in (4.13) by the Hermite interpolating splines. The original curves are shown in black and approximation curves for $\omega = 0, 16, 30$ are shown in red, green and blue colour, respectively.

18.2 and for the interpolation splines, the values are 78.9, 318 and 1139, respectively. Therefore, the optimal splines for $\omega = 0$ have the smallest average curvature. In addition, oscillations of the curvature are the smallest among other approximation splines (see Fig. 4.5).

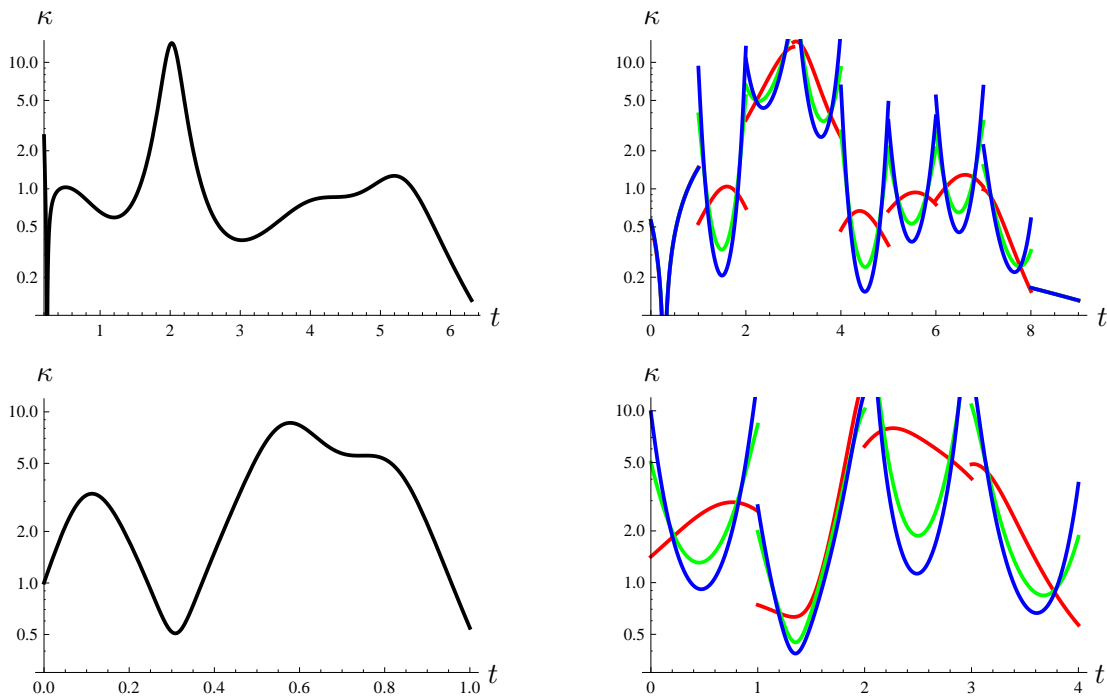


Figure 4.5: Curvature of f_1 (top left) and f_2 (bottom left) and the corresponding curvatures of approximation splines on the right. Splines for $\omega = 0, 16, 30$ are shown in red, green and blue colour, respectively.

Chapter 5

Hermite Interpolation by Cubic Triangular Patches with Small Willmore Energy

A construction of a cubic Bézier spline surface that interpolates prescribed spatial points and the corresponding normal directions of tangent planes is proposed. Boundary curves of each triangular patch minimise the approximate strain energy functional. A comparison of optimal boundary curves is given. We prove that the optimal boundary curves for parameter $\omega = 16$ coincide with boundary curves of PN triangle. The remaining undefined parameters of our interpolation spline are set in such a way that the spline patches minimise a simplified Willmore energy functional.

5.1 Interpolation Problem and PN Triangles

For a given set of points $\{\mathbf{P}_\ell\}_\ell$ in \mathbb{R}^3 and the corresponding normal vectors $\{\mathbf{n}_\ell\}_\ell$ (sampled from some smooth surface), we would like to construct a continuous, shape preserving cubic spline surface that interpolates given data and has small Willmore energy.

Let us presume that the reference linear spline surface $\mathbf{s}^\triangleright$ (i.e., a spatial triangulation), that interpolates points $\{\mathbf{P}_\ell\}_\ell$, is given in advance. The spline is a collection of linear patches $\mathbf{p}_\ell^\triangleright$, $\mathbf{s}^\triangleright =: \{\mathbf{p}_\ell^\triangleright\}_\ell$.

Since the interpolation scheme will be local, we w.l.o.g. presume that for every $\mathbf{p}_\ell^\triangleright$, the corresponding cubic Bézier surface

$$\mathbf{p} = \mathbf{p}_\ell = \sum_{|i|=3} \mathbf{c}_i B_i^3$$

interpolates points $\mathbf{P}_0, \mathbf{P}_1, \mathbf{P}_2$ and the corresponding tangent planes at its endpoints.

Let v_ℓ , $\ell = 1, 2, 3$, be a point with barycentric coordinates $(1, 0, 0)$, $(0, 1, 0)$, $(0, 0, 1)$, respectively. For $u_1 := v_2 - v_1$ and $u_2 := v_3 - v_1$ let D_{u_1}, D_{u_2} be the corresponding directional derivative operators. Let $\mathbf{n}(v) := ((D_{u_1}\mathbf{p} \times D_{u_2}\mathbf{p}) / \|D_{u_1}\mathbf{p} \times D_{u_2}\mathbf{p}\|)(v)$ be a normal to the surface \mathbf{p} at a barycentric point v . The interpolation conditions can now be written in the form

$$\begin{aligned} \mathbf{p}(v_{\ell+1}) &= \mathbf{P}_\ell, \\ \mathbf{n}(v_{\ell+1}) &= \mathbf{n}_\ell, \end{aligned} \quad \ell = 0, 1, 2. \quad (5.1)$$

In general, the interpolation problem (5.1) has several degrees of freedom. The conditions will be satisfied by constructing appropriate boundary curves in the next section.

If control points of \mathbf{p} are chosen as

$$\begin{aligned} \mathbf{c}_{300} &= \mathbf{P}_0, & \mathbf{c}_{210} &= \frac{1}{3}(2\mathbf{P}_0 + \mathbf{P}_1 - w_{10} \mathbf{n}_0), & \mathbf{c}_{120} &= \frac{1}{3}(2\mathbf{P}_1 + \mathbf{P}_0 - w_{01} \mathbf{n}_1), \\ \mathbf{c}_{030} &= \mathbf{P}_1, & \mathbf{c}_{021} &= \frac{1}{3}(2\mathbf{P}_1 + \mathbf{P}_2 - w_{21} \mathbf{n}_1), & \mathbf{c}_{012} &= \frac{1}{3}(2\mathbf{P}_2 + \mathbf{P}_1 - w_{12} \mathbf{n}_2), \\ \mathbf{c}_{003} &= \mathbf{P}_2, & \mathbf{c}_{102} &= \frac{1}{3}(2\mathbf{P}_2 + \mathbf{P}_0 - w_{02} \mathbf{n}_2), & \mathbf{c}_{201} &= \frac{1}{3}(2\mathbf{P}_0 + \mathbf{P}_2 - w_{20} \mathbf{n}_0), \\ \mathbf{c}_{111} &= \frac{1}{4}(\mathbf{c}_{210} + \mathbf{c}_{201} + \mathbf{c}_{120} + \mathbf{c}_{021} + \mathbf{c}_{102} + \mathbf{c}_{012}) - \frac{1}{6}(\mathbf{P}_0 + \mathbf{P}_1 + \mathbf{P}_2), \end{aligned}$$

where

$$w_{\ell_1 \ell_2} := \langle \mathbf{P}_{\ell_1} - \mathbf{P}_{\ell_2}, \mathbf{n}_{\ell_2} \rangle,$$

then we call \mathbf{p} a *PN triangle*. The control point \mathbf{c}_{210} is a projection of the point $1/3(2\mathbf{P}_0 + \mathbf{P}_1)$ on the plane, defined by the point \mathbf{P}_0 and the normal \mathbf{n}_0 . Similar geometric descriptions hold for other boundary control points. The point \mathbf{c}_{111} is defined by the same formula as interior control coefficient of a non-parametric cubic interpolant which preserves quadratic functions [26].

5.2 Boundary Curves

A boundary curve \mathbf{b} of a patch that satisfies interpolation conditions (5.1) is not unique. Among all feasible curves we would like to choose one with small curvature. Therefore, we will minimise a generalised strain energy functional ψ_ω in (4.3).

Let us analyse the construction of the boundary curves in more detail. Suppose that data points $\mathbf{P}_0, \mathbf{P}_1$ and the corresponding normals $\mathbf{n}_0, \mathbf{n}_1$ are prescribed. Let us denote $\Delta\mathbf{P} := \mathbf{P}_1 - \mathbf{P}_0$. We can w.l.o.g. presume that v_1 and v_2 are the adjoined domain vertices of \mathbf{b} . Since the boundary curve between points \mathbf{P}_0 and \mathbf{P}_1 is a cubic Bézier curve, it can be written as $\mathbf{b}(t) := \sum_{i+j=3} \mathbf{c}_{ij0} B_{ij0}^3(v)$, where $v = (1-t, t, 0)$, $t \in [0, 1]$. From interpolation conditions (5.1) it follows that the control points of the curve can be written in the form

$$\begin{aligned} \mathbf{c}_{300} &= \mathbf{P}_0, & \mathbf{c}_{210} &= \mathbf{P}_0 + \hat{\alpha}_0 \mathbf{d}_0, \\ \mathbf{c}_{030} &= \mathbf{P}_1, & \mathbf{c}_{120} &= \mathbf{P}_1 - \hat{\alpha}_1 \mathbf{d}_1, \end{aligned} \tag{5.2}$$

where unit vectors $\mathbf{d}_0, \mathbf{d}_1$ lie in tangent planes with normals \mathbf{n}_0 and \mathbf{n}_1 , respectively, and $\hat{\alpha}_0, \hat{\alpha}_1 > 0$. Similar formulae can be obtained for other two boundary curves of a patch. For convenience with notations in the previous chapter let $\hat{\alpha}_\ell =: 1/3\alpha_\ell$. We would like to find admissible coefficients α_0, α_1 and tangents $\mathbf{d}_0, \mathbf{d}_1$ that minimise the strain energy functional

$$\psi_\omega(\alpha_0, \alpha_1, \mathbf{d}_0, \mathbf{d}_1) = \frac{1}{\omega + 2} \left(\|\ddot{\mathbf{b}}(0)\|^2 + \omega \left\| \ddot{\mathbf{b}} \left(\frac{1}{2} \right) \right\|^2 + \|\ddot{\mathbf{b}}(1)\|^2 \right)$$

of the curve. If we fix the tangents, then the problem translates to the minimisation problem, solved in the previous chapter and the optimal coefficients are (4.5).

To find optimal boundary curves that satisfy conditions (5.2) we need to use the optimal α_0, α_1 in the functional ψ_ω and minimise it over all admissible tangent directions \mathbf{d}_0 and \mathbf{d}_1 . First, let us find admissible tangent vectors that minimise the functional ψ_{16} .

Lemma 5.1. *Let points $\mathbf{P}_0, \mathbf{P}_1$ and normals $\mathbf{n}_0, \mathbf{n}_1$ satisfy $\angle(\Delta\mathbf{P}, \mathbf{n}_\ell) \in (0, \pi)$, $\ell = 0, 1$. Then the minimum of the functional ψ_{16} ,*

$$\min_{\alpha_0, \alpha_1, \mathbf{d}_0, \mathbf{d}_1} \psi_{16}(\alpha_0, \alpha_1, \mathbf{d}_0, \mathbf{d}_1),$$

is reached if \mathbf{d}_0 and \mathbf{d}_1 are projections of $\Delta\mathbf{P}$ on tangent planes, defined by $\mathbf{P}_0, \mathbf{n}_0$ and $\mathbf{P}_1, \mathbf{n}_1$, respectively, and α_0, α_1 satisfy the equations (4.9).

Proof. For $\omega = 16$, the expression (4.7) is simplified to

$$\psi_{16}(\alpha_0, \alpha_1, \mathbf{d}_0, \mathbf{d}_1) = 2 [2\|\Delta\mathbf{P}\|^2 - 2\langle\Delta\mathbf{P}, \mathbf{d}_0\rangle\alpha_0 - 2\langle\Delta\mathbf{P}, \mathbf{d}_1\rangle\alpha_1 + \alpha_0^2 + \alpha_1^2]. \quad (5.3)$$

By inserting optimal coefficients α_0, α_1 from (4.9) into (5.3), we obtain

$$\psi_{16}(\mathbf{d}_0, \mathbf{d}_1) = 2 [2\|\Delta\mathbf{P}\|^2 - \langle\Delta\mathbf{P}, \mathbf{d}_0\rangle^2 - \langle\Delta\mathbf{P}, \mathbf{d}_1\rangle^2]$$

and the result of the lemma follows straightforwardly from properties of projections. \square

Therefore the optimal tangent vector \mathbf{d}_0 is a projection of the vector $\Delta\mathbf{P}$ on the tangent plane defined by $\mathbf{P}_0, \mathbf{n}_0$ and can be obtained as

$$\begin{aligned} \hat{\mathbf{d}}_0 &:= \Delta\mathbf{P} - w_{10} \mathbf{n}_0, \\ \mathbf{d}_0 &:= \hat{\mathbf{d}}_0 / \|\hat{\mathbf{d}}_0\|, \end{aligned} \quad (5.4)$$

and similarly for \mathbf{d}_1 .

PN triangles produce boundary curves that minimise the strain energy functional ψ_{16} .

Theorem 5.2. *Let points $\mathbf{P}_0, \mathbf{P}_1$ and normals $\mathbf{n}_0, \mathbf{n}_1$ satisfy $\angle(\Delta\mathbf{P}, \mathbf{n}_\ell) \in (0, \pi)$, $\ell = 1, 2$. Then the corresponding boundary curve of the interpolating PN triangle minimises the approximate strain energy functional ψ_{16} .*

Proof. Let us show that the minimisation of the functional ψ_{16} over all feasible parameters $\alpha_0, \alpha_1, \mathbf{d}_0, \mathbf{d}_1$ results in a boundary curve of the PN triangle. From Lemma 5.1 it follows that the boundary curve of the PN triangle has the optimal tangent vectors. Let us verify that the curves have the same inner control points. By using the formulae (5.4) and the relation

$$\|\hat{\mathbf{d}}_0\|^2 = \|\Delta\mathbf{P}\|^2 - w_{10}^2 = \langle\Delta\mathbf{P}, \Delta\mathbf{P} - w_{10}\mathbf{n}_0\rangle = \langle\Delta\mathbf{P}, \hat{\mathbf{d}}_0\rangle,$$

the PN triangle control point \mathbf{c}_{210} can be written as

$$\begin{aligned} \mathbf{c}_{210} &= \frac{1}{3}(2\mathbf{P}_0 + \mathbf{P}_1 - w_{10}\mathbf{n}_0) = \mathbf{P}_0 + \frac{1}{3}(\Delta\mathbf{P} - w_{10}\mathbf{n}_0) = \mathbf{P}_0 + \frac{1}{3}\|\hat{\mathbf{d}}_0\|\mathbf{d}_0 \\ &= \mathbf{P}_0 + \frac{1}{3}\frac{\langle\Delta\mathbf{P}, \hat{\mathbf{d}}_0\rangle}{\|\hat{\mathbf{d}}_0\|}\mathbf{d}_0 = \mathbf{P}_0 + \frac{1}{3}\langle\Delta\mathbf{P}, \mathbf{d}_0\rangle\mathbf{d}_0. \end{aligned}$$

In the last line, the point is written in the form (4.8) with the optimal coefficient (4.9). Similar expression can be obtained for \mathbf{c}_{120} . Thus the boundary curve of the PN triangle coincides with the optimal curve obtained by the minimisation of the functional ψ_{16} . \square

5 Hermite Interpolation by Cubic Patches with Small Willmore Energy

Finding admissible $\mathbf{d}_0, \mathbf{d}_1$ that minimise the general functional $\psi_\omega, \omega \neq 16$, is a harder task. By inserting the optimal coefficients α_0, α_1 (4.5) into ψ_ω , it can be written as

$$\psi_\omega(\mathbf{d}_0, \mathbf{d}_1) = \frac{72}{\omega + 2} \left(\|\Delta \mathbf{P}\|^2 - \frac{18((\omega + 20)(A^2 + B^2) + 2(\omega - 16)ABC)}{(\omega + 20)^2 - (\omega - 16)^2 C^2} \right), \quad (5.5)$$

where $A := \langle \Delta \mathbf{P}, \mathbf{d}_0 \rangle$, $B := \langle \Delta \mathbf{P}, \mathbf{d}_1 \rangle$ and $C := \langle \mathbf{d}_0, \mathbf{d}_1 \rangle$.

Let $\mathbf{n}_0, \mathbf{n}_1$ and $\Delta \mathbf{P}$ be non-coplanar vectors. Since vectors $\mathbf{n}_0 \times \Delta \mathbf{P}, \mathbf{n}_1 \times \Delta \mathbf{P}, \Delta \mathbf{P}$ form a basis in \mathbb{R}^3 , tangent vectors can be written as

$$\begin{aligned} \mathbf{d}_0 &= \alpha_1 \mathbf{n}_0 \times \Delta \mathbf{P} + \alpha_2 \mathbf{n}_1 \times \Delta \mathbf{P} + \alpha_3 \Delta \mathbf{P}, \\ \mathbf{d}_1 &= \beta_1 \mathbf{n}_0 \times \Delta \mathbf{P} + \beta_2 \mathbf{n}_1 \times \Delta \mathbf{P} + \beta_3 \Delta \mathbf{P}, \end{aligned}$$

for some scalars α_ℓ, β_ℓ . If we use the dot product of the first equation and \mathbf{n}_0 , and of the second equation and \mathbf{n}_1 , we obtain

$$\begin{aligned} \alpha_2 &= -\alpha_3 \frac{\langle \Delta \mathbf{P}, \mathbf{n}_0 \rangle}{[\mathbf{n}_1, \Delta \mathbf{P}, \mathbf{n}_0]}, \\ \beta_1 &= -\beta_3 \frac{\langle \Delta \mathbf{P}, \mathbf{n}_1 \rangle}{[\mathbf{n}_0, \Delta \mathbf{P}, \mathbf{n}_1]}. \end{aligned} \quad (5.6)$$

Here $[\bullet, \bullet, \bullet]$ denotes the mixed product of vectors. Let us define data constants

$$\begin{aligned} C_1 &= \|\mathbf{n}_0 \times \Delta \mathbf{P}\|^2, & C_2 &= \langle \mathbf{n}_0 \times \Delta \mathbf{P}, \mathbf{n}_1 \times \Delta \mathbf{P} \rangle, \\ C_3 &= \|\mathbf{n}_1 \times \Delta \mathbf{P}\|^2, & C_4 &= \|\Delta \mathbf{P}\|^2. \end{aligned}$$

Then α_1 and β_2 are the solutions of the quadratic equations $\|\mathbf{d}_0\| = 1$ and $\|\mathbf{d}_1\| = 1$, respectively,

$$\begin{aligned} \alpha_1^\pm &= \frac{-2\alpha_2 C_2 \pm \sqrt{4\alpha_2^2 C_2^2 - 4C_1(\alpha_2^2 C_3 + \alpha_3^2 C_4 - 1)}}{2C_1}, \\ \beta_2^\pm &= \frac{-2\beta_1 C_2 \pm \sqrt{4\beta_1^2 C_2^2 - 4C_3(\beta_1^2 C_1 + \beta_3^2 C_4 - 1)}}{2C_3}. \end{aligned} \quad (5.7)$$

By inserting α_1^- and β_2^- into the functional (5.5), we obtain

$$\psi_\omega(\alpha_3, \beta_3) = \frac{72}{\omega + 2} \left(\|\Delta \mathbf{P}\|^2 - \frac{18C_1 C_3 C_4^2 ((\omega + 20)C_1 C_3 (a_3^2 + b_3^2) + 2(\omega - 16)q_3 a_3 b_3)}{(\omega + 20)^2 C_1^2 C_3^2 - (\omega - 16)^2 q_3^2} \right),$$

where

$$\begin{aligned} q_1 &:= \sqrt{b_3^2 C_2^2 K_2^2 - C_3 (b_3^2 (C_4 + C_1 K_2^2) - 1)}, \\ q_2 &:= \sqrt{a_3^2 C_2^2 K_1^2 - C_1 (a_3^2 (C_4 + C_3 K_1^2) - 1)}, \\ q_3 &:= a_3 (b_3 (C_2^3 K_1 K_2 + C_1 C_3 (C_4 - C_2 K_1 K_2)) + (C_2^2 - C_1 C_3) K_1 q_1) \\ &\quad + ((C_2^2 - C_1 C_3) K_2 b_3 + C_2 q_1) q_2, \\ K_1 &:= -\langle \Delta \mathbf{P}, \mathbf{n}_0 \rangle / [\mathbf{n}_1, \Delta \mathbf{P}, \mathbf{n}_0], \\ K_2 &:= -\langle \Delta \mathbf{P}, \mathbf{n}_1 \rangle / [\mathbf{n}_0, \Delta \mathbf{P}, \mathbf{n}_1]. \end{aligned}$$

Note that it is not necessary to analyse the functional with different signs in (5.7) since all four cases are symmetric. Each case can be transformed to another by using reflections about the planes $\alpha_3 = 0$ and $\beta_3 = 0$.

The domains for α_3 and β_3 are obtained from (5.7),

$$\alpha_3^2 \leq \frac{C_1[\mathbf{n}_1, \Delta\mathbf{P}, \mathbf{n}_0]^2}{C_1 C_4[\mathbf{n}_1, \Delta\mathbf{P}, \mathbf{n}_0]^2 + \langle \Delta\mathbf{P}, \mathbf{n}_0 \rangle^2 (C_1 C_3 - C_2^2)} \leq \frac{1}{\|\Delta\mathbf{P}\|^2},$$

$$\beta_3^2 \leq \frac{C_3[\mathbf{n}_0, \Delta\mathbf{P}, \mathbf{n}_1]^2}{C_3 C_4[\mathbf{n}_0, \Delta\mathbf{P}, \mathbf{n}_1]^2 + \langle \Delta\mathbf{P}, \mathbf{n}_1 \rangle^2 (C_1 C_3 - C_2^2)} \leq \frac{1}{\|\Delta\mathbf{P}\|^2}.$$

The minimum of the functional ψ_ω can be computed by solving the nonlinear system $\partial\psi_\omega/\partial\alpha_3 = \partial\psi_\omega/\partial\beta_3 = 0$ or by applying an appropriate minimisation technique (the gradient method, e.g.). The optimal α_3 and β_3 uniquely determine the optimal tangent vectors \mathbf{d}_0 and \mathbf{d}_1 .

Minimisation algorithms for computing the optimal tangent directions can be combined with a homotopy approach. Suppose we want to compute the optimal directions for the final parameter ω_f . From Lem. 5.1 we obtain the optimal directions for the initial parameter $\omega_s = 16$. Since the energy functional ψ_ω is a continuous function of its parameters, it is reasonable to expect that the optimal directions for perturbed ω are close to the ones for ω_s . Thus the optimal directions for perturbed ω can be computed by some simple iterative method, e.g. Newton's method for the gradient of ψ_ω , and by taking the optimal vectors for ω_s as an initial parameter. By gradually changing the parameter ω and computing new local minimum for every step of iteration we can obtain the optimal directions for every final parameter ω_f . The homotopic transformation of the optimal curve for ω_s to the optimal one for ω_f is presented as Alg. 1. The parameter ω is changing by a constant factor in each of m iteration steps.

Algorithm 1 Construction of optimal tangents $\mathbf{d}_0, \mathbf{d}_1$ by using homotopy.

Input: $\psi_\omega, \omega_s, \omega_f, \{\mathbf{d}_0, \mathbf{d}_1\}$ (the initial parameter), m

Output: $\{\mathbf{d}_0, \mathbf{d}_1\}$

$\omega = \omega_s$

for $j = 1, 2, \dots, m$ **do**

$\omega = \omega + (\omega_f - \omega_s)/m$

 find local minimum of ψ_ω for initial vectors $\mathbf{d}_0, \mathbf{d}_1$

 update vectors $\mathbf{d}_0, \mathbf{d}_1$

end for

In Fig. 5.1, optimal boundary curves for different parameters ω are presented. In the top left figure, where the tangent planes are almost in the horizontal position, the optimal curves are practically indistinguishable. In the following examples where the data are taken from more diverse surfaces, bigger differences between the curves can be seen. Curves for $\omega = 0$ produce the most visually pleasant round shapes. By increasing the value of the parameter, the curves tend to be more flat.

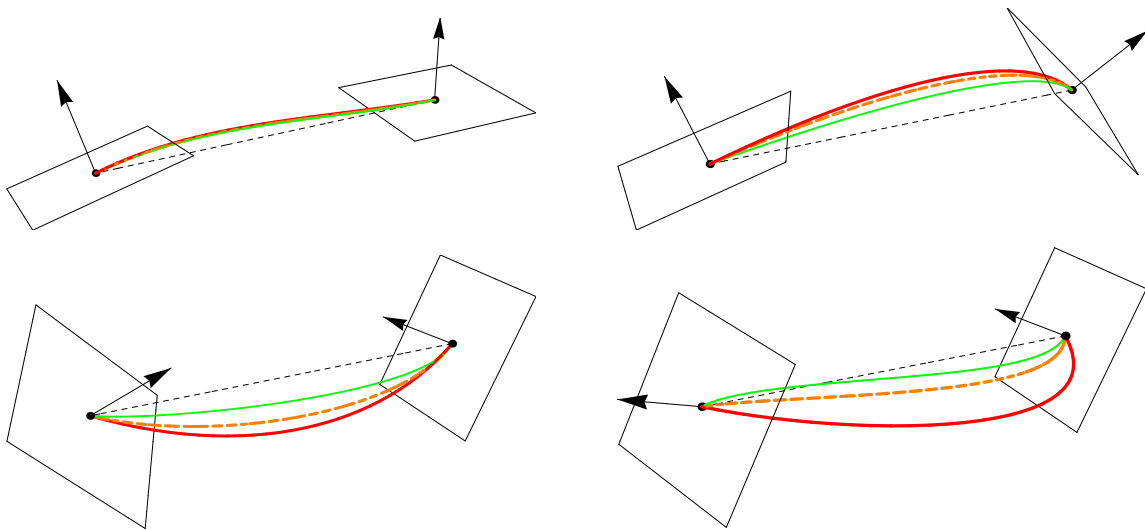


Figure 5.1: Optimal boundary curves for ψ_ω , $\omega = 0, 4, 16$, are interpolating different tangent planes. They are represented by red, orange and green curves, respectively.

5.3 Interior Control Point and Approximate Willmore Energy

Let points $\mathbf{P}_0, \mathbf{P}_1, \mathbf{P}_2$, normals $\mathbf{n}_0, \mathbf{n}_1, \mathbf{n}_2$ and boundary control points of a Bézier patch \mathbf{p} be fixed. Presume that the normals point in the same half-space, defined by $\mathbf{P}_0, \mathbf{P}_1, \mathbf{P}_2$. We are left to set the remaining point \mathbf{c}_{111} so that Willmore energy of \mathbf{p} will be small. Let us first presume that the optimal \mathbf{c}_{111} lie on a line that is parallel to an average of normals $\mathbf{n}_0, \mathbf{n}_1, \mathbf{n}_2$ and intersects $\mathbf{p}^\triangleright$ at its barycenter,

$$\mathbf{c}_{111}(r) := \frac{\sum_{\ell=0}^2 \mathbf{n}_\ell}{\|\sum_{\ell=0}^2 \mathbf{n}_\ell\|} r + \frac{1}{3} \sum_{\ell=0}^2 \mathbf{P}_\ell, \quad r \in \mathbb{R}. \quad (5.8)$$

Let us use the standard notation for the first and the second fundamental form coefficients of the surface. They are defined as

$$\begin{aligned} E &:= \langle D_{u_1} \mathbf{p}, D_{u_1} \mathbf{p} \rangle, & L &:= \langle D_{u_1} D_{u_1} \mathbf{p}, \mathbf{n} \rangle, \\ F &:= \langle D_{u_1} \mathbf{p}, D_{u_2} \mathbf{p} \rangle, & M &:= \langle D_{u_1} D_{u_2} \mathbf{p}, \mathbf{n} \rangle, \\ G &:= \langle D_{u_2} \mathbf{p}, D_{u_2} \mathbf{p} \rangle, & N &:= \langle D_{u_2} D_{u_2} \mathbf{p}, \mathbf{n} \rangle. \end{aligned} \quad (5.9)$$

Note that all coefficients are functions of v . Recall that Willmore energy of \mathbf{p} is

$$\mathcal{W}(\mathbf{p}) = \frac{1}{4} \int_{\mathbf{p}} (\kappa_1 - \kappa_2)^2 dA,$$

where κ_ℓ are the principal curvatures of \mathbf{p} and dA is the area form of \mathbf{p} . The principal curvatures are the solutions of the quadratic equation

$$\det \left(\begin{bmatrix} L & M \\ M & N \end{bmatrix} - \kappa \begin{bmatrix} E & F \\ F & G \end{bmatrix} \right) = 0.$$

Simple calculus yields

$$\mathcal{W}(\mathbf{p}) = \frac{1}{4} \int_D f(v) dv,$$

where $D := \{v = (\alpha, \beta, 1 - \alpha - \beta) : \alpha \in [0, 1], \beta \in [0, 1 - \alpha]\}$ is the integration domain triangle and

$$f := \frac{G^2 L^2 - 4FGLM + (4F^2 - 2EG)LN + 4EGM^2 - 4EFMN + E^2 N^2}{(EG - F^2)^{3/2}}. \quad (5.10)$$

Let us use the notation $f(v; r)$ since f only depends on the barycentric point v and parameter r once all the boundary control points of the patch are fixed. The optimal r could be obtained by solving the equation

$$\frac{d}{dr} \mathcal{W}(\mathbf{p}(r)) = \frac{1}{4} \frac{d}{dr} \int_D f(v; r) dv = 0.$$

The first obstacle is that the integral cannot be calculated analytically in general. A common approach is to approximate the integral with an appropriate quadrature formula. In order to obtain a minimisation problem where a unique solution is easily computed, the points of discretisation have to be carefully chosen.

Let us define trapezoidal approximation of \mathcal{W} on four points. Let

$$v_c := \frac{1}{3} (v_1 + v_2 + v_3)$$

denote the triangle barycenter. We obtain

$$\mathcal{W}(\mathbf{p}) = \frac{1}{4} \int_D f dv \approx \frac{1}{4} A_D \bar{f} = \frac{1}{8} \frac{\bar{f}_1 + \bar{f}_2 + \bar{f}_3}{3}, \quad (5.11)$$

where A_D is the area of the triangle D and \bar{f}_ℓ is mean value of f at vertices $v_\ell, v_{\ell+1}, v_c$,

$$\bar{f}_\ell(r) = \frac{f(v_\ell; r) + f(v_{\ell+1}; r) + f(v_c; r)}{3}.$$

Here $v_4 := v_1$. A simplification of the right-hand side of (5.11) leads to *approximate Willmore energy functional*

$$\mathcal{W}_t(r) := \frac{1}{36} \sum_{\ell=1}^3 f(v_\ell; r) + \frac{1}{24} f(v_c; r). \quad (5.12)$$

Note that $\mathcal{W}_t \geq 0$ since $f \geq 0$.

Let us denote the Hermite interpolating patch that minimises \mathcal{W}_t and has boundary curves that minimise the functionals ψ_ω by $HI-\omega$.

Theorem 5.3. *The energy functional \mathcal{W}_t in (5.12) has a unique minimum.*

Proof. Let $v \in \{v_1, v_2, v_3\}$. It can easily be verified that all $D_{u_1}\mathbf{p}$, $D_{u_2}\mathbf{p}$, $D_{u_1}D_{u_1}\mathbf{p}$ and $D_{u_2}D_{u_2}\mathbf{p}$ are independent of r at v . Thus E, F, G, L, N are also independent of r at v . Since $D_{u_1}D_{u_2}\mathbf{p}(v)$ is linear in \mathbf{c}_{111} , it follows that $M(v)$ is linear in r . It can be seen from (5.10) that $f(v; r) = C_v r^2 + \mathcal{O}(r)$ and $C_v > 0$ since $EG > 0$.

It can easily be verified that $D_{u_1}\mathbf{p}$ and $D_{u_2}\mathbf{p}$ are independent of r at v_c . Thus the functions E, F, G are independent of r at v_c . Since the functions L, M, N are linear in r , it follows that $f(v_c; r)$ is a quadratic function of r .

Let us show that \mathcal{W}_t is not a linear nor a constant function. Energy \mathcal{W}_t can not be linear since $\mathcal{W}_t \geq 0$. Presume that \mathcal{W}_t is a constant function. Since $f(v_\ell; r) = C_{v_\ell} r^2 + \mathcal{O}(r)$, $C_{v_\ell} > 0$, it follows that $f(v_c; r) = C_{v_c} r^2 + \mathcal{O}(r)$, $C_{v_c} < 0$. Then $f(v_c; r)$ is negative for r large enough, a contradiction with the definition of f . Thus \mathcal{W}_t is a quadratic function and has a unique minimum at parabola's turning point. \square

To achieve better results we can take a quadrature rule on more than four points. In this case the optimal parameter r can only be obtained numerically, for instance by Newton's method on the derivative of f . The optimal r from the functional \mathcal{W}_t can then be regarded as a good initial parameter for the minimisation method.

As an example, let us sample the data from the function $g(x, y) = \sin((x + 1)y)$ (see Fig. 1.2) at points $(-1, -1)$, $(1, -1)$, $(0, 0)$ and construct our interpolant, based on various approximations of the energy functional. Let $\mathcal{W}^{(d)}$ denote a trapezoidal approximation of the Willmore energy functional on domain points $\{\mathbf{i}/d : |\mathbf{i}| = d\}$, written in barycentric coordinates (for instance, $\mathcal{W}^{(10)}$ is discretised in 66 domain points). Plots of functionals with different discretisations are presented in Fig. 5.2. Clearly, the minimum of the

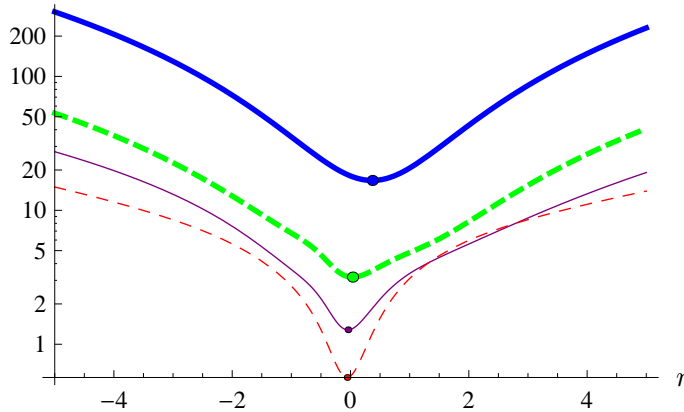


Figure 5.2: Discrete Willmore energy functionals \mathcal{W}_t , $\mathcal{W}^{(3)}$, $\mathcal{W}^{(5)}$, $\mathcal{W}^{(10)}$ are represented by a blue, green, purple and red curve, respectively.

functional \mathcal{W}_t is a good approximation of the minima of functionals defined on finer grids.

Now let us generalise the problem (5.8) by setting the control point $\mathbf{c}_{111} =: \mathbf{r}$ to be an arbitrary point in \mathbb{R}^3 and

$$\mathcal{W}_t(\mathbf{r}) := \frac{1}{36} \sum_{\ell=1}^3 f(v_\ell; \mathbf{r}) + \frac{1}{24} f(v_c; \mathbf{r}). \tag{5.13}$$

In the rest of the section we show that the energy functional (5.13) has a unique minimum at mild presumptions.

Lemma 5.4. *The function*

$$C(v) := \frac{2(G^2 - 2FG + 4F^2 - EG - 2EF + E^2)}{3(EG - F^2)^{3/2}}$$

is non-negative. Moreover, C is a positive function unless $E = G = 2F$ holds true.

Proof. The function C can be written as

$$C = \frac{2[(E - G)^2 + (E - 2F)(G - 2F)]}{3(EG - F^2)^{3/2}}. \quad (5.14)$$

The function $g(F) := (E - 2F)(G - 2F)$ has the minimum at $(E + G)/4$. Thus $g(F) \geq -(E - G)^2/4$ and

$$C(v) \geq \frac{(E - G)^2}{2(EG - F^2)^{3/2}} \geq 0 \quad (5.15)$$

for all v . The last claim of the lemma follows straightforwardly from (5.14) and (5.15). \square

Let \mathbf{n}_c be the normal to the surface at $\mathbf{p}(v_c)$. Note that \mathbf{n}_c does not depend on the point \mathbf{r} . Let $B := [\mathbf{n}_0 \ \mathbf{n}_1 \ \mathbf{n}_2 \ \mathbf{n}_c]^T$.

Theorem 5.5. *The discrete energy \mathcal{W}_t in (5.13) has a minimum. If the matrix B has a full rank, then the minimum of \mathcal{W}_t is unique iff vectors $\mathbf{n}_0, \mathbf{n}_1, \mathbf{n}_2$ are linearly independent or the equation $E = G = 2F$ is not satisfied at v_c .*

Proof. The only fundamental coefficient that depends on $\mathbf{r} = (x, y, z)$ at v_ℓ , $\ell = 1, 2, 3$, is M . At v_c all coefficients of the first fundamental form are independent of the parameter \mathbf{r} . Thus the energy functional \mathcal{W}_t can be written as

$$\begin{aligned} \mathcal{W}_t(\mathbf{r}) &= \frac{1}{36} \sum_{\ell=1}^3 [a_\ell M^2(v_\ell) + b_\ell M(v_\ell) + c_\ell] + \frac{1}{24} \sum_{\ell=4}^9 a_\ell K_\ell(v_c) \\ &= \sum_{\ell=1}^3 \hat{a}_\ell \langle \mathbf{n}_{\ell-1}, \mathbf{r} \rangle^2 + C(v_c) \langle \mathbf{n}_c, \mathbf{r} \rangle^2 + \mathcal{O}(\mathbf{r}), \end{aligned}$$

where $a_\ell, b_\ell, c_\ell, \hat{a}_\ell$ are constants and

$$K_\ell := [L^2 \quad LM \quad LN \quad M^2 \quad MN \quad N^2]_{\ell-3}, \quad \ell = 4, 5, \dots, 9.$$

A straightforward calculation of the Hessian of \mathcal{W}_t leads to

$$H(\mathcal{W}_t) = \begin{bmatrix} \mathcal{W}_{t,xx} & \mathcal{W}_{t,xy} & \mathcal{W}_{t,xz} \\ \mathcal{W}_{t,yx} & \mathcal{W}_{t,yy} & \mathcal{W}_{t,yz} \\ \mathcal{W}_{t,zx} & \mathcal{W}_{t,zy} & \mathcal{W}_{t,zz} \end{bmatrix} = 2B^T A B, \quad (5.16)$$

5 Hermite Interpolation by Cubic Patches with Small Willmore Energy

where $A = \text{diag}(\hat{a}_1, \hat{a}_2, \hat{a}_3, C(v_c))$. Constants \hat{a}_ℓ are positive since

$$\frac{4EG}{(EG - F^2)^{3/2}}(v_\ell) > 0, \quad \ell = 1, 2, 3,$$

and $C(v_c)$ is non-negative by Lemma 5.4. Let $\mathbf{x} \in \mathbb{R}^3$ be arbitrary. It follows

$$\mathbf{x}^T H \mathbf{x} = 2 \|A^{1/2} B \mathbf{x}\|_2^2 \geq 0,$$

hence H is semi-positive definite and \mathcal{W}_t has a minimum.

Let B have the full rank. The Hessian H is positive definite iff $\det H > 0$. By using the Cauchy-Binet formula on the right-hand side of (5.16), the determinant of H can be written in the form

$$\det H = 8 \hat{a}_1 \hat{a}_2 \hat{a}_3 (\det [\mathbf{n}_0 \quad \mathbf{n}_1 \quad \mathbf{n}_2])^2 + 8 \sum_{1 \leq \ell_1 < \ell_2 \leq 3} \hat{a}_{\ell_1} \hat{a}_{\ell_2} C(v_c) (\det [\mathbf{n}_{\ell_1-1} \quad \mathbf{n}_{\ell_2-1} \quad \mathbf{n}_c])^2.$$

The determinant is positive iff presumptions of the theorem hold true. Since \mathcal{W}_t has a unique minimum iff H is positive definite, the proof is complete. \square

For practical applications, it is advised to minimise \mathcal{W}_t in (5.12) prior to (5.13). The shape of a patch that minimises the latter functional does not outweigh a more expensive minimisation.

5.4 Algorithm

Let us summarise the main steps of our interpolation scheme. The procedure is presented as Alg. 2. In the algorithm we use the same parameter ω for all boundary curves. Alternatively, we could straightforwardly implement different shape parameter ω for every boundary curve.

Algorithm 2 Hermite interpolation with small Willmore energy, HI- ω scheme

Input: $\{\mathbf{P}_\ell, \mathbf{n}_\ell\}_\ell$ (sets of points and the normal vectors), $\mathbf{s}^\triangleright$ (spatial triangulation), ω

Output: $\{\mathbf{p}_\ell\}_\ell$ (set of triangular patches)

for every patch \mathbf{p}_ℓ **do**

for every boundary curve **do**

 set the tangent directions by (5.4)

if $\omega \neq 16$ **then**

 compute the directions from Alg. 1

end if

 compute boundary control points from (5.2) and (4.5)

end for

 obtain the interior point \mathbf{c}_{111} by minimising the functional \mathcal{W}_t in (5.12) or (5.13)

end for

Chapter 6

Geometric Interpolation by Bivariate Parametric Macro-Elements

In this chapter, Hermite interpolation by two types of parametric C^1 macro-elements on triangulations is considered. Cubic triangular splines interpolate points and the corresponding tangent planes at domain vertices and approximate tangent planes at midpoints of domain edges. Quintic splines additionally interpolate normal curvature forms at the vertices. Control points of the interpolants are constructed in two steps. In the first one, uniformly distributed control points of a linear spline interpolant are projected to the interpolation planes. To satisfy smoothness conditions between patches, a correction of control points is obtained as the solution of a least square minimisation. The construction of the approximant is local and fast.

6.1 Motivation: Non-Parametric Macro-Elements

Constructions of parametric macro-elements will be derived from constructions of the standard functional counterparts. In [51], a *nodal minimal determining set*, i.e., a set of Hermite data that uniquely determines an interpolating spline, is constructed for every macro-element space. The conditions involve interpolation of partial and directional derivatives of a function. The following two interpolation problems will be tackled in the parametric setting.

Let D_x and D_y be standard partial derivative operators in x and y direction. For an edge $e = (v_0, v_1) \in \mathcal{E}$, let $v_e := 1/2(v_0 + v_1)$ and let e' be a normalised vector that is obtained by rotating e for $\pi/2$ in positive direction. Let $D_{e'}$ be directional derivative operator in the direction e' .

Theorem 6.1 ([51], Thm. 6.3.). *For sets of interpolation data $\{z_v, z_v^{(x)}, z_v^{(y)}, z_v^{(xx)}, z_v^{(xy)}, z_v^{(yy)} \in \mathbb{R}\}$, $v \in \mathcal{V}$, and $\{z_e \in \mathbb{R}\}$, $e \in \mathcal{E}$, there exists a unique spline $s \in \mathcal{S}_5^{1,2}(\Delta)$ that solves the following interpolation problem:*

$$\begin{aligned} s(v) &= z_v, \\ D_x s(v) &= z_v^{(x)}, & D_y s(v) &= z_v^{(y)}, & v &\in \mathcal{V}, \\ D_x D_x s(v) &= z_v^{(xx)}, & D_x D_y s(v) &= z_v^{(xy)}, & D_y D_y s(v) &= z_v^{(yy)}, \\ D_{e'} s(v_e) &= z_e, & e &\in \mathcal{E}. \end{aligned}$$

Theorem 6.2 ([51], Thm. 6.7.). *Let \mathcal{V} and \mathcal{E} be sets of vertices and edges of the original triangulation Δ . For sets of interpolation data $\{z_v, z_v^{(x)}, z_v^{(y)} \in \mathbb{R}\}$, $v \in \mathcal{V}$, and $\{z_e \in \mathbb{R}\}$, $e \in \mathcal{E}$, there exists a unique spline $s \in \mathcal{S}_3^{1,1}(\Delta_{CT})$ that solves the following interpolation problem:*

$$\begin{aligned} s(v) &= z_v, & v \in \mathcal{V}, \\ D_x s(v) &= z_v^{(x)}, & D_y s(v) &= z_v^{(y)}, \\ D_{e'} s(v_e) &= z_e, & e \in \mathcal{E}. \end{aligned}$$

Though the following two Hermite schemes can be straightforwardly generalised to the parametric case, that approach is not practical since the interpolation data would consist of a large amount of parametrisation depended data, such as derivatives for every component of the spline $\mathbf{s} = (s_x, s_y, s_z)$. Instead, we would like a method that interpolates geometric data that are more appropriate in parametric spline constructions.

6.2 Interpolation Conditions and Minimising Cells

In this section we will investigate how to determine control points of interpolant \mathbf{s} that are related to the following three types of interpolation constraints. At every vertex, we will interpolate a tangent plane and the corresponding normal curvature form. The conditions will replace the interpolation of the first and the second derivatives of a function in the non-parametric setting (see § 6.1). At midpoints of edges we will approximate tangent planes. The conditions will be a replacement of the directional derivatives interpolation of a function. Since the geometric interpolation conditions will not set the control points \mathbf{c}_i uniquely, we will use the remaining degrees of freedom to approximate uniform distribution of control points of a linear spline $\mathbf{s}^\triangleright$ of polynomial degree d .

The control points of \mathbf{s} must satisfy given interpolation and smoothness conditions. Therefore the construction of control points will be split into two parts. Firstly, control points of the linear spline will be projected onto interpolation planes with an oblique projection. The obtained projected points \mathbf{d}_i will not be feasible with respect to the mutual continuity conditions. Hence, corrections of points, obtained as the solution of a least square minimisation, will be applied.

The constructions in this section will be carried out for a general polynomial degree d . The results will be applied in the next section for $d = 3, 5$. We will need the following definitions of sets of control points.

Definition 6.3. *Let $\mathbf{p} = \sum \mathbf{c}_i B_i^d$ be a patch defined on triangle $\tau = (v_0, v_1, v_2)$. A set of control points*

$$\mathcal{D}_m(v_0, \mathbf{p}) := \{\mathbf{c}_i : |\mathbf{i}| = d, i \geq d - m\}$$

is a disk of \mathbf{p} with center v_0 and radius m , $0 \leq m \leq d$. Similarly we define disks for v_1 and v_2 . If $v_3 \neq v_\ell$, $\ell = 0, 1, 2$, then $\mathcal{D}_m(v_3, \mathbf{p}) := \{\}$.

A disk with center v and radius m is

$$\mathcal{D}_m(v) := \bigcup_{\tau \in \Delta} \left\{ \mathbf{c}_i^{[\tau]} : \mathbf{c}_i^{[\tau]} \in \mathcal{D}_m(v, \mathbf{p}^{[\tau]}) \right\}.$$

A ring with center v and radius m , $1 \leq m \leq d$, is defined as

$$\mathcal{R}_m(v) := \mathcal{D}_m(v) \setminus \mathcal{D}_{m-1}(v).$$

Definition 6.4. Let $\mathbf{p} = \sum \mathbf{c}_i B_i^d$ be a patch defined on triangle $\tau = (v_0, v_1, v_2)$. For odd d and edge $e = (v_0, v_1)$ let

$$\mathcal{D}_e(\mathbf{p}) := \{\mathbf{c}_{(d-1)/2, (d-1)/2, 1}\}$$

be the control point associated to the edge e . Similarly we define the associated points for other two edges. If τ does not contain an edge \tilde{e} , $\mathcal{D}_{\tilde{e}}(\mathbf{p}) := \{\}$.

For $e \in \mathcal{E}$ we define a set of associated control points

$$\mathcal{D}_e := \bigcup_{\tau \in \Delta} \left\{ \mathbf{c}_i^{[\tau]} : \mathbf{c}_i^{[\tau]} \in \mathcal{D}_e(\mathbf{p}^{[\tau]}) \right\}.$$

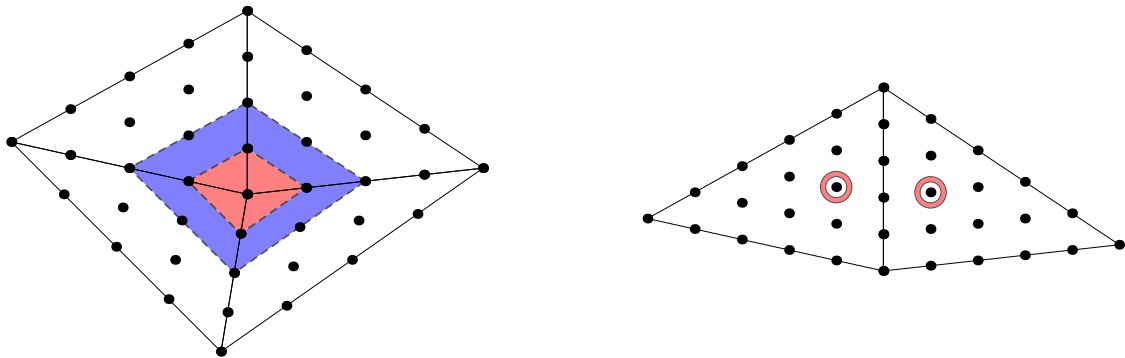


Figure 6.1: The sets $\mathcal{D}_1(v)$ and $\mathcal{D}_2(v)$ are represented with black dots in red and red+blue area, respectively (left). The set \mathcal{D}_e for an interior edge e consists of two control points, marked with red borders (right).

The set \mathcal{D}_e consist of one or two control points. An example of sets $\mathcal{D}_m(v)$ and \mathcal{D}_e is shown in Fig. 6.1. In the remainder of this section we will discuss how to construct control points for three types of sets, $\mathcal{D}_1(v)$ and $\mathcal{R}_2(v)$ for $v \in \mathcal{V}$, and \mathcal{D}_e , $e \in \mathcal{E}$. Because the conditions between sets for different vertices v and edges e will not overlap, the construction of macro-elements will be local.

6.2.1 Tangent Plane Interpolation and Minimising Cell for $\mathcal{R}_1(v)$

At every vertex $v \in \mathcal{V}$ we would like to interpolate a prescribed point \mathbf{P} and the associated tangent plane Π , defined by the point \mathbf{P} and a normal vector \mathbf{n} . To satisfy the first condition, the control point in $\mathcal{D}_0(v)$ must be equal to \mathbf{P} . To interpolate the plane Π , the constraints

$$\langle \mathbf{c}_i - \mathbf{P}, \mathbf{n} \rangle = 0, \quad \mathbf{c}_i \in \mathcal{R}_1(v), \quad (6.1)$$

must be satisfied. The points in $\mathcal{R}_1(v)$ are connected by smoothness conditions (see Thm. 2.2, page 13). Hence if we assign positions of control points in $\mathcal{D}_1(v, \mathbf{p}) \setminus \mathcal{D}_0(v, \mathbf{p})$

for some patch \mathbf{p} , then the rest in $\mathcal{R}_1(v)$ are uniquely determined by the C^1 continuity conditions. Therefore, the above restrictions give a 4-parametric family of control points.

Since the interpolation conditions are not sufficient to uniquely determine the set $\mathcal{D}_1(v)$, the remaining degrees of freedom will be used so that the points $\mathcal{R}_1(v)$ will be close to projected points, obtained from the points $\mathcal{R}_1^\triangleright(v)$ of the linear spline approximant. By applying this condition, the tangents of the boundary curves at \mathbf{P} will point in similar directions as the boundary curves of the linear spline. This is a desired property since the conditions imply small geodesic curvature of the patches.

Presume that points in the sets $\mathcal{R}_1(v)$ and $\mathcal{R}_1^\triangleright(v)$ are denoted by \mathbf{c}_ℓ and $\mathbf{c}_\ell^\triangleright$ for $\ell = 1, 2, \dots, n$, respectively. Let the elements in both sets have the same ordering that corresponds to ordering of vertices around the central vertex in a cell (see page 13, Fig. 2.1, right, and Fig. 6.2). Furthermore, let us presume geometric restrictions

$$(\mathbf{c}_\ell^\triangleright - \mathbf{P}) \nparallel \mathbf{n}, \quad \ell = 1, 2, \dots, n. \quad (6.2)$$

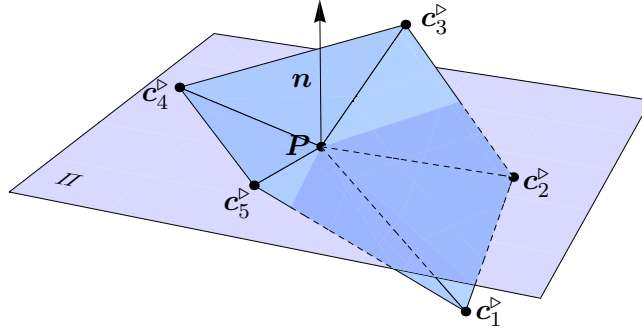


Figure 6.2: Control points in $\mathcal{R}_1^\triangleright(v)$.

To satisfy (6.1), the most straightforward approach would be to apply the orthogonal projection

$$\text{proj}_{\mathbf{P}, \Pi} := \bullet - \langle \bullet - \mathbf{P}, \mathbf{n} \rangle \mathbf{n}$$

on the points $\mathcal{R}_1^\triangleright(v)$ and set the resulting points as starting points for $\mathcal{R}_1(v)$. But the procedure does not give the best results since the projected points are often too close to \mathbf{P} and the corresponding patches tend to be too flat.

Instead of projecting in the direction \mathbf{n} , we propose a oblique projection with the property $(\mathbf{c}_\ell^\triangleright - \mathbf{P}) \perp (\mathbf{d}_\ell - \mathbf{c}_\ell^\triangleright)$ where \mathbf{d}_ℓ is a projected point of $\mathbf{c}_\ell^\triangleright$. The projection direction \mathbf{m}_ℓ is obtained by orthogonally projecting \mathbf{n} onto plane, orthogonal to $\mathbf{c}_\ell^\triangleright - \mathbf{P}$,

$$\mathbf{m}_\ell := \mathbf{n} - \frac{\langle \mathbf{c}_\ell^\triangleright - \mathbf{P}, \mathbf{n} \rangle}{\|\mathbf{c}_\ell^\triangleright - \mathbf{P}\|^2} (\mathbf{c}_\ell^\triangleright - \mathbf{P}). \quad (6.3)$$

The point $\mathbf{c}_\ell^\triangleright$ is projected onto Π in the direction \mathbf{m}_ℓ (see Fig. 6.3),

$$\mathbf{d}_\ell := \mathbf{c}_\ell^\triangleright - \frac{\langle \mathbf{c}_\ell^\triangleright - \mathbf{P}, \mathbf{n} \rangle}{\langle \mathbf{m}_\ell, \mathbf{n} \rangle} \mathbf{m}_\ell. \quad (6.4)$$

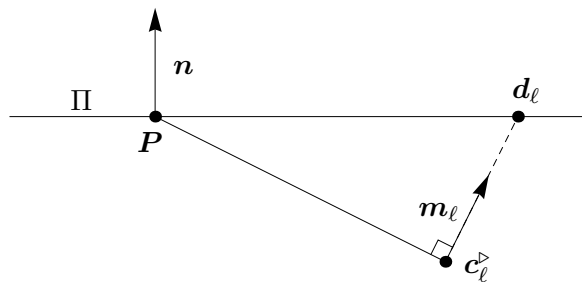


Figure 6.3: Point \mathbf{d}_ℓ is a projection of $\mathbf{c}_\ell^\triangleright$ onto Π .

The projected points are well defined since conditions (6.2) imply $\langle \mathbf{m}_\ell, \mathbf{n} \rangle \neq 0$, $\ell = 1, 2, \dots, n$. The obtained projection is a natural transference from the non-parametric case where control points are moved only in the direction orthogonally to the domain.

If the condition (6.2) is not fulfilled for some ℓ then the point $\mathbf{c}_\ell^\triangleright$ must be projected in a different way. For example, we could define that $\mathbf{d}_\ell - \mathbf{P}$ lies on the bisector of vectors $\mathbf{d}_{\ell-1} - \mathbf{P}$ and $\mathbf{d}_{\ell+1} - \mathbf{P}$ and its length is $\|\mathbf{d}_\ell - \mathbf{P}\| = 1/2 (\|\mathbf{d}_{\ell-1} - \mathbf{P}\| + \|\mathbf{d}_{\ell+1} - \mathbf{P}\|)$. A case where two consecutive indices $\ell, \ell + 1$ would not satisfy (6.2) cannot occur in practice.

If we would set $\mathbf{c}_\ell := \mathbf{d}_\ell$, $\ell = 1, 2, \dots, n$, a spline \mathbf{s} would interpolate the plane Π but would not be C^1 smooth in the neighbourhood of the point \mathbf{P} . Therefore, let us find an admissible set of control points \mathbf{c}_ℓ with respect to the smoothness conditions that is relatively close to the projected points \mathbf{d}_ℓ . We would like to solve the following least square minimisation problem

$$\min_{\{\mathbf{c}_1, \mathbf{c}_2\}} \varphi((\mathbf{c}_\ell)_{\ell=1}^n), \quad (6.5)$$

where the functional φ measures relative distances between the two sets of points,

$$\varphi((\mathbf{c}_\ell)_{\ell=1}^n) := \sum_{\ell=1}^n \frac{\|\mathbf{c}_\ell - \mathbf{d}_\ell\|^2}{\|\mathbf{d}_\ell - \mathbf{P}\|^2}. \quad (6.6)$$

Note that by Thm. 2.2 the control points \mathbf{c}_ℓ are connected by C^1 smoothness conditions at the vertex,

$$\mathbf{c}_\ell = \langle v_\ell(\tau_{\ell-2}), (\mathbf{P}, \mathbf{c}_{\ell-2}, \mathbf{c}_{\ell-1}) \rangle, \quad \ell \geq 3. \quad (6.7)$$

Here v_ℓ is the vertex that is associated to the point \mathbf{c}_ℓ and τ_ℓ the triangle that corresponds to the points $\mathbf{c}_\ell, \mathbf{c}_{\ell+1}$. The problem (6.5) can be written as a normal equation and it has a unique solution. We call the optimal set of points $\mathcal{R}_1(v)$ a *minimising cell*. An example of it is shown in Fig. 6.4.

Remark 6.5. *If a vertex $v \in \mathcal{V}$ is boundary, then the corresponding minimising cell influences the boundary curves of the spline \mathbf{s} . In this case, it is sometimes better to modify the minimisation problem (6.5) to enforce more control on the shape of boundary curves of the spline. Therefore, we could minimise the functional $\varphi((\mathbf{c}_1, \mathbf{c}_n))$ to obtain the desired tangents of boundary curves of \mathbf{s} at \mathbf{P} . An example is shown in Fig. 6.5.*

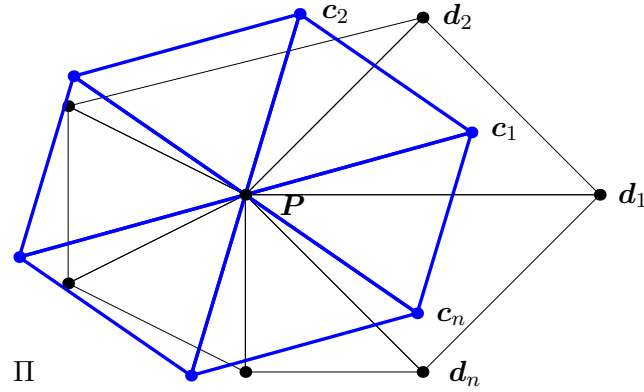


Figure 6.4: Points \mathbf{c}_ℓ of the minimising cell are determined in such a way that they are as close to points \mathbf{d}_ℓ as possible, i.e., they minimise the functional φ in (6.6). Here, all barycentric coordinates are $v_\ell(\tau_{\ell-2}) = (1, -1, 1)$.

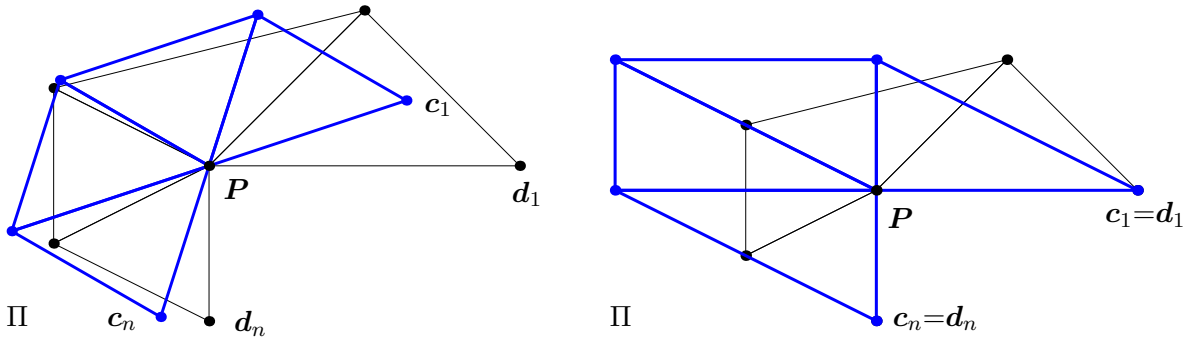


Figure 6.5: Two minimising cells at a boundary point \mathbf{P} . The obtained points \mathbf{c}_ℓ minimise $\varphi((\mathbf{c}_\ell)_{\ell=1}^n)$ (left) and $\varphi((\mathbf{c}_1, \mathbf{c}_n))$ (right).

Control points of the minimising cell satisfy the tangent plane interpolation conditions (6.1). Hence, the interpolation conditions are preserved after the correction of points.

Proposition 6.6. *Let $\mathcal{M} := \{\mathbf{c}_\ell\}_{\ell=1}^n$ be the minimising cell of $\mathcal{R}_1(v)$. Then the points of \mathcal{M} lie on the plane Π .*

Proof. We prove the proposition by a contradiction. Presume that the points \mathcal{M} do not lie on the plane Π . Let \mathcal{M}' denote a set of points \mathcal{M} that are projected orthogonally on the plane Π . It is easy to verify that the points of \mathcal{M}' are closer to the points $\{\mathbf{d}_\ell\}_{\ell=1}^n$ than points of \mathcal{M} and furthermore they satisfy the continuity constraints (6.7). Therefore \mathcal{M} is not the minimising cell. \square

The minimising cell must fulfil an additional requirement

$$\langle (\mathbf{c}_1 - \mathbf{P}) \times (\mathbf{c}_2 - \mathbf{P}), \mathbf{n} \rangle > 0$$

which ensures preservation of the surface orientation. If the minimisation (6.5) gives an inadmissible solution, a different approach for obtaining the points \mathbf{c}_ℓ should be applied (e.g., adding a penalty term for inadmissible orientation of points). However, an inadmissible solution rarely appears in practical applications.

6.2.2 Normal Curvature Interpolation and Minimising Cell for $\mathcal{R}_2(v)$

In this subsection we presume that the set of points $\mathcal{D}_1(v)$, $v \in \mathcal{V}$, is already fixed (e.g., it is determined by the procedure in §6.2.1) so that the spline \mathbf{s} interpolates a point \mathbf{P} at v and a tangent plane with a normal \mathbf{n} . The remaining points in $\mathcal{D}_2(v)$ will be used to interpolate a given *normal curvature form* at v . The form is described by a set

$$\{\mathbf{u}_1^*, \mathbf{u}_2^*, \kappa_1, \kappa_2\}, \quad (6.8)$$

where \mathbf{u}_ℓ^* and κ_ℓ are the principal directions and the corresponding normal curvatures of a surface at v . A well-known property from differential geometry states that the normal curvature $\kappa_n(\mathbf{u})$ of the spline \mathbf{s} in a direction \mathbf{u} , $\|\mathbf{u}\| = 1$, is

$$\kappa_n(\mathbf{u}) = \kappa_1 \langle \mathbf{u}, \mathbf{u}_1^* \rangle^2 + \kappa_2 \langle \mathbf{u}, \mathbf{u}_2^* \rangle^2.$$

In this subsection we will additionally presume that $\mathbf{s} \in C^2(v)$. The presumption will ensure the consistency of the curvature form of the neighbouring patches. Note that enforcing additional smoothness at vertices is a common approach in spline theory to overcome certain dimension problems or in some cases to ensure the full approximation order of the spline space [2, 12, 51].

Before dealing with the construction of control points, we need the following lemma that states the connection between the normal curvatures and the control points.

Lemma 6.7. *Fix a patch $\mathbf{p} = \sum \mathbf{c}_i B_i^d$ and two points $v_1 = (1, 0, 0)$, $v_2 = (0, 1 - \mu, \mu)$, $\mu \in [0, 1]$, written in barycentric coordinates. Let \mathbf{b} be a parametric curve, obtained as a restriction of \mathbf{p} to domain line $\{(1 - \lambda)v_1 + \lambda v_2 : \lambda \in [0, 1]\}$,*

$$\mathbf{b}(\lambda) := \mathbf{p}((1 - \lambda)v_1 + \lambda v_2), \quad \lambda \in [0, 1].$$

Let $\mathbf{b} = \sum_{\ell=0}^d \mathbf{b}_\ell B_\ell^d$ be represented in Bézier form, where B_ℓ^d are the univariate Bernstein basis polynomials. Then normal curvature κ_n of \mathbf{p} at $\mathbf{p}(v_1)$ in the direction $\mathbf{u} = \dot{\mathbf{b}}(0)/\|\dot{\mathbf{b}}(0)\|$ is

$$\kappa_n(\mathbf{u}) = \frac{d-1}{d} \frac{\langle \mathbf{b}_2 - \mathbf{b}_1, \mathbf{n} \rangle}{\|\mathbf{b}_1 - \mathbf{b}_0\|^2}. \quad (6.9)$$

Proof. Let $u_1 := (-1, 1, 0)$ and $u_2 := (-1, 0, 1)$ be vectors written in barycentric coordinates. Vector \mathbf{u} corresponds to the direction $u := (1 - \mu)u_1 + \mu u_2$ in the domain. For a general surface, the normal curvature is

$$\kappa_n(\mathbf{u}) = \frac{\begin{bmatrix} 1 - \mu & \mu \end{bmatrix} \begin{bmatrix} L & M \\ M & N \end{bmatrix} \begin{bmatrix} 1 - \mu \\ \mu \end{bmatrix}}{\begin{bmatrix} 1 - \mu & \mu \end{bmatrix} \begin{bmatrix} E & F \\ F & G \end{bmatrix} \begin{bmatrix} 1 - \mu \\ \mu \end{bmatrix}},$$

where E, F, G are the first and L, M, N are the second fundamental form coefficients of the surface (see explicit formulae in (5.9), page 42). For patch \mathbf{p} the expression simplifies to

$$\kappa_n(\mathbf{u}) = \frac{\langle \ddot{\mathbf{b}}(0), \mathbf{n} \rangle}{\langle \dot{\mathbf{b}}(0), \dot{\mathbf{b}}(0) \rangle} = \frac{d(d-1) \langle \mathbf{b}_2 - \mathbf{b}_1 - (\mathbf{b}_1 - \mathbf{b}_0), \mathbf{n} \rangle}{d^2 \|\mathbf{b}_1 - \mathbf{b}_0\|^2} = \frac{d-1}{d} \frac{\langle \mathbf{b}_2 - \mathbf{b}_1, \mathbf{n} \rangle}{\|\mathbf{b}_1 - \mathbf{b}_0\|^2}.$$

□

The points \mathbf{b}_ℓ in the previous lemma can be obtained by the blossom algorithm [64, 28],

$$\mathbf{b}_\ell := \mathbf{p}[v_1^{\langle d-\ell \rangle}, v_2^{\langle \ell \rangle}], \quad \ell = 0, 1, 2, \dots, d.$$

From (6.9) it can be observed that if $\mu \in \{0, 1\}$, the normal curvature $\kappa_n(\mathbf{u})$ is in a unique correspondence to the distance of \mathbf{b}_2 ($\mathbf{c}_{d-2,2,0}$ and $\mathbf{c}_{d-2,0,2}$, respectively) from the tangent plane at v , once the points $\mathbf{b}_0, \mathbf{b}_1$ are fixed. Similarly, for $\mu \notin \{0, 1\}$ the curvature is in one-to-one correspondence to the distance of \mathbf{b}_2 from the tangent plane if the points $\mathbf{c}_{d,0,0}, \mathbf{c}_{d-1,1,0}, \mathbf{c}_{d-1,0,1}, \mathbf{c}_{d-2,2,0}, \mathbf{c}_{d-2,0,2}$ are fixed.

The points in $\mathcal{R}_2(v)$ are connected by C^2 smoothness conditions (see Thm. 2.2). Let \mathbf{p} be a patch, adjoined to the domain vertex v . If we fix all control points in $\mathcal{D}_2(v, \mathbf{p}) \setminus \mathcal{D}_1(v, \mathbf{p})$, then the rest in $\mathcal{R}_2(v)$ are uniquely determined by C^2 continuity constraints. The above conditions give us a 6-parametric family of control points (3 out of 9 degrees of freedom of $\mathcal{D}_2(v, \mathbf{p}) \setminus \mathcal{D}_1(v, \mathbf{p})$ are determined from the normal curvature form).

The remaining 6 parameters will be obtained from the minimising cell. Let us presume that the control points $\mathcal{R}_1(v) =: \{\mathbf{c}_\ell\}_{\ell=1}^n$ of \mathbf{s} are ordered as in §6.2.1. Let points in $\mathcal{R}_2(v) =: \{\mathbf{c}_\ell\}_{\ell=n+1}^{n+n'}$ and $\mathcal{R}_2^\triangleright(v) =: \{\mathbf{c}_\ell^\triangleright\}_{\ell=n+1}^{n+n'}$ be indexed with the same ordering as $\mathcal{R}_1(v)$ (see Fig. 6.6). Here, $n' = 2n$ if v is interior and $n' = 2n - 1$, otherwise.

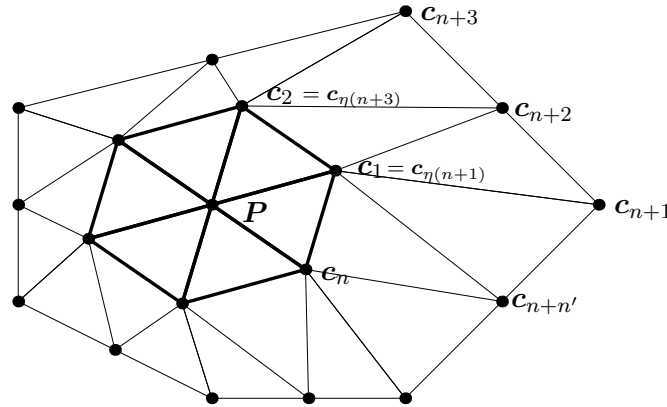


Figure 6.6: Points in $\mathcal{R}_1(v)$ and $\mathcal{R}_2(v)$ are indexed with the same ordering.

The projected points \mathbf{d}_ℓ are obtained similarly as in (6.4),

$$\mathbf{d}_\ell := \mathbf{c}_\ell^\triangleright - \frac{\langle \mathbf{c}_\ell^\triangleright - \mathbf{P}, \mathbf{n} \rangle - k_\ell}{\langle \mathbf{m}_\ell, \mathbf{n} \rangle} \mathbf{m}_\ell, \quad \ell = n+1, n+2, \dots, n+n'. \quad (6.10)$$

The direction vector \mathbf{m}_ℓ is defined in (6.3). The additional, normal curvature term is obtained from (6.9),

$$k_\ell := \begin{cases} \frac{d}{d-1} \|\mathbf{c}_{\eta(\ell)} - \mathbf{P}\|^2 \kappa_n(\mathbf{u}_\ell), & \text{if } \ell - n \text{ is odd,} \\ \frac{2d}{d-1} \|\mathbf{c}_{\eta(\ell)} - \mathbf{P}\|^2 \kappa_n(\mathbf{u}_\ell) \\ \quad - \frac{1}{2} \langle \mathbf{d}_{\ell-1} - \mathbf{c}_{\eta(\ell-1)} + \mathbf{d}_{\ell+1} - \mathbf{c}_{\eta(\ell+1)}, \mathbf{n} \rangle, & \text{if } \ell - n \text{ is even,} \end{cases} \quad (6.11)$$

and

$$\begin{aligned} \mathbf{c}_{\eta(\ell)} &:= \frac{1}{2}(\mathbf{c}_{\lfloor(\ell-n+1)/2\rfloor} + \mathbf{c}_{\lceil(\ell-n+1)/2\rceil}), \\ \mathbf{u}_\ell &:= \frac{1}{\|\mathbf{c}_{\eta(\ell)} - \mathbf{P}\|}(\mathbf{c}_{\eta(\ell)} - \mathbf{P}). \end{aligned}$$

In (6.10) we first need to compute the points \mathbf{d}_ℓ where $\ell - n$ is odd.

Setting $\mathbf{c}_\ell := \mathbf{d}_\ell$, $\ell = n+1, n+2, \dots, n+n'$, would result in a spline \mathbf{s} that interpolates the normal curvature form at v but is not C^1 smooth. Therefore, we need to find a set of points that satisfies the smoothness constraints and is close to the points \mathbf{d}_ℓ . Hence, we use the functional φ , introduced in (6.6), and solve the minimisation problem

$$\min_{\{\mathbf{c}_{n+1}, \mathbf{c}_{n+2}, \mathbf{c}_{n+3}\}} \varphi \left((\mathbf{c}_\ell)_{\ell=n+1}^{n+n'} \right). \quad (6.12)$$

The control points \mathbf{c}_ℓ , $\ell > n+3$, are uniquely set from the first three points by the corresponding C^2 smoothness conditions at v (see Thm. 2.2).

As in the tangent plane interpolation problem, we are left to verify that the control points in the minimising cell satisfy the normal curvature interpolation conditions. Let Π_ℓ denote a plane defined by the point \mathbf{d}_ℓ and the normal vector \mathbf{n} . Then the curvature constraints are transformed to

$$\mathbf{c}_\ell \in \Pi_\ell, \quad \ell = n+1, n+2, \dots, n+n'. \quad (6.13)$$

Lemma 6.8. *Let the points in the set $\mathcal{D}_2(v)$ satisfy C^2 smoothness conditions at v . The conditions $\mathbf{c}_\ell \in \Pi_\ell$ hold true for $\ell = n+1, n+2, n+3$ iff they hold true for $\ell > n+3$.*

Proof. Let the first three control points satisfy the constraints $\mathbf{c}_\ell \in \Pi_\ell$. Therefore, the corresponding patch interpolates the normal curvature form defined by $\{\mathbf{u}_1^*, \mathbf{u}_2^*, \kappa_1, \kappa_2\}$ (see (6.8)). The C^2 continuity constraints at the vertex v uniquely determine all the control points in the set $\mathcal{D}_2(v)$. Since $\mathbf{s} \in C^2(v)$, every patch, adjoined to the domain vertex v , interpolates the normal curvature form at v . Hence, $\mathbf{c}_\ell \in \Pi_\ell$ holds for all $\ell > n$.

The converse holds true by similar arguments. \square

Proposition 6.9. *Let $\mathcal{M} := \{\mathbf{c}_\ell\}_{\ell=n+1}^{n+n'}$ be the minimising cell for (6.12). Then the points of \mathcal{M} satisfy conditions (6.13).*

Proof. We will prove the proposition by a contradiction. Assume that $\mathbf{c}_\ell \notin \Pi_\ell$ for some ℓ . From the previous lemma it follows that for some ℓ , $\ell = n+1, n+2, n+3$, the condition $\mathbf{c}_\ell \in \Pi_\ell$ is not satisfied. Let $\mathcal{M}' := \{\mathbf{c}'_\ell\}_{\ell=n+1}^{n+n'}$ be a cell that is obtained from \mathcal{M} by orthogonally projecting \mathbf{c}_ℓ onto Π_ℓ for $\ell = n+1, n+2, n+3$ and computing the rest by the smoothness conditions. From Lemma 6.8 it follows that all of the points in \mathcal{M}' satisfy the conditions (6.13).

We are left to verify that points \mathbf{c}'_ℓ are closer to the points \mathbf{d}_ℓ than \mathbf{c}_ℓ . We can w.l.o.g. presume that $\mathbf{n} = (0, 0, 1)$ and hence the projection is in z -direction. The smoothness conditions connect the control points componentwise. Hence all the points \mathbf{c}'_ℓ are obtained from z -projection of \mathbf{c}_ℓ onto planes Π_ℓ . After projection, the x - and y -distances remain unchanged but z -components of \mathbf{c}'_ℓ and \mathbf{d}_ℓ coincide.

The cell \mathcal{M}' is an admissible solution that is closer to the set $\{\mathbf{d}_\ell\}_\ell$ than \mathcal{M} . Therefore \mathcal{M} is not the minimising cell, a contradiction with proposition presumptions. \square

6.2.3 Tangent Plane Approximation at Midpoint of an Edge

In the last part of the section we will analyse the problem on how to determine the set \mathcal{D}_e , $e \in \mathcal{E}$, in order to interpolate given data and to minimise the correction of points needed to achieve a required smoothness.

Let d be odd and let $\mathbf{p}^{[\tau_1]}$ and $\mathbf{p}^{[\tau_2]}$ be adjacent patches defined on triangles $\tau_1 = (v_0, v_1, v_2)$ and $\tau_2 = (v_0, v_2, v_3)$, respectively, joining with C^1 smoothness conditions across $e := (v_0, v_2)$ (see Thm. 2.1). Let us denote $\{\mathbf{c}_\ell\} := \mathcal{D}_e(\mathbf{p}^{[\tau_\ell]})$ for $\ell = 1, 2$. Let us presume that all of control points

$$\begin{aligned} \{\mathbf{c}_i^{[\tau_1]} : |\mathbf{i}| = d, j = 0, 1\} \setminus \{\mathbf{c}_1\}, \\ \{\mathbf{c}_i^{[\tau_2]} : |\mathbf{i}| = d, k = 0, 1\} \setminus \{\mathbf{c}_2\} \end{aligned} \quad (6.14)$$

are fixed. We would like to set the remaining two points in such a way that the tangent plane of $\mathbf{p}^{[\tau_1]}$ at the barycentric point $v = (1/2, 0, 1/2)$ approximates a given plane Π .

For the convenience, let $\mathbf{c}_i := \mathbf{c}_i^{[\tau_1]}$. The tangent plane passes through de Casteljau points $\mathbf{c}_{e_\ell}^{(d-1)}(v)$, $\ell = 1, 2, 3$. Since the points $\mathbf{c}_{e_1}^{(d-1)}(v)$ and $\mathbf{c}_{e_3}^{(d-1)}(v)$ are determined from the set in (6.14), it is not possible to interpolate an arbitrary plane Π . Therefore an approximation of it will be considered instead.

Let \mathbf{n}_Π denote the normal vector of the plane Π . To obtain the best approximation of Π , the tangent plane normal \mathbf{n} of the patch $\mathbf{p}^{[\tau_1]}$ should be set in such a way that $\|\mathbf{n} - \mathbf{n}_\Pi\|$ is minimal. Note that the vector \mathbf{n} lies in a plane Σ , defined by $\mathbf{P} := \mathbf{c}_0^{(d)}(v)$ and a normal vector that is parallel to $\mathbf{c}_{e_3}^{(d-1)}(v) - \mathbf{c}_{e_1}^{(d-1)}(v)$. Thus, \mathbf{n} should be set as orthogonal projection of \mathbf{n}_Π onto Σ . Let $\Pi_{\mathbf{P}}$ denote the obtained tangent plane.

The problem of approximating the tangent plane Π is transformed to interpolation of the newly obtained tangent plane $\Pi_{\mathbf{P}}$,

$$\langle \mathbf{c}_{e_2}^{(d-1)}(v) - \mathbf{P}, \mathbf{n} \rangle = 0. \quad (6.15)$$

The intermediate de Casteljau point is obtained from control points of $\mathbf{p}^{[\tau_1]}$ in the following way,

$$\mathbf{c}_{e_2}^{(d-1)}(v) = \frac{1}{2^{d-1}} \sum_{\ell=0}^{d-1} \binom{d-1}{\ell} \mathbf{c}_{\ell,1,d-\ell-1}. \quad (6.16)$$

Combining (6.15) and (6.16) yields

$$\langle \mathbf{c}_1 - \mathbf{P}_1, \mathbf{n} \rangle = 0,$$

where

$$\mathbf{P}_1 := \frac{1}{\binom{d-1}{(d-1)/2}} \left(2^{d-1} \mathbf{P} - \sum_{\substack{\ell=0 \\ \ell \neq (d-1)/2}}^{d-1} \binom{d-1}{\ell} \mathbf{c}_{\ell,1,d-\ell-1} \right). \quad (6.17)$$

Similarly, we obtain the point \mathbf{P}_2 for the patch $\mathbf{p}^{[\tau_2]}$. Let Π_ℓ denote a plane that is defined by the point \mathbf{P}_ℓ and the normal \mathbf{n} (see Fig. 6.7). Then

$$(6.15) \iff \mathbf{c}_{e_2}^{(d-1)}(v) \in \Pi_{\mathbf{P}} \iff \mathbf{c}_1 \in \Pi_1 \iff \mathbf{c}_2 \in \Pi_2.$$

The points $\mathbf{c}_1, \mathbf{c}_2$ are not uniquely determined from (6.15). The remaining two parameters are obtained by minimising the distances from the points $\mathbf{c}_\ell^\triangleright, \{\mathbf{c}_\ell^\triangleright\} := \mathcal{D}_e(\mathbf{p}^{[\tau_\ell], \triangleright})$, where $\mathbf{p}^{[\tau_\ell], \triangleright}$ is the linear patch that corresponds to $\mathbf{p}^{[\tau_\ell]}$. Let $\hat{\mathbf{P}} := \mathbf{p}^{[\tau_1], \triangleright}(v) = 1/2(\mathbf{c}_{d00} + \mathbf{c}_{00d})$. Similarly as in the previous cases, we define the directions of the oblique projections,

$$\mathbf{m}_\ell := \mathbf{n} - \frac{\langle \mathbf{c}_\ell^\triangleright - \hat{\mathbf{P}}, \mathbf{n} \rangle}{\|\mathbf{c}_\ell^\triangleright - \hat{\mathbf{P}}\|^2} (\mathbf{c}_\ell^\triangleright - \hat{\mathbf{P}}), \quad \ell = 1, 2, \quad (6.18)$$

and the projected points are

$$\mathbf{d}_\ell := \mathbf{c}_\ell^\triangleright - \frac{\langle \mathbf{c}_\ell^\triangleright - \hat{\mathbf{P}}, \mathbf{n} \rangle}{\langle \mathbf{m}_\ell, \mathbf{n} \rangle} \mathbf{m}_\ell, \quad \ell = 1, 2. \quad (6.19)$$

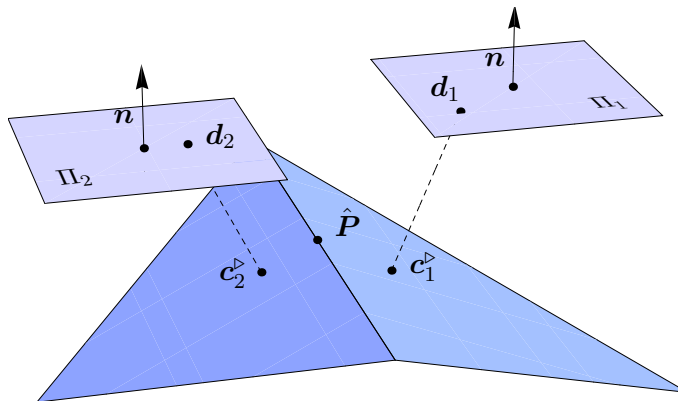


Figure 6.7: Points $\mathbf{c}_\ell^\triangleright$ are projected onto planes Π_ℓ .

Next, let the two unset control points be the solution of the minimisation problem

$$\min_{\{\mathbf{c}_1\}} \hat{\varphi}((\mathbf{c}_\ell)_\ell),$$

where the functional $\hat{\varphi}$ is defined as

$$\hat{\varphi}((\mathbf{c}_\ell)_{\ell=1}^2) := \sum_{\ell=1}^2 \frac{\|\mathbf{c}_\ell - \mathbf{d}_\ell\|^2}{\|\mathbf{d}_\ell - \hat{\mathbf{P}}\|^2}. \quad (6.20)$$

The direction \mathbf{m}_ℓ in (6.18), the point \mathbf{d}_ℓ in (6.19) and the functional $\hat{\varphi}$ are slightly modified objects of (6.3), (6.4) and (6.6), respectively. Here, the interpolation point \mathbf{P} is replaced by $\hat{\mathbf{P}}$ since the spline does not interpolate any point at v . It can easily be verified (see the previous subsection) that the optimal points \mathbf{c}_ℓ satisfy the conditions $\mathbf{c}_\ell \in \Pi_\ell, \ell = 1, 2$. If the edge e is boundary, then the expression (6.20) simplifies to only one summand and $\mathbf{c}_1 = \mathbf{d}_1$.

6.2.4 Algorithms

Let us summarise the algorithms of this chapter. Procedures for constructing the sets $\mathcal{R}_1(v)$ (see § 6.2.1), $\mathcal{R}_2(v)$ (see § 6.2.2) and \mathcal{D}_e (see § 6.2.3) are presented as Alg. 3, 4, 5, respectively.

Algorithm 3 Construction of the set $\mathcal{R}_1(v)$, $v \in \mathcal{V}$

Input: a cell with center v , $\mathcal{R}_1^\triangleright(v)$ (list of control points $\mathbf{c}_\ell^\triangleright$), $\{\mathbf{P}, \Pi\}$ (interpolation data)

Output: $\mathcal{R}_1(v)$

for $\ell = 1, 2, \dots, n$ **do**

 compute \mathbf{d}_ℓ as a projection of $\mathbf{c}_\ell^\triangleright \in \mathcal{R}_1^\triangleright(v)$ onto Π by using (6.3) and (6.4)

end for

compute the minimising cell $\mathcal{R}_1(v)$ by minimising the functional φ in (6.6) with constraints (6.7)

Algorithm 4 Construction of the set $\mathcal{R}_2(v)$, $v \in \mathcal{V}$

Input: a cell with center v , a set $\mathcal{D}_1(v)$ (determined by Alg. 3), $\mathcal{R}_2^\triangleright(v)$ (list of control points $\mathbf{c}_\ell^\triangleright$), $\{\mathbf{P}, \Pi, \mathbf{u}_1^*, \mathbf{u}_2^*, \kappa_1, \kappa_2\}$ (interpolation data)

Output: $\mathcal{R}_2(v)$

for $\ell = n + 1, n + 3, \dots, 2\lfloor(n' - 1)/2\rfloor + n + 1$ **do**

 compute k_ℓ from (6.11)

 compute \mathbf{d}_ℓ as a projection of $\mathbf{c}_\ell^\triangleright \in \mathcal{R}_2^\triangleright(v)$ by using (6.3) and (6.10)

end for

for $\ell = n + 2, n + 4, \dots, 2\lfloor n'/2\rfloor + n$ **do**

 compute k_ℓ from (6.11)

 compute \mathbf{d}_ℓ as a projection of $\mathbf{c}_\ell^\triangleright \in \mathcal{R}_2^\triangleright(v)$ by using (6.3) and (6.10)

end for

compute the minimising cell $\mathcal{R}_2(v)$ by solving the least square problem (6.12)

Algorithm 5 Construction of the set \mathcal{D}_e , $e \in \mathcal{E}$

Input: triangles containing edge e , control points in (6.14), $\{\mathbf{c}_1^\triangleright, \mathbf{c}_2^\triangleright\}$, Π (tangent plane)

Output: \mathcal{D}_e

for $\ell = 1, 2$ **do**

 compute \mathbf{P}_ℓ from (6.17)

 compute \mathbf{d}_ℓ as a projection of $\mathbf{c}_\ell^\triangleright$ onto Π_ℓ by using (6.18) and (6.19)

end for

compute \mathcal{D}_e by minimising functional $\hat{\varphi}$ in (6.20)

6.3 Macro-Elements

In this section, we present parametric extensions of two well-known macro-element spaces, polynomial $\mathcal{S}_5^{1,2}(\Delta)$ and Clough–Tocher $\mathcal{S}_3^{1,1}(\Delta_{CT})$ one. Each macro-element solves a particular interpolation problem. The remaining degrees of freedom are determined by constructing appropriate minimising cells with respect to the linear spline interpolant.

A very convenient tool to represent free parameters of a spline $\mathbf{s} \in \mathcal{S}_d^{r,\rho}(\Delta)$ and to determine the dimension of the spline space is the following definition of set of control points.

Definition 6.10. *A set of control points*

$$\mathcal{C} \subset \mathcal{A} := \bigcup_{\tau \in \Delta} \bigcup_{|\mathbf{i}|=d} \{ \mathbf{c}_i^{[\tau]} \}$$

is minimal determining set for a spline space $\mathcal{S}_d^{r,\rho}(\Delta)$, if control points in \mathcal{C} uniquely determine spline $\mathbf{s} \in \mathcal{S}_d^{r,\rho}(\Delta)$. Control points in $\mathcal{A} \setminus \mathcal{C}$ are uniquely determined by \mathcal{C} via smoothness conditions of the spline space.

Each spline $\mathbf{s} \in \mathcal{S}_d^{r,\rho}(\Delta)$ is in unique correspondence to its minimal determining set. We will use the sets of the macro-element spaces to verify that our interpolation schemes uniquely and consistently determine the spline. The interpolation conditions will be solved by applying the algorithms in § 6.2.

Let $T_v \mathbf{s}$ and $C_v \mathbf{s}$ denote the tangent plane and the normal curvature form of a spline \mathbf{s} at vertex v .

6.3.1 Polynomial Macro-Element in $\mathcal{S}_5^{1,2}(\Delta)$

With a small modification of Thm 6.1 (and its proof) in [51] we can prove the following theorem.

Theorem 6.11. *For every $v \in \mathcal{V}$, let $d_v = \mathcal{D}_2(v, \mathbf{p}^{[\tau]})$ for some $\tau \in \Delta$ with vertex at v . For every $e \in \mathcal{E}$, let $d_e = \mathcal{D}_e(\mathbf{p}^{[\tau]})$ for some $\tau \in \Delta$ containing edge e . Then*

$$\mathcal{C} := \bigcup_{v \in \mathcal{V}} d_v \cup \bigcup_{e \in \mathcal{E}} d_e$$

is minimal determining set for $\mathcal{S}_5^{1,2}(\Delta)$. Its cardinality is $6|\mathcal{V}| + |\mathcal{E}|$ and therefore the dimension of the space $\mathcal{S}_5^{1,2}(\Delta)$ is $18|\mathcal{V}| + 3|\mathcal{E}|$.

We would like to uniquely set the control points in the set \mathcal{C} in such a way that the spline \mathbf{s} solves the following interpolation/approximation problem,

$$\begin{aligned} \mathbf{s}(v) &= \mathbf{P}_v, \\ T_v \mathbf{s} &= \Pi_v, & v \in \mathcal{V}, \\ C_v \mathbf{s} &= \{ \mathbf{u}_1^*(v), \mathbf{u}_2^*(v), \kappa_1(v), \kappa_2(v) \}, \\ T_{\frac{1}{2}(v_0+v_1)} \mathbf{s} &\approx \Pi_{\frac{1}{2}(v_0+v_1)}, & (v_0, v_1) \in \mathcal{E}. \end{aligned} \tag{6.21}$$

The first three conditions refer to the interpolation constraints: interpolation of points, tangent planes and normal curvature forms (see (6.8)), respectively. The last condition describes an approximation of a tangent plane since not enough degrees of freedom are left for the interpolation once the first two conditions are applied (see § 6.2.3). The problem (6.21) is a parametric version of the interpolation problem in Thm. 6.1.

First, we construct the reference linear spline surface $\mathbf{s}^\triangleright$ of polynomial degree $d = 5$ that interpolates points \mathbf{P}_v at $v \in \mathcal{V}$. The approximation conditions (6.21) for \mathbf{s} are applied in the order as they are listed. Interpolation of points and tangent plane constraints fix $5|\mathcal{V}|$ parameters. The remaining $4|\mathcal{V}|$ parameters that uniquely determine the sets $\mathcal{D}_1(v)$, $v \in \mathcal{V}$, are obtained from the minimising cells. The procedure is summarised as Alg. 3. Next, interpolation of the normal curvature form assigns values of $3|\mathcal{V}|$ parameters. The remaining $6|\mathcal{V}|$ ones, obtained from the minimising cells, determine the unset parameters in $\mathcal{D}_2(v)$ (see Alg. 4 and Fig. 6.8). Finally, the remaining $3|\mathcal{E}|$ parameters are fixed by approximation of tangent planes and the applied minimising cells for \mathcal{D}_e , $e \in \mathcal{E}$ (see Alg. 5). The number of all parameters, $18|\mathcal{V}| + 3|\mathcal{E}|$, is equal to the dimension of the space (see Thm. 6.11). Therefore, the interpolation spline $\mathbf{s} \in \mathcal{S}_5^{1,2}(\Delta)$ is uniquely and consistently determined.

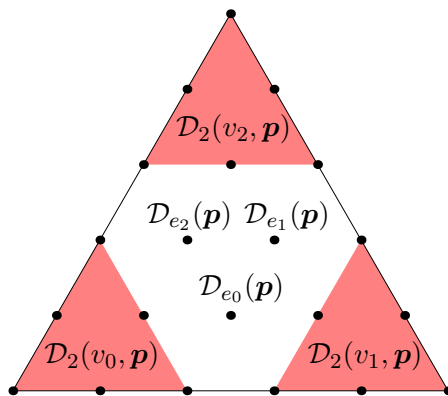


Figure 6.8: Control points (represented by black dots) of polynomial macro-element patch $\mathbf{p} \in \mathcal{P}_5^3$ are divided into sets $\mathcal{D}_2(v, \mathbf{p})$ (red areas) and $\mathcal{D}_e(\mathbf{p})$.

6.3.2 Clough–Tocher Macro-Element in $\mathcal{S}_3^{1,1}(\Delta_{CT})$

As for the previous macro-element space let us present a set of control points that uniquely determines a spline $\mathbf{s} \in \mathcal{S}_3^{1,1}(\Delta_{CT})$. In this section, let \mathcal{V} and \mathcal{E} denote sets of vertices and edges of the original triangulation Δ . By applying minor modifications of Thm 6.5 in [51] we can prove the following theorem.

Theorem 6.12. *For every $v \in \mathcal{V}$, let $d_v = \mathcal{D}_1(v, \mathbf{p}^{[\tau]})$ for some $\tau \in \Delta_{CT}$ with vertex at v . For every $e \in \mathcal{E}$, let $d_e = \mathcal{D}_e(\mathbf{p}^{[\tau]})$ for some $\tau \in \Delta_{CT}$ containing edge e . Then*

$$\mathcal{C} := \bigcup_{v \in \mathcal{V}} d_v \cup \bigcup_{e \in \mathcal{E}} d_e$$

is minimal determining set for the space $\mathcal{S}_3^{1,1}(\Delta_{CT})$. Its cardinality is $3|\mathcal{V}| + |\mathcal{E}|$ and the dimension of the space is $9|\mathcal{V}| + 3|\mathcal{E}|$.

We would like to solve the following interpolation/approximation problem

$$\begin{aligned}
 \mathbf{s}(v) &= \mathbf{P}_v, & v \in \mathcal{V}, \\
 T_v \mathbf{s} &= \Pi_v, & \\
 T_{\frac{1}{2}(v_0+v_1)} \mathbf{s} &\approx \Pi_{\frac{1}{2}(v_0+v_1)}, & (v_0, v_1) \in \mathcal{E}.
 \end{aligned} \tag{6.22}$$

The problem (6.22) is a parametric version of the interpolation problem in Thm. 6.2.

First, we construct the linear spline $\mathbf{s}^\triangleright$ of polynomial degree $d = 3$ on Δ_{CT} that interpolates the points \mathbf{P}_v at $v \in \mathcal{V}$. Additionally, at barycenters of original triangles $\tau =: (v_0, v_1, v_2) \in \Delta$ the linear patches interpolate points $1/3(\mathbf{P}_{v_0} + \mathbf{P}_{v_1} + \mathbf{P}_{v_2})$.

The interpolation conditions (6.22) for points and tangent planes at vertices and the minimising cell parameters fix $5|\mathcal{V}| + 4|\mathcal{E}|$ degrees of freedom of the spline \mathbf{s} (the construction is presented as Alg. 3). At every edge $e \in \mathcal{E}$, the set \mathcal{D}_e is determined from the approximation of the tangent plane and by computing the minimising cell (see Alg. 5). Hence, the remaining $|\mathcal{E}| + 2|\mathcal{E}|$ parameters are assigned. Therefore, all the control points \mathbf{c}_ℓ , $\ell = 1, 2, \dots, 15$, for every macro-triangle are consistently set (see Fig. 6.9).

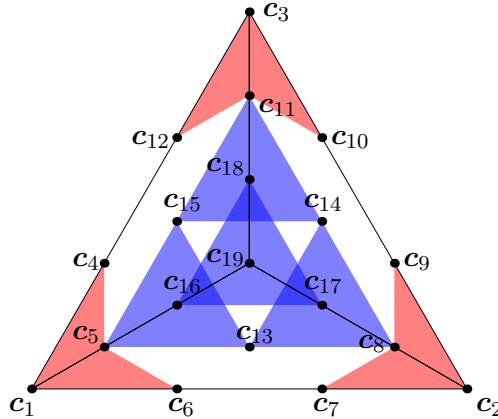


Figure 6.9: Control points of a macro-triangle in $\mathcal{S}_3^{1,1}(\Delta_{\text{CT}})$ are enumerated by indices $\ell = 1, 2, \dots, 19$. Control points connected by red regions are determined by interpolation conditions at vertices. C^1 continuity constraints at interior boundaries are presented by blue regions.

The rest of interior control points are computed from C^1 smoothness conditions across boundaries of micro-triangles:

$$\begin{aligned}
 \mathbf{c}_{16} &= \frac{1}{3}(\mathbf{c}_5 + \mathbf{c}_{13} + \mathbf{c}_{15}), & \mathbf{c}_{17} &= \frac{1}{3}(\mathbf{c}_8 + \mathbf{c}_{13} + \mathbf{c}_{14}), \\
 \mathbf{c}_{18} &= \frac{1}{3}(\mathbf{c}_{11} + \mathbf{c}_{14} + \mathbf{c}_{15}), & \mathbf{c}_{19} &= \frac{1}{3}(\mathbf{c}_{16} + \mathbf{c}_{17} + \mathbf{c}_{18}).
 \end{aligned}$$

Since the number of determined parameters $9|\mathcal{V}| + 3|\mathcal{E}|$ is equal to the dimension of the space $\mathcal{S}_3^{1,1}(\Delta_{\text{CT}})$ (see Thm. 6.12), the interpolating spline $\mathbf{s} \in \mathcal{S}_3^{1,1}(\Delta_{\text{CT}})$ is uniquely determined and no inconsistency can arise.

6.4 Remarks

Let us conclude the chapter by some remarks and properties of the derived interpolation scheme.

Remark 6.13. *It can easily be verified that both of the presented approximation methods in § 6.3 are local. Hence, interpolation data at a vertex or an edge only influence the adjoining patches. As opposed to the standard functional splines, where every patch is uniquely determined only from Hermite data inside the corresponding triangle (see Thm. 6.1 and Thm. 6.5 in [51], e.g.), in our schemes also the data of adjacent triangles affect the patch. Namely, control points of the parametric patch are obtained by computing different minimising cells. The latter depend on control points of the adjacent linear spline patches.*

Remark 6.14. *Standard functional macro-elements in $\mathcal{S}_d^{r,\rho}(\Delta)$ have the optimal approximation order since they reproduce polynomials of total degree $\leq d$ in the corresponding Hermite problem. This is not true for the presented parametric counterparts since not all degrees of freedom are used to interpolate data. Despite this fact, if the interpolation data are dense enough, the shape differences between the two approximants are small.*

Interpolation problems in Thm. 6.1 and Thm. 6.2 can be regarded as special cases of (6.21) and (6.22), respectively (e.g., partial derivatives of the first order uniquely determine an interpolation plane, etc.). Let us denote control points of a non-parametric patch on triangle τ by $\mathbf{c}_i^{(f)} := (\langle \mathbf{i}/d, \tau \rangle, c_i) \in \mathbb{R}^3$, $|\mathbf{i}| = d$. From geometric point of view, the interpolation problem is solved by projecting control points $\mathbf{c}_i^{(f)}$ in z -direction onto interpolation planes (Fig. 6.10). On the other hand, control points of a parametric patch are projected in the direction, orthogonal to $\mathbf{c}_i^{(f)} - \mathbf{P}$. If the interpolation data are dense,

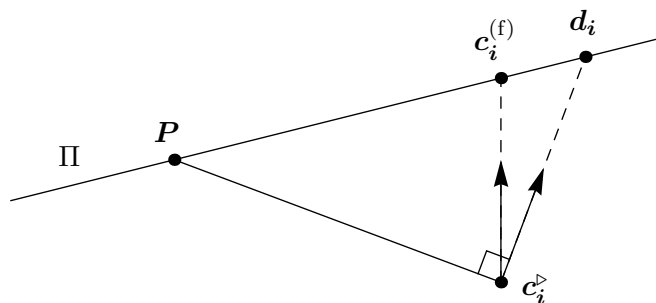


Figure 6.10: Different projection directions are chosen to compute control points of a functional and a parametric macro-element.

the projected points \mathbf{d}_i are close to $\mathbf{c}_i^{(f)}$ and the parametric spline resembles the functional one.

Remark 6.15. *In practice, triangulated domain is not provided in advance. Usually only scattered spatial points are given. A construction of a suitable triangulation from a collection of points is a non-trivial task and it is not analysed in the thesis. In some cases, a triangulation can be constructed by unfolding the linear spline reference surface to a plane.*

Chapter 7

Numerical Examples

The derived Hermite schemes are tested and compared with some well-known methods in various examples. Hermite interpolants HI- ω are presented in Chapter 5 and parametric macro-elements in Chapter 6. Construction of PN triangles [68] is recalled in §5.1.

Farin's G^1 quartic scheme solves the standard Hermite problem (interpolation of points and the corresponding tangent plane) and produces a visually smooth spline [26]. The algorithm consists of the following main steps:

- construct cubic boundary curves of the patches,
- compute the remaining interior control points,
- apply Clough–Tocher subdivision on every patch and raise degree of cubic patches to four,
- correct original boundaries to ensure G^1 smoothness between patches and
- apply corrections of points to obtain C^1 connections between the subpatches.

The methods are tested by approximating different surfaces: a unit sphere, a torus and a more general free-form surface. The quality of a resulting shape is measured by different criteria such as the visual quality of the shape, maximal error, Willmore energy and curvature distribution. By approximating a non-parametric function, a comparison between parametric and non-parametric macro-elements is made. An example of surface reconstruction from scattered points is presented afterwards. At the end of the chapter, our schemes are applied to solve a simple hole filling problem.

7.1 Surface Approximation

7.1.1 Sphere Approximation

In the first example we examine a unit sphere approximation – the most natural test for HI- ω interpolants. Let us sample 6 points and the corresponding radial normals from an octahedron inscribed in the unit sphere. In Tab. 7.1, spline approximants and the corresponding residual functions, defined as a function of radial distances from the approximation spline to the sphere, are presented. For every spline, Willmore energy (\mathcal{W}) and the maximal value of the residual (e_r) are computed. Note that Willmore energy of the surface is obtained as the sum of energies of the patches.

7 Numerical Examples

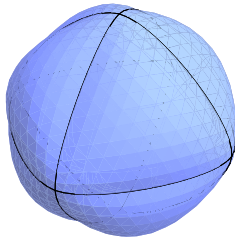
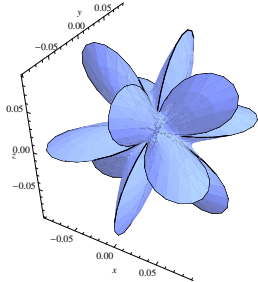
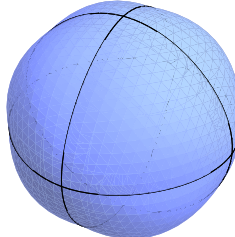
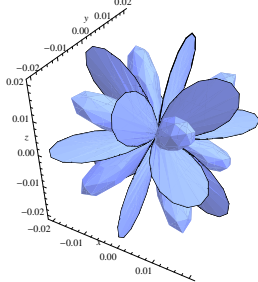
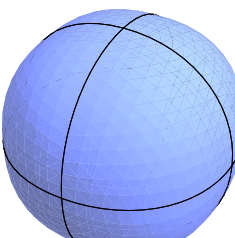
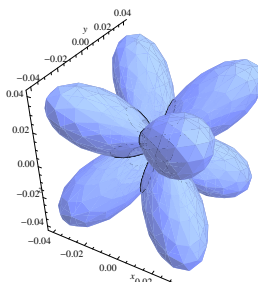
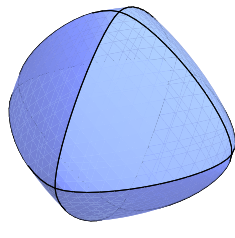
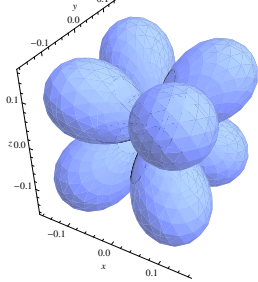
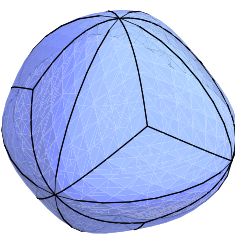
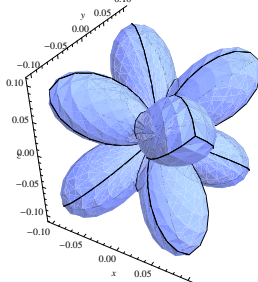
	Spline	Residual
HI-16 $\mathcal{W} = 4.40$ $e_r = 0.116$		
HI-4 $\mathcal{W} = 0.502$ $e_r = 0.0277$		
HI-0 $\mathcal{W} = 0.223$ $e_r = 0.0649$		
PN $\mathcal{W} = 0.897$ $e_r = 0.230$		
Farin's scheme $\mathcal{W} = 2.19$ $e_r = 0.157$		

Table 7.1: An approximation of the unit sphere. Data are obtained from the octahedron.

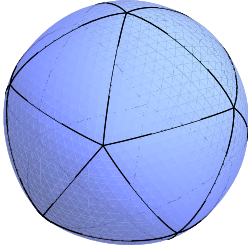
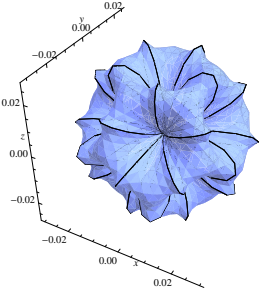
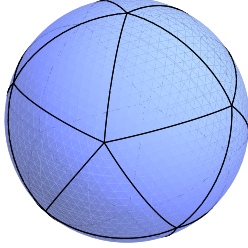
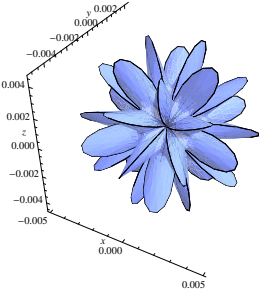
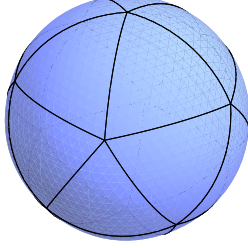
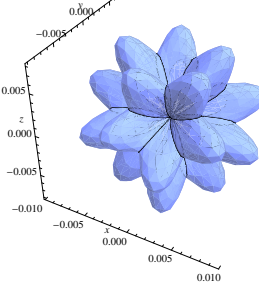
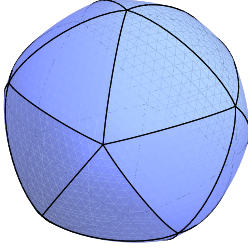
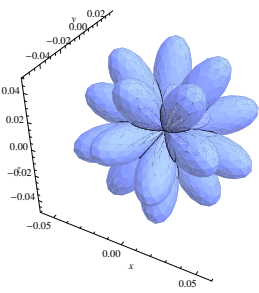
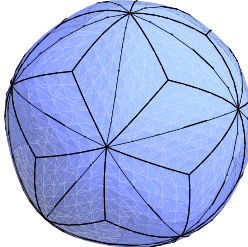
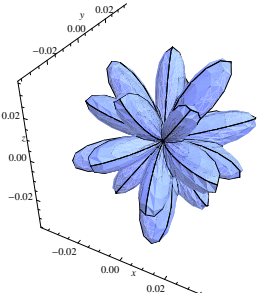
	Spline	Residual
HI-16 $\mathcal{W} = 0.920$ $e_r = 0.0318$		
HI-4 $\mathcal{W} = 0.0390$ $e_r = 0.00524$		
HI-0 $\mathcal{W} = 0.0247$ $e_r = 0.00990$		
PN $\mathcal{W} = 0.300$ $e_r = 0.0589$		
Farin's scheme $\mathcal{W} = 0.595$ $e_r = 0.0422$		

Table 7.2: An approximation of the unit sphere. Data are sampled from the icosahedron.

7 Numerical Examples

In the second example we increase the number of data and take 12 points from the inscribed icosahedron and the corresponding radial normals (Tab. 7.2). In both examples, HI- ω splines of lower parameters ω give better approximations. The result is expected since boundary curves of lower parameters have smaller curvature variation. The spline consisting of HI-4 patches produces the best approximation considering the residual function. HI-0 patches have the smallest Willmore energy. The PN patches tend to be more flat than patches produced with other algorithms. Increasing the number of patches naturally improves the quality of the approximation in all the cases.

Macro-element interpolants cannot approximate a sphere due to the strict C^r smoothness conditions. Nevertheless, an approximation of a larger part of the sphere is considered to obtain some comparison to other interpolation schemes. Additional tangent plane normals at midpoints of the edges are obtained as an average of normals at the vertices. For the quintic case, principal curvatures $\kappa_1 = \kappa_2 = 1$ are sampled at each vertex. By overlooking holes of both approximants in bottom hemispheres (see Tab. 7.3), the shapes of the splines are comparable to the ones in Tab. 7.1. Although the polynomial quintic macro-element has a larger radial error than the Clough–Tocher cubic counterpart, its shape resembles the shape of the sphere better which is also confirmed by values of Willmore energy. Undesired bulges of the cubic spline can be seen in centers of Clough–Tocher splits.

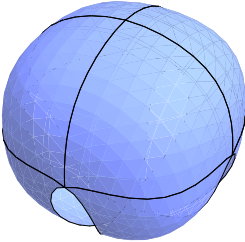
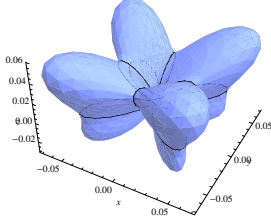
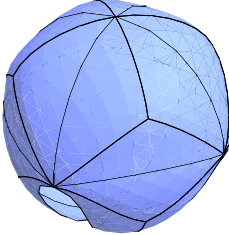
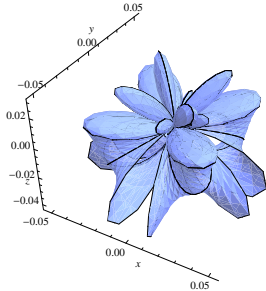
	Spline	Residual
polynomial m.e. $\mathcal{W} = 0.702$ $e_r = 0.105$		
Clough– Tocher m.e. $\mathcal{W} = 2.62$ $e_r = 0.0657$		

Table 7.3: Approximation of the unit sphere by macro-elements. Data are obtained from the octahedron.

7.1.2 Torus Approximation

Let us approximate a torus with $R = 2$ (the distance from the center of the tube to the center of the torus) and $r = 1$ (the radius of the tube). By identifying boundary

vertices and edges of the domain triangulation, we construct a triangulation, suitable for approximating a torus (see Fig. 7.1).

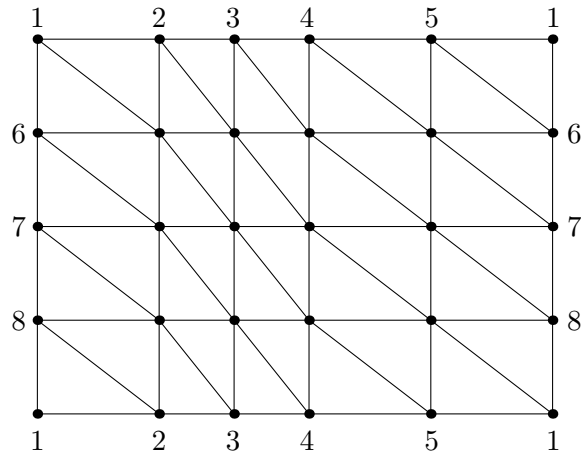


Figure 7.1: A triangulation, where vertices with the same indices and the corresponding edges are identified.

The torus is approximated by five Hermite interpolation schemes (see Fig. 7.2). To reduce number of similar results we only test HI- ω method for $\omega = 0$, which produced the best sphere approximation in terms of Willmore energy. Some quantitative differences between the approximants are shown in Tab. 7.4. The results are satisfying even though a small number of patches is used. In all the cases, the shapes on the right-hand side segments are better since the interpolation data in that area are denser. HI-0 interpolant and macro-elements have comparable Hausdorff distance errors which are smaller than in the case of PN triangles and Farin’s interpolant.

	d	# of \mathbf{p}	# of \mathbf{c}_i	# of i.d.	error	\mathcal{W}
HI-0	3	40	400	40	0.205	25.2
polynomial m.e.	5	40	840	120	0.218	143
Clough-T. m.e.	3	120	1200	100	0.220	186
PN triangles	3	40	400	40	0.481	28.0
Farin’s scheme	4	120	1800	40	0.372	170

Table 7.4: Some quantitative comparisons of the torus approximation splines. Notations in the first row are abbreviations of *polynomial degree*, *number of patches*, *number of control points*, *number of interpolation data*, *Hausdorff error* and *Willmore energy*.

As expected, HI-0 spline has the smallest Willmore energy. Surface of PN triangles has a comparable energy, whereas other spline have a considerable greater value. Note that the value of the energy is not be the best criterion to determine the quality of surface. Namely, a linear spline surface has Willmore energy equal to zero since the quick changes of the shape across the boundary curves are not captured by the energy functional.

Some undesired shape defects can detected on the Farin’s interpolant on lower part of the figure. Only Clough-Tocher macro-element produces boundary curves on the top of

7 Numerical Examples

the surface that resemble horizontal contours of the torus. For all the other schemes, the corresponding curves are close to linear segments. The boundary curves of the quintic macro-element could be improved if we would take a better reference surface instead of a linear spline.

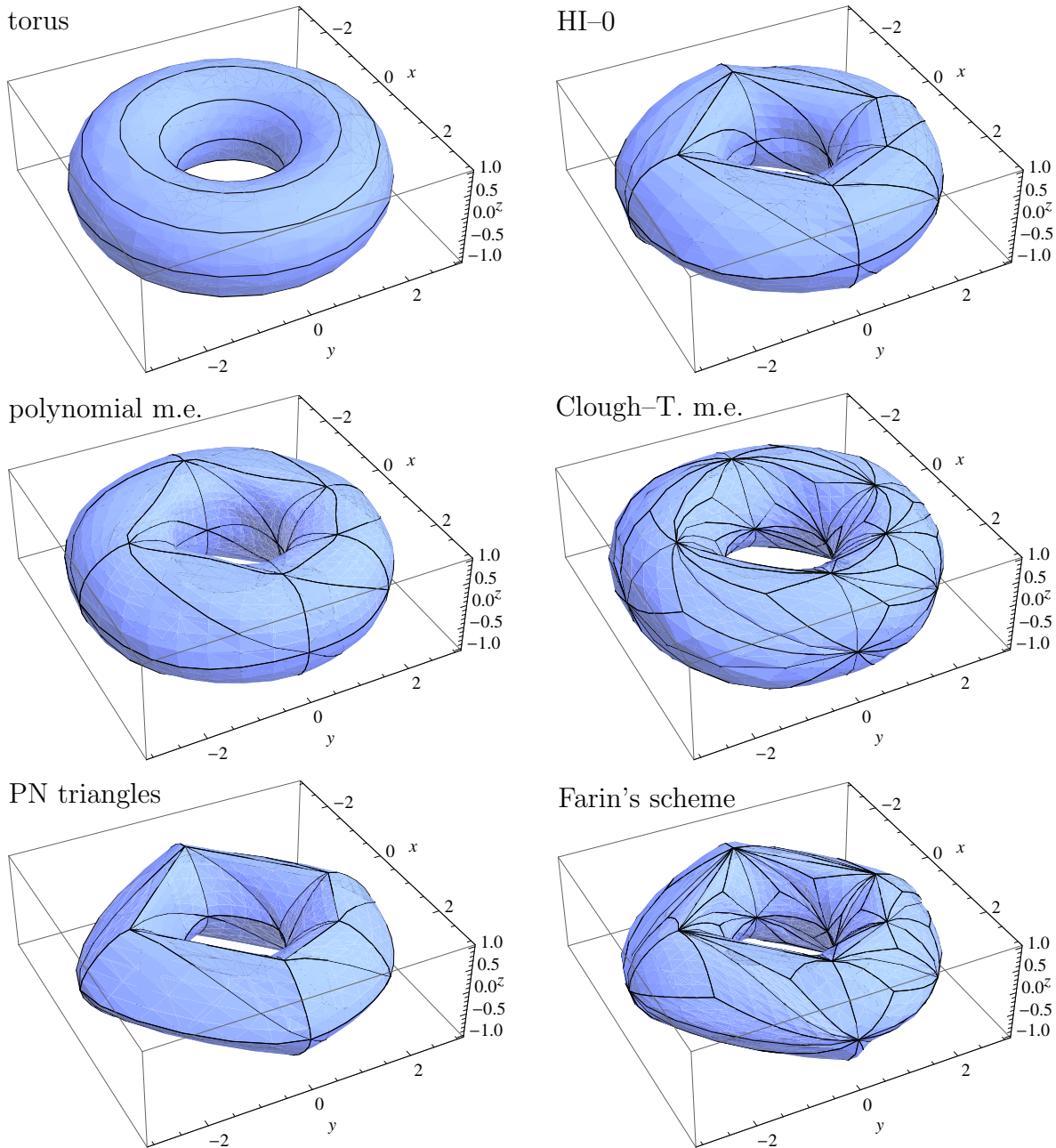


Figure 7.2: Approximation of the torus by Hermite interpolation schemes.

Quality of a surface is sometimes measured by distribution of Gaussian curvature $K = \kappa_1 \kappa_2$, where κ_ℓ are the principal curvatures of the surface. Fig. 7.3 shows that all of the interpolants have a considerably greater curvature oscillations than the original surface. Extreme curvatures can be detected mostly on the boundaries of the interpolation patches. HI-0 spline surface has the smallest oscillations of Gaussian curvature. Although

the polynomial macro-element is the only spline that interpolates the principal curvatures at the interpolation vertices, its overall Gaussian curvature distribution is not better compared to other splines.

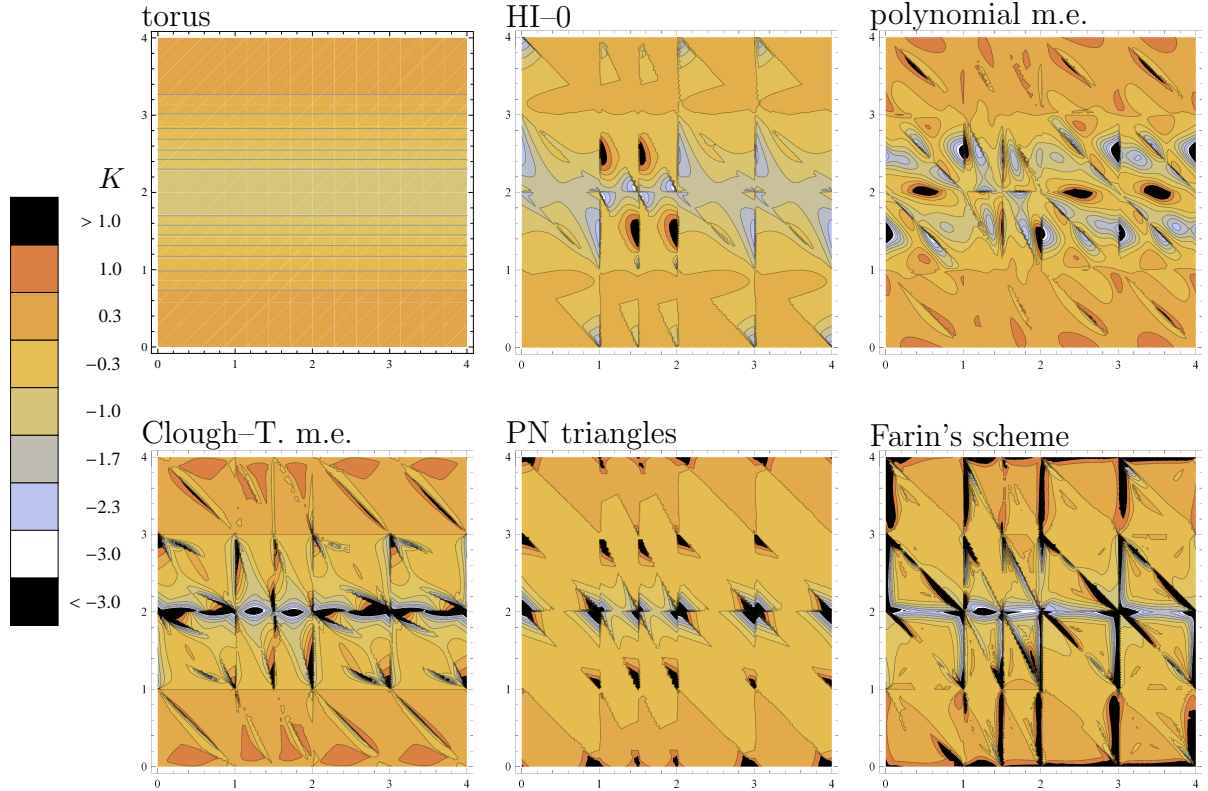


Figure 7.3: Gaussian curvature of the torus and its Hermite interpolating splines.

7.1.3 Free-Form Surface Approximation

In the following example of surface approximation let us approximate a more general free-form surface with a more diverse curvature distribution. Let

$$\begin{aligned} \mathbf{f} &: [-3, 3]^2 \rightarrow \mathbb{R}^3, \\ \mathbf{f}(u, v) &:= \left(u + \frac{v^2}{12}, v - \cos(u), \frac{1}{3}u^2 + \sin(v) \right). \end{aligned} \quad (7.1)$$

Plots of \mathbf{f} and the corresponding interpolation schemes are shown in Fig. 7.4. Some quantitative differences between the approximants such as a number of patches and interpolation data are shown in Tab. 7.5. All interpolation algorithms give satisfying results and no significant shape defects can be detected. The macro-elements give the best results when Hausdorff error is considered. This is not surprisingly since they also interpolate a greater number of data. Surface made of PN triangles gives the biggest Hausdorff error among all schemes since its patches are the most flat.

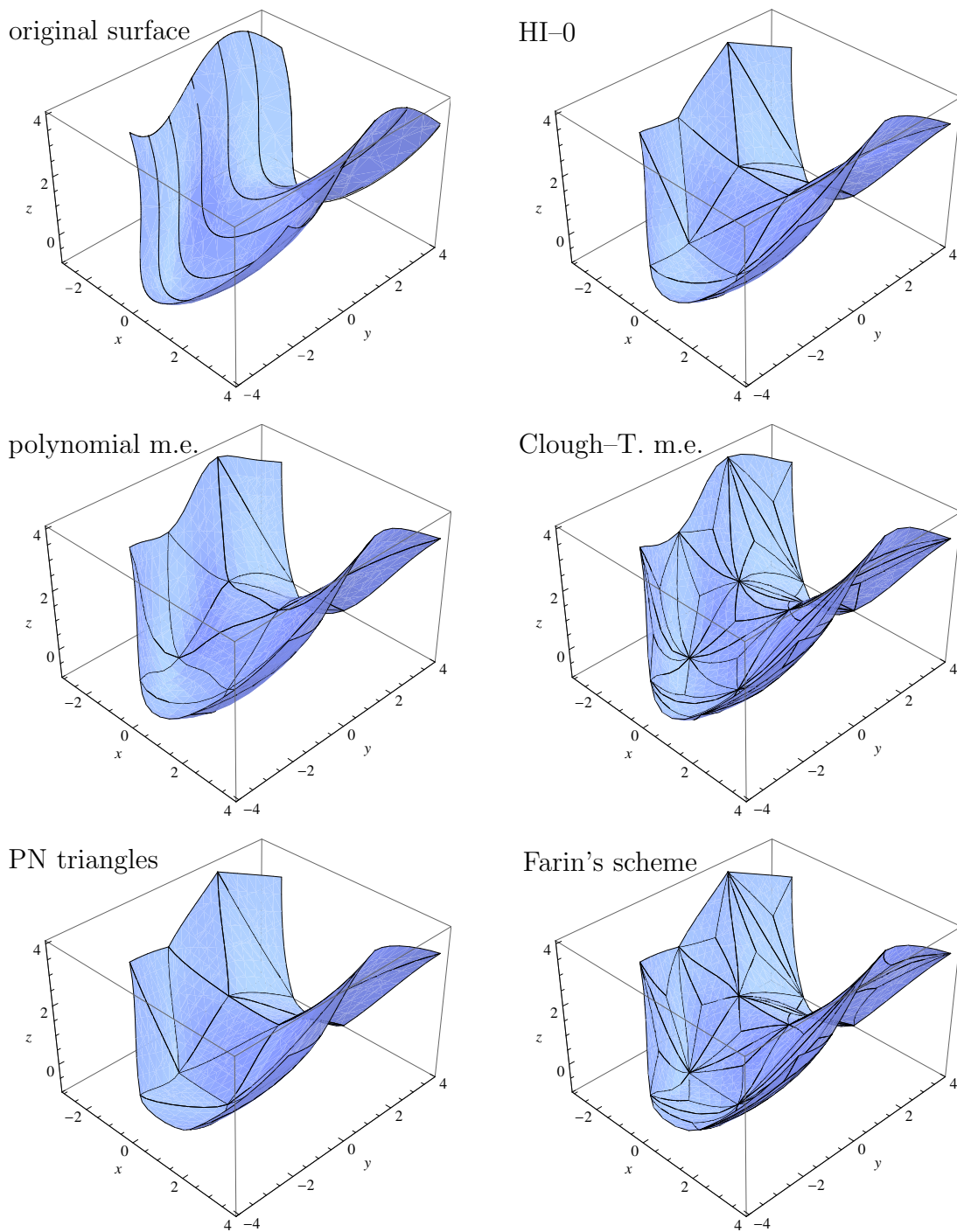


Figure 7.4: Approximation of function f in (7.1) by Hermite interpolants.

7.1.4 Comparison of Parametric and Non-Parametric Macro-Elements

An important property of the parametric macro-element interpolants is the resemblance to their standard functional counterparts if the interpolation data are dense enough (see §6.4). This property is verified by the following example.

	d	# of \mathbf{p}	# of \mathbf{c}_i	# of i.d.	error
HI-0	3	18	180	32	0.290
polynomial m.e.	5	18	378	81	0.203
Clough–T. m.e.	3	54	540	65	0.214
PN triangles	3	18	180	32	0.593
Farin’s scheme	4	54	810	32	0.409

Table 7.5: Some quantitative comparisons of splines that approximate \mathbf{f} in (7.1). Notations in the first row are abbreviations of *polynomial degree*, *number of patches*, *number of control points*, *number of interpolation data* and *Hausdorff error*.

A function $f(x, y) := 1/2 \sin(xy)$ is approximated on domain $\Omega = [-2, 2]^2$ by polynomial and Clough–Tocher macro-element together with their non-parametric interpolation schemes. At domain vertices and edge midpoints, parametric splines interpolate the geometric data. On the other hand, the functional splines interpolate values of f and its partial and directional derivatives (see § 6.1). The parametric and their non-parametric counterparts are visually almost indistinguishable (Fig. 7.5). A bigger difference can be observed on the plots of residual error functions $|m - f|$, where $m : \Omega \rightarrow \mathbb{R}$ is a functional representation of a macro-element. Maximal z -errors are 0.122 (polynomial m.e.), 0.199 (functional polynomial m.e.), 0.435 (Clough–Tocher m.e.) and 0.382 (functional Clough–Tocher m.e.). The quintic splines outperform the cubic ones since they interpolate more data even though they consist of fewer number of patches.

7.2 Surface Reconstruction

A common problem in optimal shape design is that not all of the processes are performed by a single software package. For example, a part of car surface, aeroplane or a turbine can be designed in a different software than the afterward processes such as CFD (computational fluid dynamics), stiffness or noise analysis. Exportation of data between programs can lead to certain losses and in some cases the data need to be transformed in advance to a specific format before exporting.

In order to avoid problems of exporting a complicated surface, it is a common procedure to sample a dense grid of points of the surface only. The surface is then reconstructed only from the given points. A non-trivial problem to construct a suitable spatial triangulation that connects the interpolation points needs to be solved firstly. Since its construction do not fall within the scope of the thesis, let us presume that it is obtained in advance. Therefore, we presume that a linear spline $\mathbf{s}^\triangleright$ is given and all the remaining data need to be extracted or approximated from it. Afterwards, the procedure to construct the surface is the same as in previous cases.

We will construct appropriate interpolation data in the following way. Normal \mathbf{n} of a tangent plane at point \mathbf{P} is computed as a weighted average of normals of the adjoining linear patches of $\mathbf{s}^\triangleright$. The weights are proportional to the angles between the connecting edges. Similarly, at the midpoint of an edge, let normal of the tangent plane be the average of normals of the adjoining linear patches.

7 Numerical Examples

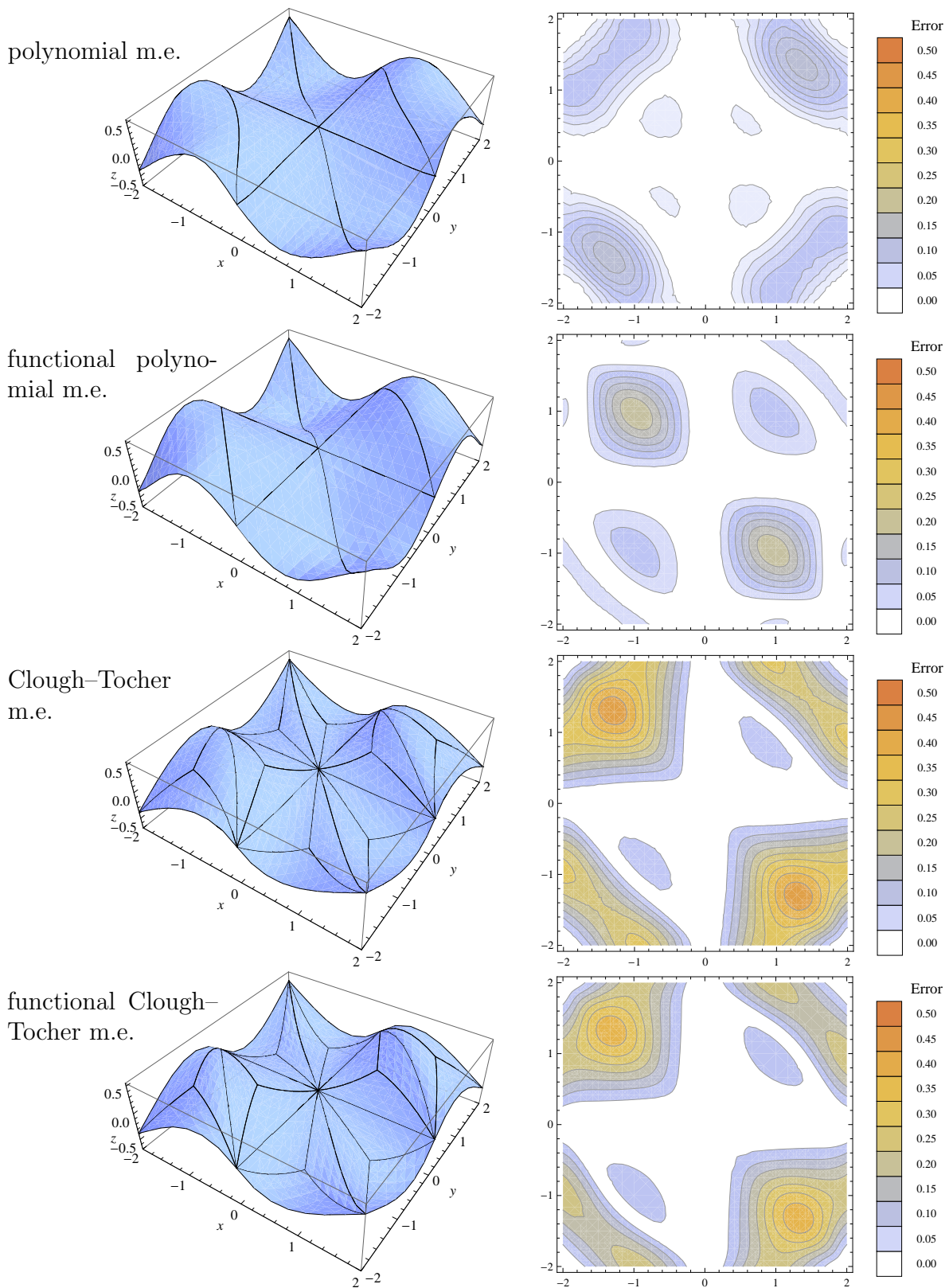


Figure 7.5: Approximation of a function $(x, y) \rightarrow 1/2 \sin(xy)$ by different macro-elements m . The corresponding error functions $|m - f|$ are shown on the right.

Normal curvature form at \mathbf{P} is obtained by the following procedure. Let $\{\mathbf{P}_\ell\}_\ell$ be a set of points adjacent to \mathbf{P} . Points $\mathbf{P}, \mathbf{P}_\ell$ and normal \mathbf{n} uniquely determine an interpolation circle (see Fig. 7.6). Let r_ℓ be a signed radius of the circle (r_ℓ is positive iff

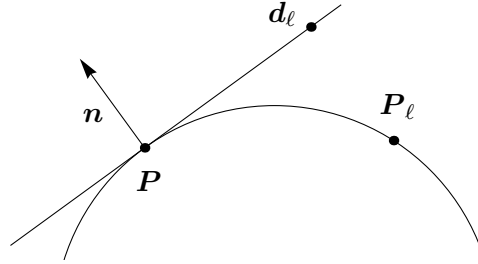


Figure 7.6: Normal curvature is computed via construction of the interpolation circle.

$\langle \mathbf{P}_\ell - \mathbf{P}, \mathbf{n} \rangle > 0$). Let \mathbf{d}_ℓ be the orthogonal projection of \mathbf{P}_ℓ onto the plane, defined by \mathbf{P} and \mathbf{n} . Then let normal curvature at \mathbf{P} in the direction of $\mathbf{d}_\ell - \mathbf{P}$ be $1/r_\ell$. To simplify the problem, the principal curvatures are

$$\kappa_1 = \max_\ell \{r_\ell\}_\ell, \quad \kappa_2 = \min_\ell \{r_\ell\}_\ell.$$

If the corresponding principal directions are not orthogonal, a correction of directions with minimal change of the corresponding angles is applied.

Since all the main procedures of surface reconstruction are presented, let us test our schemes in the following example. Let us construct a segment of a draft tube of a Francis water turbine. Data consist of sampled points and the associated linear spline $\mathbf{s}^\triangleright$ (Fig. 7.7).

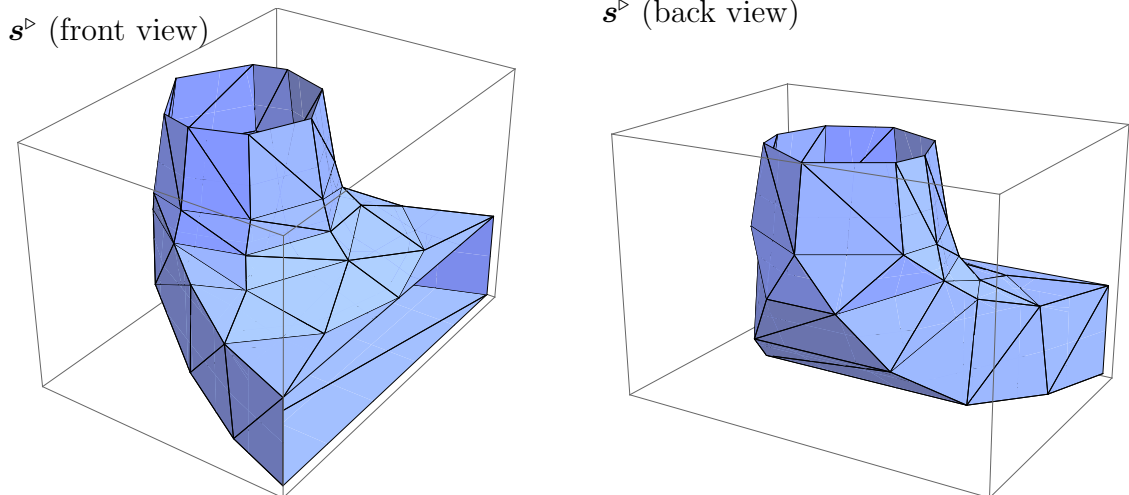


Figure 7.7: Draft tube segment (courtesy of Turboinštitut d.d.) is reconstructed by linear spline interpolant.

The data are sufficient to construct the HI- ω interpolant. To construct a macro-element, the corresponding domain triangulation needs to be built first. We obtain it by unfolding spatial triangulation $\mathbf{s}^\triangleright$ to a plane (Fig. 7.8). Details how to construct it will be skipped here. Note that the construction is not unique and it is advised that the

7 Numerical Examples

domain triangulation locally resembles the original spline \mathbf{s}^p . To obtain a better quality of the surface, triangulations with small angles should be avoided.

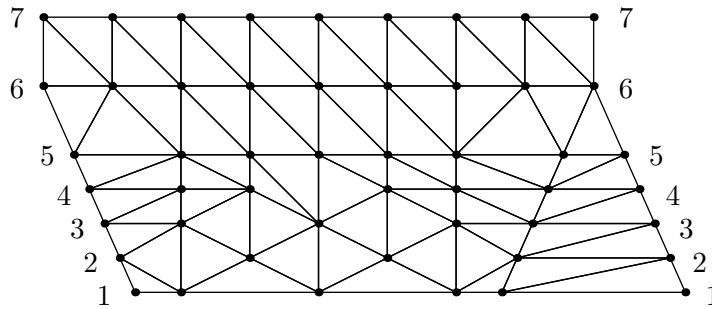


Figure 7.8: Domain triangulation for the draft tube. Vertices with the same indices and the corresponding edges are identified.

In Fig. 7.9, the shape of the draft tube is obtained by HI-0 patches and the polynomial macro-element. Both schemes produce a visually satisfying shape on most parts of the surface. In both cases, an undesired undulations can be seen on the front edge of the draft tube segment. The artefacts are result of two properties. At that region, normals of tangent planes change quickly and the triangular patches are too thin. The shape could be improved considerably by taking a denser grid of interpolation points. Some smaller undulations can also be detected on the left-center sides of the plots.

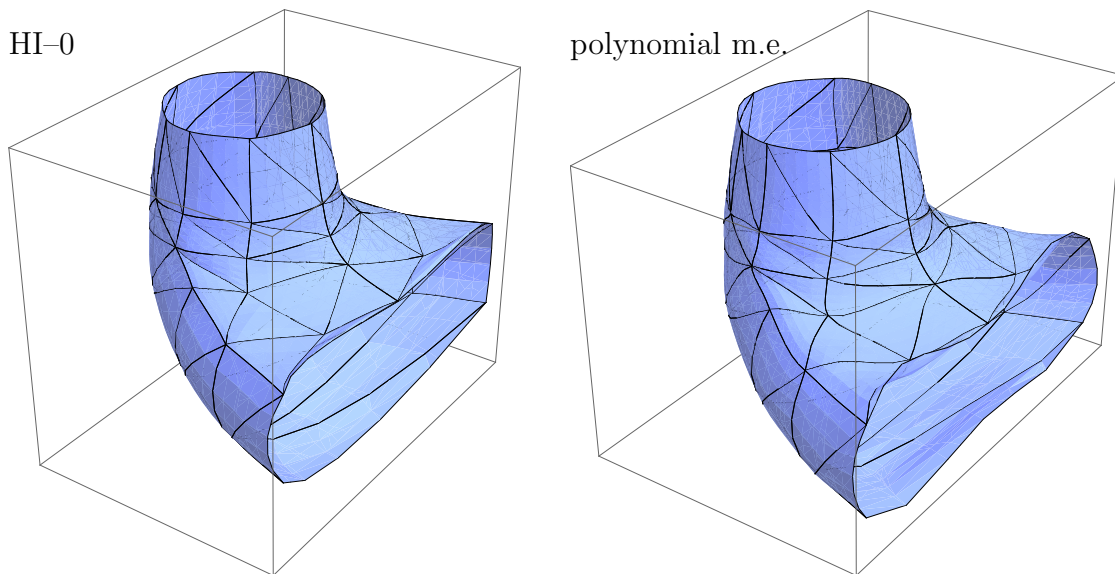


Figure 7.9: Draft tube segment is constructed by our interpolation schemes.

Although it is usually desirable, that the shape of the interpolant is smooth, in some cases it is useful to apply non-smooth connections. In the case of a draft tube, non-smooth connections contribute to a simpler geometry that is cheaper to physically construct in a factory. Non-smooth edges can easily be applied in our schemes. Firstly, the interpolation data need to be adjusted. At this type of edges we need to distinguish between different interpolation tangent planes for the corresponding adjoining patches.

At non-smooth edges, the corresponding boundary curves of HI- ω need to be constructed slightly differently than in Alg. 2 (page 46). Each of the tangent directions of the boundary curve needs to satisfy two different tangent plane conditions. Hence, each direction is uniquely determined by the intersection of the corresponding tangent planes and not by minimising the energy functional ψ_ω .

Similar technique can be applied for macro-elements. If control points of the linear spline are taken as the reference points, gaps on the spline surface at non-smooth edges might appear. Corrected control points of the boundary curves are obtained at the intersection of interpolation planes to preserve the interpolation conditions. After the applied corrections, smoothness conditions at the neighbouring edges might not be satisfied anymore. Since the applied corrections are usually small, mismatch of the smoothness conditions is small and not visually detectable. If we would want to preserve the positions of the corrected control points and to fix the smoothness restrictions, a construction of minimising cells that preserve boundaries could be applied (see Rmk. 6.5, page 51). But note that the sought minimising cells would not always exist. To preserve the boundary control points, the minimum of the corresponding nonnegative functional φ should be zero which is not always the case.

In Fig. 7.10, the draft tube segment with non-smooth edges is reconstructed. The shapes of both interpolation surfaces are almost indistinguishable and are a satisfactory representation of the original surface. Undulations in the front are removed. Some smaller artefacts can be seen in the center of the figures, where non-smooth edges transform into smooth ones.

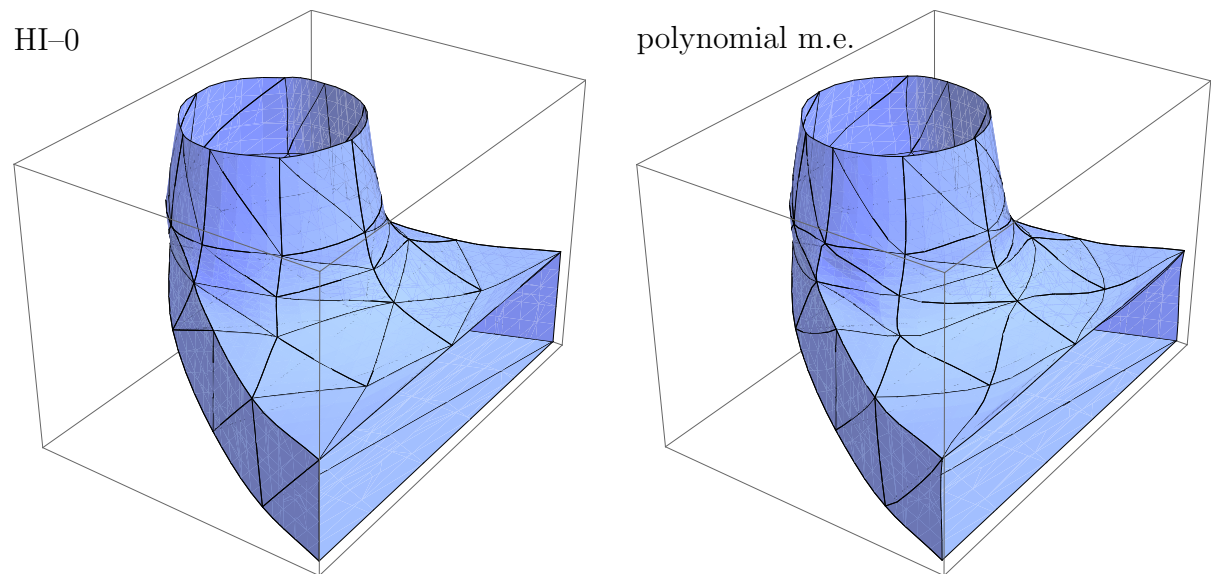


Figure 7.10: Draft tube segment with non-smooth edges is constructed by our interpolation schemes.

7.3 Hole Filling Problem

Hole filling problem occurs in practical applications when certain parts of a surface need to be restored or reconstructed. Smaller parts of the surface are lost, damaged or have

7 Numerical Examples

an undesirable shape and are consequently removed from the surface. The obtained holes need to be filled by new patches to get a required representation of the surface.

In this section we will show a simple example how to fill the holes with our interpolants. To achieve continuity between the original surface and the newly constructed patches, we need to presume that the boundary curves at the holes are Bézier curves of appropriate polynomial degree. The construction of the spline will only depend on sampled control points of the boundary curves. A problem to fill a larger hole will not be dealt, since we would need analyse how to generate reasonable interpolation data also in the interior of the hole.

Let \mathbf{m} be C^1 Clough–Tocher macro-element (see [50]) approximation of function \mathbf{f} ,

$$\mathbf{f} : [0, 3]^2 \rightarrow \mathbb{R}^3,$$

$$\mathbf{f}(x, y) := \left(x, y, \frac{1}{2} \sin(xy) + \frac{1}{8} \cosh(y) \right),$$

with the interior part of the surface, that corresponds to $[1, 2]^2$, removed. Spline \mathbf{m} and its triangulation are shown in Fig. 7.11.

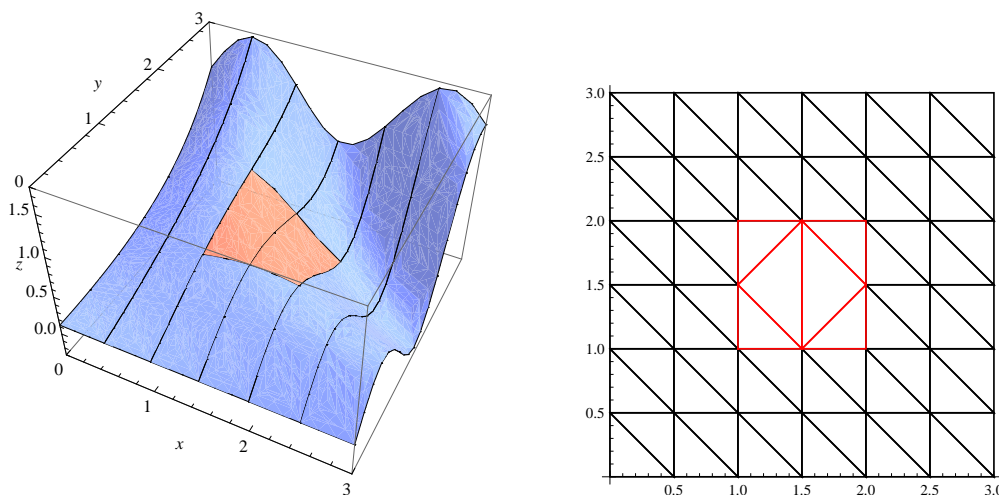


Figure 7.11: Interior part of \mathbf{m} , shown in red colour, is removed (left). Domain triangulation of \mathbf{m} , together with new triangles (in red) of the hole filling surface (right).

All interpolation data for the HI- ω scheme are obtained from control points of \mathbf{m} . Only the interior boundary curves of HI- ω spline minimise the strain energy functional ψ_ω since the rest are determined by C^0 continuity conditions. To construct a hole filling macro-element, additional interpolation data need to be approximated, similarly as in the previous section. The normal curvature forms are obtained as in § 7.2 and let tangent plane normal at every edge midpoint be computed as the average of normals at the edge endpoints. As the procedure in the previous section, a correction of boundary control points are applied to obtain continuity between the original surface and the macro-element.

The hole is filled with six patches, obtained by HI-0 and polynomial macro-element scheme (with the associated triangulation shown in Fig. 7.11, right). Plots of the surfaces and the corresponding residual functions are presented in Fig. 7.12. The constructed

splines give a satisfactory approximation of the removed part. Residual functions reveal that the error distribution of HI-0 spline is slightly better than of the macro-element. The maximal z -errors are 0.0132 and 0.0161, respectively.

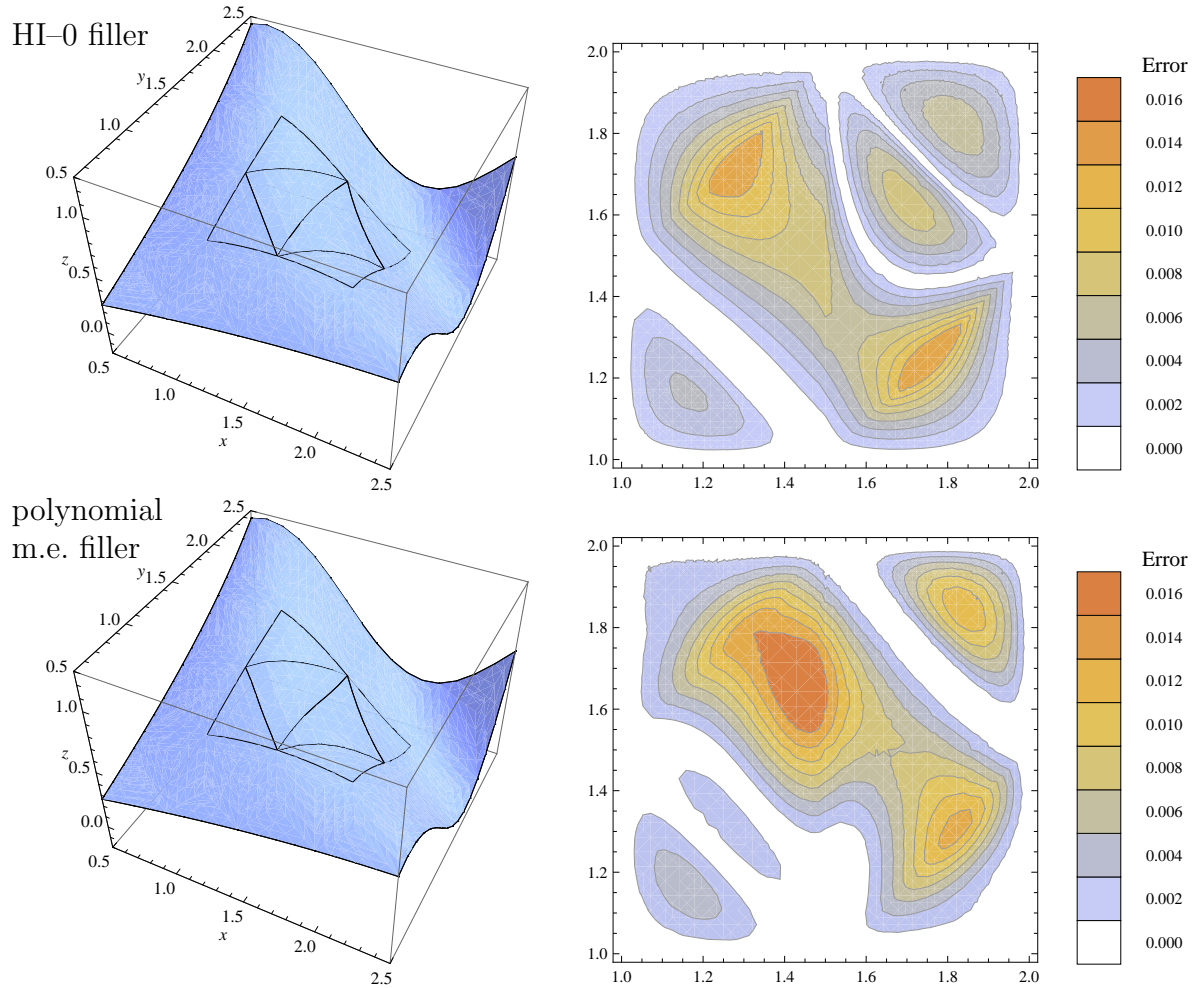


Figure 7.12: The hole in surface m is filled by our interpolation surfaces. The corresponding z -error functions are shown on the right.

Chapter 8

Conclusions

In the thesis, we present some theoretical results as well as practical applications for solving interpolation problems by splines on triangulations.

The presented results on positivity of the principal minors provide an important theoretical background for solving constrained Lagrange interpolation problems. The latter is a significant step to construct Lagrange interpolation splines. Although the positivity of the minors for uniformly distributed domain points remains an open problem for polynomial degree ≥ 18 , the verified properties are satisfactory for practical applications. Namely, use of polynomials of higher degrees is not recommended due to their tendency to oscillate. The Lagrange problem can be extended by studying generalised domain points. The existence and uniqueness of the solution is only investigated for polynomial degree ≤ 4 . At higher degrees, the problem becomes considerably more complicated and many configurations of points need to be analysed. Generalised positions of interpolation points can easily be applied in some existing Lagrange interpolation scheme to provide more freedom on how to choose the interpolation parameters. In the thesis, only correctness of the problem is studied. The optimal positions of domain points, i.e., points yielding the best approximation properties, are not studied and this remains an open problem for future work.

Extension of the Lagrange problems to parametric case should also be investigated in the future. Although the constructions of functional spline interpolants could straightforwardly be implemented in the parametric case, the approach would not exploit the advantages of geometric interpolations. Namely, in the geometric interpolation problems, the number of interpolation data can be higher since the interpolation parameters are not predetermined but obtained as a solution of nonlinear equations to maximise the number of interpolation points.

Hermite interpolation problem by parametric triangular splines is tackled by two novel methods. Since boundary curves of the patches greatly influence the quality of the spline surface, the construction in the first scheme is focused on this problem. The scheme is a generalisation of the Hermite cubic interpolation method for curves with small strain energy to surfaces. The construction is local, efficient and leads to unique interpolant. Although the derived patches do not join with G^1 continuity, smooth transitions of the surface at triangle vertices imply small differences of tangent plane directions across common edges.

The shape of the patch is greatly influenced by its boundary curves. Thus, we compare

the optimal boundary curves for different shape parameters. From numerical examples we conclude that it is better to apply boundary curves that correspond to lower values of the shape parameter.

The interior control points are set in such a way that the simplified Willmore energy functional has a unique minimum. The minimum of the functional could be used as a good starting point for minimising the original Willmore energy functional with an iterative solver if higher accuracy is needed.

The steps for constructing boundary curves and computing the optimal interior control points are not inseparable. Each of the procedures could be applied in other algorithms. For example, the algorithm to construct strain energy minimising curves could be integrated in a different interpolation scheme for surfaces and approximate Willmore energy functional could be applied for condensing free parameters of a spline.

The second scheme is an extension of the standard interpolation algorithm for macro-elements to the parametric setting. Hermite data from the functional case are adequately replaced by geometric data, suitable to describe parametric surfaces. The derived method inherits properties such as local construction and linear complexity. Free parameters are applied to approximate positions of uniformly distributed control points of a linear spline interpolant. On a denser grid of interpolation data, the parametric patches resemble the functional ones of standard macro-elements.

To obtain a scheme that can approximate a surface of arbitrary topology, the analysis of G^1 contacts between certain patches remains an open problem for future work. For practical applications, a relaxation on approximate smoothness conditions would also be an interesting research topic. Drawback of the scheme is an inseparable dependence of the spline shape to the domain triangulation which in practice is rarely given in advance. Therefore, a development of a new or integration of some existing efficient algorithm for constructing domain triangulation from the interpolation data should be investigated in the future. By replacing a linear spline interpolant as a reference surface with a better approximant (e.g., a quadratic spline), better distribution of control points could be obtained.

Numerical test show that the derived schemes are comparable to other established interpolation methods. In most cases, macro-elements outperform other algorithms. The results can be justified by the fact that the latter interpolate a greater number of data than other schemes. Also, the spline construction ensures the control points are more uniformly distributed, which usually contributes to better curvature distribution and a visually more appealing shape of the spline. For comparison, construction of control points in the Farin's G^1 interpolation scheme are subjected to satisfy complex continuity conditions between patches rather than obtaining the best possible shape. But the resulting scheme is local and can approximate a surface of arbitrary topology.

Cubic interpolants with small Willmore energy consists of lower number of control points than aforementioned methods. Splines with the boundary curves for smaller shape parameters give a round, visually satisfying shape and are an adequate choice when a simpler construction is preferred. It needs to be mentioned that in some cases the scheme might not perform as desired. If the data are taken from a coarse mesh, unwanted artefacts could occur. The patches tend to approximate parts of small spheres where

flat patches would give a better approximation. By applying a quadrature rule on more points the artefacts disappear or are reduced.

By introducing minor changes to our interpolation schemes, the algorithms can be applied in practical applications such as surface reconstruction from points, hole filling problem or to enforce certain non-smooth connections between patches.

Since no interpolation scheme is perfect, it is an important property that the obtained spline can easily be modified locally afterwards if undesired shape is spotted. Straightforward modifications can easily be implemented in our schemes since they do not integrate processes that change representation of the surface or number of control points such as subdivision or blending algorithms. The shape can be changed by applying a correction on arbitrary control points of Willmore minimising splines and on control points of the minimal determining sets of macro-elements.

Bibliography

- [1] P. ALFELD AND L. L. SCHUMAKER, *Smooth macro-elements based on Powell-Sabin triangle splits*, Adv. Comp. Math., 16 (2002), pp. 29–46.
- [2] —, *Upper and lower bounds on the dimension of superspline spaces*, Constr. Approx., 19 (2003), pp. 145–161.
- [3] A. ARNAL AND J. MONTERDE, *A third order partial differential equation for isotropic boundary based triangular Bézier surface generation*, J. Comput. Appl. Math., 236 (2011), pp. 184–195.
- [4] V. BARAMIDZE, *Minimal energy spherical splines on Clough-Tocher triangulations for Hermite interpolation*, Appl. Numer. Math., 62 (2012), pp. 1077–1088.
- [5] J. W. BARRETT, H. GARCKE, AND R. NÜRNBERG, *Parametric approximation of Willmore flow and related geometric evolution equations*, SIAM J. Sci. Comput., 31 (2008), pp. 225–253.
- [6] A. BOBENKO AND P. SCHRÖDER, *Discrete willmore flow*, in Eurographics Symposium on Geometry Processing, M. Desbrun and H. Pottmann, eds., Eurographics Association, Vienna, 2005, pp. 101–110.
- [7] L. BOS, M. CALIARI, S. DE MARCHI, M. VIANELLO, AND Y. XU, *Bivariate Lagrange interpolation at the Padua points: The generating curve approach*, J. Approx. Theory, 143 (2006), pp. 15–25.
- [8] L. BOS, S. DE MARCHI, AND S. WALDRON, *On the Vandermonde determinant of Padua-like points*, Dolomites Research Notes on Approximation, vol. 2, (2009), pp. 1–15.
- [9] L. BOS, S. D. MARCHI, A. SOMMARIVA, AND M. VIANELLO, *Computing multivariate Fekete and Leja points by numerical linear algebra*, SIAM J. Numerical Analysis, 48 (2010), pp. 1984–1999.
- [10] J. M. BRUNAT AND A. MONTES, *The power-compositions determinant and its application to global optimization*, SIAM J. Matrix Anal. Appl., 23 (2001), pp. 459–471.
- [11] J. M. CARNICER, M. GASCA, AND T. SAUER, *Interpolation lattices in several variables*, Numer. Math., 102 (2006), pp. 559–581.
- [12] C. K. CHUI AND T. X. HE, *On the dimension of bivariate superspline spaces*, Math. Comp., 53 (1989), pp. 219–234.

- [13] C. K. CHUI, G. HECKLIN, G. NÜRNBERGER, AND F. ZEILFELDER, *Optimal Lagrange interpolation by quartic C^1 splines on triangulations*, J. Comput. Appl. Math., 216 (2008), pp. 344–363.
- [14] C. K. CHUI AND M. J. LAI, *Vandermonde determinants and Lagrange interpolation in \mathbb{R}^s* , Nonlinear and Convex Analysis, B.L. Lin and S. Simons (eds.), (1987), pp. 23–32.
- [15] K. C. CHUNG AND T. H. YAO, *On lattices admitting unique Lagrange interpolations*, SIAM J. Numer. Anal., 14 (1977), pp. 735–743.
- [16] R. W. CLOUGH AND J. L. TOCHER, *Finite element stiffness matrices for analysis of plates in bending*, in Proceedings of the Conference on Matrix Methods in Structural Mechanics, Wright Patterson A.F.B, Ohio, 1965, pp. 515–545.
- [17] C. CONTI AND R. MORANDI, *Piecewise C^1 -shape-preserving Hermite interpolation*, Computing, 56 (1996), pp. 323–341.
- [18] S. COOPER AND S. WALDRON, *The diagonalisation of the multivariate Bernstein operator*, J. Approx. Theory, 117 (2002), pp. 103–131.
- [19] P. COSTANTINI AND M. L. SAMPOLI, *A general scheme for shape preserving planar interpolating curves*, BIT, 43 (2003), pp. 297–317.
- [20] G. E. COXSON, *The P -matrix problem is co-NP-complete*, Math. Programming, 64 (1994), pp. 173–178.
- [21] I. CRAVERO AND C. MANNI, *Shape-preserving interpolants with high smoothness*, J. Comput. Appl. Math., 157 (2003), pp. 383–405.
- [22] C. DE BOOR, *A practical guide to splines*, vol. 27 of Applied Mathematical Sciences, Springer-Verlag, New York, revised ed., 2001.
- [23] C. DE BOOR AND R. DEVORE, *A geometric proof of total positivity for spline interpolation*, Math. Comp., 45 (1985), pp. 497–504.
- [24] C. DE BOOR, K. HÖLLIG, AND M. SABIN, *High accuracy geometric Hermite interpolation*, Comput. Aided Geom. Design, 4 (1987), pp. 269–278.
- [25] T. DEROSE, *Necessary and sufficient conditions for tangent plane continuity of Bézier surfaces*, Comput. Aided Geom. Design, 7 (1990), pp. 165–179.
- [26] G. FARIN, *Smooth interpolation to scattered 3D data*, in Surfaces in computer aided geometric design (Oberwolfach, 1982), R. Barnhill and W. Boehm, eds., North-Holland, Amsterdam, 1983, pp. 43–63.
- [27] —, *Triangular Bernstein-Bezier patches*, Comput. Aided Geom. Design, 3 (1986), pp. 83–127.
- [28] —, *Curves and surfaces for computer-aided geometric design*, Computer Graphics and Geometric Modeling, Academic Press Inc., San Diego, CA, fifth ed., 2002.

- [29] G. E. FASSHAUER AND L. L. SCHUMAKER, *Minimal energy surfaces using parametric splines*, *Comput. Aided Geom. Design*, 13 (1996), pp. 45–79.
- [30] M. GASCA, *Spline functions and total positivity*, *Revista Mathematica*, 9 (1996), pp. 125–139.
- [31] M. GASCA AND J. I. MAEZTU, *On Lagrange and Hermite interpolation in \mathbb{R}^k* , *Numer. Math.*, 39 (1982), pp. 1–14.
- [32] M. GASCA AND C. A. MICCHELLI, *Total positivity and its applications*, *Mathematics and Its Applications*, vol. 359, Springer, 1996.
- [33] M. GASCA AND T. SAUER, *Polynomial interpolation in several variables*, *Adv. Comput. Math.*, 12 (2000), pp. 377–410. Multivariate polynomial interpolation.
- [34] T. N. T. GOODMAN AND K. UNSWORTH, *Shape-preserving interpolation by parametrically defined curves*, *SIAM J. Numer. Anal.*, 25 (1988), pp. 1453–1465.
- [35] S. HAHMANN AND G.-P. BONNEAU, *Triangular G^1 interpolation by 4-splitting domain triangles*, *Comput. Aided Geom. Design*, 17 (2000), pp. 731–757.
- [36] G. HERRON, *Smooth closed surfaces with discrete triangular interpolants*, *Comput. Aided Geom. Design*, 2 (1985), pp. 297–306.
- [37] K. HÖLLIG AND J. KOCH, *Geometric Hermite interpolation with maximal order and smoothness*, *Comput. Aided Geom. Design*, 13 (1996), pp. 681–695.
- [38] G. JAKLIČ, *On the dimension of the bivariate spline space $S_3^1(\Delta)$* , *Int. J. Comput. Math.*, 82 (2005), pp. 1355–1369.
- [39] G. JAKLIČ, J. KOZAK, M. KRAJNC, V. VITRIH, AND E. ŽAGAR, *Three-pencil lattices on triangulations*, *Numer. Algorithms*, 45 (2007), pp. 49–60.
- [40] —, *On geometric Lagrange interpolation by quadratic parametric patches*, *Comput. Aided Geom. Design*, 25 (2008), pp. 373–384.
- [41] G. JAKLIČ, J. KOZAK, M. KRAJNC, AND E. ŽAGAR, *On geometric interpolation by planar parametric polynomial curves*, *Math. Comp.*, 76 (2007), pp. 1981–1993.
- [42] G. JAKLIČ AND E. ŽAGAR, *Shape preserving interpolation by cubic G^1 splines in \mathbb{R}^3* , *Ann. Univ. Ferrara Sez. VII Sci. Mat.*, 54 (2008), pp. 259–267.
- [43] —, *Curvature variation minimizing cubic Hermite interpolants*, *Appl. Math. Comput.*, 218 (2011), pp. 3918–3924.
- [44] —, *Planar cubic Hermite G^1 splines with small strain energy*, *J. Comput. Appl. Math.*, 235 (2011), pp. 2758–2765.
- [45] G. JAKLIČ AND T. KANDUČ, *On positivity of principal minors of bivariate Bézier collocation matrix*, submitted, (2011).

- [46] —, *Hermite and Lagrange interpolation in \mathbb{R}^d by G^1 cubic splines with small strain energy*, submitted, (2012).
- [47] —, *Geometric interpolation by bivariate parametric macro-elements*, submitted, (2013).
- [48] —, *Hermite interpolation by triangular cubic patches with small Willmore energy*, accepted in *Int. J. Comput. Math.*, (2013).
- [49] G. JAKLIČ, T. KANDUČ, S. PRAPROTNİK, AND E. ŽAGAR, *Energy minimizing mountain ascent*, *J. Optim. Theory. Appl.*, 155 (2012), pp. 680–693.
- [50] M.-J. LAI AND L. L. SCHUMAKER, *Macro-elements and stable local bases for splines on Clough-Tocher triangulations*, *Numer. Math.*, 88 (2001), pp. 105–119.
- [51] —, *Spline functions on triangulations*, vol. 110 of *Encyclopedia of Mathematics and its Applications*, Cambridge University Press, Cambridge, 2007.
- [52] S. L. LEE AND G. M. PHILLIPS, *Construction of lattices for Lagrange interpolation in projective space*, *Constr. Approx.*, 7 (1991), pp. 283–297.
- [53] C. T. LOOP, *A G^1 triangular spline surface of arbitrary topological type*, *Comput. Aided Geom. Design*, 11 (1994), pp. 303–330.
- [54] S. MANN, M. LOUNSBERY, C. LOOP, D. MEYERS, J. PAINTER, T. DEROSE, AND K. SLOAN, *A survey of parametric scattered data fitting using triangular interpolants*, in *Curve and Surface Design*, G. E. Farin, R. E. Barnhill, and H. Hagen, eds., SIAM, 1992, pp. 145–172.
- [55] D. S. MEEK AND D. J. WALTON, *Geometric Hermite interpolation with Tschirnhausen cubics*, *J. Comput. Appl. Math.*, 81 (1997), pp. 299–309.
- [56] K. G. MURTY, *On a characterization of P -matrices*, *SIAM J. Applied Mathematics*, 20 (1971), pp. 378–384.
- [57] G. NÜRNBERGER, V. RAYEVSKAYA, L. L. SCHUMAKER, AND F. ZEILFELDER, *Local Lagrange interpolation with C^2 splines of degree seven on triangulations*, *Advances in Constructive Approximation: Vanderbilt 2003*, M. Neamtu and E. Saff (eds.), (2004), pp. 345–370.
- [58] —, *Local Lagrange interpolation with bivariate splines of arbitrary smoothness*, *Constr. Approx.*, 23 (2005), pp. 33–59.
- [59] G. NÜRNBERGER, L. L. SCHUMAKER, AND F. ZEILFELDER, *Lagrange interpolation by C^1 cubic splines on triangulated quadrangulations*, *Adv. Comput. Math.*, 21 (2004), pp. 357–380.
- [60] G. NÜRNBERGER AND F. ZEILFELDER, *Lagrange interpolation by bivariate C^1 -splines with optimal approximation order*, *Adv. Comput. Math.*, 21 (2004), pp. 381–419.

- [61] N. OLISCHLÄGER AND M. RUMPF, *Two step time discretization of willmore flow*, in IMA Conference on the Mathematics of Surfaces, E. R. Hancock, R. R. Martin, and M. A. Sabin, eds., volume 5654 of Lecture Notes in Computer Science, Springer, 2009, pp. 278–292.
- [62] L. PERES HARI, D. GIVOLI, AND J. RUBINSTEIN, *Computation of open Willmore-type surfaces*, Appl. Numer. Math., 37 (2001), pp. 257–269.
- [63] A. RABABAH, *High order approximation method for curves*, Comput. Aided Geom. Design, 12 (1995), pp. 89–102.
- [64] L. RAMSHAW, *Blossoms are polar forms*, Comput. Aided Geom. Design, 6 (1989), pp. 323–358.
- [65] N. S. SAPIDIS, ed., *Designing fair curves and surfaces*, Geometric Design Publications, Society for Industrial and Applied Mathematics (SIAM), Philadelphia, PA, 1994. Shape quality in geometric modeling and computer-aided design.
- [66] M. SCHWARZ, M. STAGINSKI, AND M. STAMMINGER, *GPU-based rendering of PN triangle meshes with adaptive tessellation*, in Proceedings of Vision, Modeling, and Visualization, L. Kobbelt, T. Kuhlen, T. Aach, and R. Westermann, eds., Akademische Verlagsgesellschaft Aka GmbH, Berlin, Aachen, 2006, pp. 161–168.
- [67] W.-H. TONG AND T.-W. KIM, *High-order approximation of implicit surfaces by G^1 triangular spline surfaces*, Comput. Aided Design, 41 (2009), pp. 441–455.
- [68] A. VLACHOS, J. PETERS, C. BOYD, AND J. L. MITCHELL, *Curved PN triangles*, in ACM Symposium on Interactive 3D Graphics, J. F. Hughes and C. H. Sequin, eds., New York: ACM Press, North Carolina, 2001, pp. 159–166.
- [69] J. WALLNER, *Note on curve and surface energies*, Comput. Aided Geom. Design, 24 (2007), pp. 494–498.
- [70] D. J. WALTON AND D. S. MEEK, *A triangular G^1 patch from boundary curves*, Comput. Aided Design, 28 (1996), pp. 113–123.
- [71] J.-H. YONG AND F. CHENG, *Geometric Hermite curves with minimum strain energy*, Comput. Aided Geom. Design, 21 (2004), pp. 281–301.
- [72] T. ZHOU, D. HAN, AND M.-J. LAI, *Energy minimization method for scattered data Hermite interpolation*, Appl. Numer. Math., 58 (2008), pp. 646–659.
- [73] M. ZLÁMAL, *On the finite element method*, Numer. Math., 12 (1968), pp. 394–409.

Index

- Bézier
 - patch, 11
 - representation, 11
- Bernstein basis polynomial, 11
- collocation matrix, 3, 16
- continuity conditions
 - C^r continuity conditions, 12
 - geometric continuity, 4
- control coefficient, 12
- control point, 12

- de Casteljau algorithm, 12
- disk, 48
- domain point, 3, 15
 - generalised domain point, 26

- HI- ω patch, 43

- intermediate de Casteljau point, 12
- interpolation
 - constrained interpolation, 3, 15
 - correctness, 2, 16
 - Hermite interpolation, 2, 29, 37, 47, 48
 - Lagrange interpolation, 2, 15

- lattice, 2

- macro-element, 4, 47, 59
 - Clough–Tocher macro-element, 60
 - polynomial macro-element, 59
- minimal determining set, 59
- minimising cell, 51

- nodal minimal determining set, 47
- normal curvature form, 53

- P-matrix, 3
- PN triangle, 6, 38

- ring, 49

- spline, 1, 12
 - spline space, 12
- strain energy, 29
 - approximate strain energy, 29

- triangulation, 11
 - Clough–Tocher refinement, 11
 - macro-triangles, 11
 - micro-triangles, 11

- Willmore energy, 6, 42
 - approximate Willmore energy, 43

Razširjeni povzetek

Zlepki so zelo uporabno matematično orodje pri aproksimaciji in predstavitvi različnih objektov, kot so krivulje, ploskve in telesa. Nepogrešljivi so pri računalniško podprtem geometrijskem oblikovanju (CAGD). V praksi jih uporabljamo za modeliranje raznovrstnih objektov v različnih panogah industrije (avtomobilska industrija, aeronavtika, industrija filmov in računalniških iger), obdelavi slik, reševanju diferencialnih enačb itd. Vsebujejo veliko zaželenih lastnosti, kot so baza z lokalnimi nosilci, hitra in stabilna konstrukcija, ohranjanje oblike, dobre konvergenčne lastnosti, direktna povezava med obliko zlepka in njegovo kontrolno mrežo itd. V primerjavi z enorazsežnimi zlepkami, ki so dobro raziskani, ostaja mnogo osnovnih vprašanj za dvorazsežne (večrazsežne) zlepke odprtih. Mednje sodijo dimenzija prostora zlepkov, konstrukcija baze, korektnost interpolacije, geometrijska zveznost in problem primerne določitve prostih parametrov zlepka.

V uporabi so bolj poznane Bézierove ploskve iz tenzorskih produktov, ki so direktna posplošitev Bézierovih krivulj. V zadnjih letih se je močno razvila teorija Bézierovih ploskev na triangulacijah. Zlepki na triangulacijah so bolj upogljivi od ploskev na pravokotnih domenah in lahko posledično opišejo bolj splošne površine.

Večina teorije sloni na neparametričnih zlepkah (površine, ki jih opišemo s funkcijo $s : \Omega \subset \mathbb{R}^2 \rightarrow \mathbb{R}$). Slabost slednjih je, da ne morejo opisati zapletenih 3D objektov, saj nimajo dovolj prostostnih stopenj. V takih primerih uporabljamo parametrične zlepke (površine, vložene v \mathbb{R}^3 , ki so parametrizirane z domeno $\Omega \subset \mathbb{R}^2$).

Interpolacijske probleme na zlepkah v grobem delimo na Lagrangeeve in Hermiteove. V prvem so interpolacijski podatki sestavljeni le iz vrednosti funkcije, pri drugem pa nastopajo tudi odvodi. V parametričnem primeru namesto vrednosti in odvodov nastopajo geometrijski podatki, kot so točke, tangentne ravnine in forme, ki so povezane z višjimi odvodi funkcije. Dokazovanje korektnosti problema (obstoj in enoličnost interpolacijskega problema) pogosto prevedemo na študij nesingularnosti pripadajočih kolokacijskih matrik.

Z omejitvami pogojena Lagrangeeva interpolacija na trikotniku

Polinomski Lagrangeev interpolacijski problem je v več spremenljivkah bistveno zahtevnejši, kot je v enorazsežnem primeru, saj je korektnost problema odvisna od položaja interpolacijskih točk. Potrebni in zadostni pogoji na razporeditev interpolacijskih točk na trikotniku ostaja odprt problem. Večina konstrukcij, ki izpolnjuje zadostne pogoje, sloni na t.i. mrežah (angl. *lattice*) [15, 52, 39, 11].

Z $\mathcal{I}_d := \{\mathbf{i} := (i, j, k) : i + j + k = d, i, j, k \in \mathbb{Z}_+\}$ označimo množico šibkih 3-kompozicij števila d . Poseben primer omenjenih konfiguracij točk je naslednja množica enakomerno razporejenih točk v domeni

$$\mathcal{D}_{d,\tau} := \{\xi_{\mathbf{i}} : \mathbf{i} \in \mathcal{I}_d\},$$

kjer so točke $\xi_{\mathbf{i}} := \xi_{ijk} := \mathbf{i}/d$ izražene v baricentričnih koordinatah glede na dani trikotnik τ . Za opis polinomov nad trikotniki je namesto potenčne baze bolj prikladno in numerično

stabilnejše uporabljati bazo Bernsteinovih polinomov

$$\{B_{\mathbf{i}}^d = B_{ijk}^d : \mathbf{i} \in \mathcal{I}_d\},$$

zapisano v baricentričnem koordinatnem sistemu glede na trikotnik τ . Poljuben neparametričen polinom p ali parametričen polinom \mathbf{p} totalne stopnje $\leq d$ lahko zapišemo Bézierovi obliki,

$$p = \sum_{\mathbf{i} \in \mathcal{I}_d} c_{\mathbf{i}} B_{\mathbf{i}}^d, \quad \text{oziroma} \quad \mathbf{p} = \sum_{\mathbf{i} \in \mathcal{I}_d} \mathbf{c}_{\mathbf{i}} B_{\mathbf{i}}^d,$$

kjer so $c_{\mathbf{i}} := c_{ijk} \in \mathbb{R}$ kontrolni koeficient in $\mathbf{c}_{\mathbf{i}} := \mathbf{c}_{ijk} \in \mathbb{R}^3$ kontrolne točke.

L. L. Schumaker je postavil domnevo, da če vzamemo poljubno podmnožico $\Gamma \subset \mathcal{I}_d$, potem lahko s polinomi $\{B_{\mathbf{i}}^d : \mathbf{i} \in \Gamma\}$ interpoliramo poljubne vrednosti v točkah $\{\xi_{\mathbf{i}} : \mathbf{i} \in \Gamma\}$ [51]. Domneva govori tudi o strožji zahtevi, da determinanta pripadajoče kolokacijske matrike ni le neničelna, temveč je pozitivna. Problemu recimo z omejitvami pogojena Lagrangeeva interpolacija, saj imamo za izbrane bazne polinome vnaprej določene pripadajoče kontrolne koeficiente. Težava pri dokazovanju predstavljenega problema je, da rešitve problema ne iščemo v celotnem prostoru polinomov temveč v njegovem podprostoru, za katerega pa ne veljajo nekatere lepe lastnosti prostorov.

V disertaciji pokažemo, da so za enakomerno razporejene interpolacijske točke $\mathcal{D}_{d,\tau}$ na trikotniku in $d \leq 17$ glavni minorji pripadajoče kolokacijske matrike pozitivni. Pozitivnost minorjev obravnavamo tudi za nekatere posebne konfiguracije točk. Osnovno domnevo razširimo s postavitvijo natančne spodnje meje za vrednosti minorjev. V zadnjem delu predstavimo nekaj rezultatov za posplošeno razporeditev točk v domeni. Korektnost obravnavamo z neposredno analizo pripadajočih kolokacijskih matrik.

Pozitivnost glavnih minorjev Bézierove kolokacijske matrike

Predstavimo domnevo o interpolaciji bolj podrobno.

Domneva 1 ([51]). *Za izbran trikotnik τ in neprazno množico $\Gamma = \{\mathbf{i}_1, \mathbf{i}_2, \dots, \mathbf{i}_n\} \subset \mathcal{I}_d$ je pripadajoča kolokacijska matrika*

$$M_{\Gamma} := [B_j^d(\xi_{\mathbf{i}})]_{\mathbf{i}, j \in \Gamma} = \begin{bmatrix} B_{\mathbf{i}_1}^d(\xi_{\mathbf{i}_1}) & B_{\mathbf{i}_2}^d(\xi_{\mathbf{i}_1}) & \cdots & B_{\mathbf{i}_n}^d(\xi_{\mathbf{i}_1}) \\ B_{\mathbf{i}_1}^d(\xi_{\mathbf{i}_2}) & B_{\mathbf{i}_2}^d(\xi_{\mathbf{i}_2}) & \cdots & B_{\mathbf{i}_n}^d(\xi_{\mathbf{i}_2}) \\ \vdots & \vdots & \ddots & \vdots \\ B_{\mathbf{i}_1}^d(\xi_{\mathbf{i}_n}) & B_{\mathbf{i}_2}^d(\xi_{\mathbf{i}_n}) & \cdots & B_{\mathbf{i}_n}^d(\xi_{\mathbf{i}_n}) \end{bmatrix}$$

nesingularna. Velja tudi $\det M_{\Gamma} > 0$.

Če vzamemo $\Gamma = \mathcal{I}_d$, potem je M_{Γ} kolokacijska matrika za standardni interpolacijski problem, ki je nesingularna.

S potrditvijo domneve 1 bi dobili naslednji rezultat. Naj bo $\Gamma \subset \mathcal{I}_d$ in $\mathcal{L}(\{B_{\mathbf{i}}^d\}_{\mathbf{i} \in \Gamma})$ dan prostor polinomov. Potem bi bil interpolacijski problem za točke $\{\xi_{\mathbf{i}}\}_{\mathbf{i} \in \Gamma}$ v domeni korekten. Domneva je pomembna pri konstrukciji interpolacijskih ploskev na triangulacijah, saj so nekateri kontrolni koeficienti iskane ploskve določeni iz pogojev gladkosti, preostali pa iz interpolacijskih pogojev [57, 58, 51].

Matrika M_Γ ni simetrična. Vrednost determinante M_Γ je neodvisna od vrstnega reda elementov Γ , če le vzamemo enako urejenost tako za vrstice kot za stolpce matrike. S primerno izbiro urejenosti elementov lahko dosežemo, da je matrika $M_{\mathcal{I}_d}$ bločno spodnjetrokotna [10]. Tako se osnovni problem zmanjša na obravnavo $\binom{d-1}{2} \times \binom{d-1}{2}$ velike podmatrike, ki pripada interpolacijskim točkam, ki so v strogi notranjosti trikotnika. Preostali bloki namreč pripadajo enorazsežnim Bézierovim kolokacijskim matrikam, ki so po [23] totalno nenegativne in imajo pozitivne glavne minorje.

Glavni rezultat razdelka je naslednji izrek.

Izrek 2. *Naj bo $d \leq 17$. Potem domneva 1 drži, t.j. $\det M_\Gamma > 0$ za vsako neprazno podmnožico $\Gamma \subset \mathcal{I}_d$.*

Rezultat sloni na pozitivnosti lastnih vrednosti matrike $M_{\mathcal{I}_d} + M_{\mathcal{I}_d}^T$. Žal se izkaže, da za $d \geq 18$ vedno obstajajo tudi negativne lastnosti vrednosti, zato omenjenega pristopa ne moremo uporabiti za splošen dokaz domneve. Kljub vsemu je rezultat pomemben za praktično uporabo, saj imajo interpolacijski polinomi visokih stopenj neželene lastnosti.

Iz izreka 2 neposredno sledi naslednji rezultat.

Izrek 3. *Naj bo $\Gamma \subset \mathcal{I}_d$ in $d \leq 17$. Potem za poljubne vrednosti $\{z_i\}_{i \in \Gamma}$ obstaja enoličen polinom*

$$p := \sum_{i \in \Gamma} c_i B_i^d,$$

za katerega velja

$$p(\xi_i) = z_i, \quad i \in \Gamma.$$

Označimo podmnožico vseh kompozicij, ki imajo ℓ ničel, z $\mathcal{I}_d^{(\ell)} \subset \mathcal{I}_d$, $\ell = 0, 1, 2$. Pozitivnost minorjev lahko dokažemo za naslednje izbire Γ in poljuben d .

Izrek 4. *Naj bo d poljuben in naj Γ zadošča eni izmed naslednjih predpostavk:*

- (a) $|\Gamma| \leq 2$,
- (b) naj bo ena izmed komponent kompozicije (i, j, k) fiksna za vse elemente množice Γ ,
- (c) $\Gamma = \mathcal{I}_d$,
- (d) $\Gamma = \{(i, j, k) \in \mathcal{I}_d : i \geq i_0, j \geq j_0, k \geq k_0\}$ za fiksna nenegativna cela števila i_0, j_0, k_0 ,
- (e) $\Gamma \subset \mathcal{I}_d^{(2)} \cup \mathcal{I}_d^{(1)}$,
- (f) $\Gamma = \Gamma_1 \cup \Gamma_2$, kjer je Γ_1 množica iz (a), (b) ali (d) in Γ_2 množica iz (e).

Potem velja $\det M_\Gamma > 0$.

S postavitvijo natančne spodnje za vrednosti minorjev razširimo osnovno domnevo.

Domneva 5. Za fiksno d velja

$$\min_{\substack{\Gamma \subset \mathcal{I}_d \\ \Gamma \neq \emptyset}} \det M_\Gamma = \det M_{\mathcal{I}_d} > 0.$$

Domnevo smo preverili z računalnikom za $d \leq 7$. Spodnjo mejo lahko s pomočjo [10] eksaktno izračunamo,

$$\det M_{\mathcal{I}_d} = d^{-d \binom{d+2}{2}} \prod_{\mathbf{i} \in \mathcal{I}_d} \binom{d}{\mathbf{i}} \prod_{\ell_1=1}^{\min\{d,3\}} \left(d^{\binom{d-1}{\ell_1}} \prod_{\ell_2=1}^{d-\ell_1+1} \ell_2^{\binom{d-\ell_2+1}{\ell_1-2}} \right)^{\binom{3}{\ell_1}}.$$

O interpolaciji za posplošeno lego točk

Do sedaj smo študirali problem z omejitvami pogojene interpolacije samo za enakomerno razporejene točke $\mathcal{D}_{d,\tau}$. Zastavi se nam naravno vprašanje, kako splošne so lahko konfiguracije točk, da ostane problem korekten.

Posplošene točke $\zeta_{\mathbf{i}} =: (\alpha_{\mathbf{i}}, \beta_{\mathbf{i}}, \gamma_{\mathbf{i}})$, $\mathbf{i} \in \mathcal{I}_d$, naj ležijo znotraj trikotnika τ , torej $\alpha_{\mathbf{i}}, \beta_{\mathbf{i}}, \gamma_{\mathbf{i}} \geq 0$. Za $\Gamma = \mathcal{I}_d$ dobimo standardni Lagrangeev interpolacijski problem, ki je v literaturi obsežno obravnavan. Po drugi strani je zelo malo znanega za primer $\emptyset \neq \Gamma \subsetneq \mathcal{I}_d$. Nekaj zadostnih pogojev za pozitivnost minorjev predstavimo s pomočjo obravnave kolokacijskih matrik.

Zaradi lastnosti Bernsteinovih baznih polinomov se je smiselno omejiti na primer, da točka $\zeta_{\mathbf{i}}$ leži na robu trikotnika τ natanko tedaj, ko velja $\mathbf{i} \notin \mathcal{I}_d^{(0)}$. Na ta način interpolacijski problem ločimo na dva podproblema, za robne in notranje točke trikotnika. Za točke na robu iz [23] enostavno sledi zadosten pogoj, da morajo biti točke linearno urejene na vsakem robu. Torej, če označimo z v_ℓ , $\ell = 1, 2, 3$, vozlišča trikotnika τ , morajo za prvi rob veljati pogoji

$$\zeta_{i j 0} = (1 - \lambda_j) v_1 + \lambda_j v_2, \quad (i, j, 0) \in \Gamma,$$

kjer je

$$\lambda_0 = 0, \lambda_d = 1 \quad \text{in} \quad \lambda_{j_1} < \lambda_{j_2} \iff j_1 < j_2.$$

Za notranje točke se zaradi kompleksnosti problema za višje d omejimo le na primer $d \leq 4$. V tem primeru so v notranjosti trikotnika kvečjemu tri točke in potrebno je preučiti le tri nesimetrične primere.

Predstavljeno posplošitev lege točk bi lahko enostavno uporabili v nekaj obstoječih Lagrangeevih shemah na triangulacijah, na primer v [59, 60, 13, 39].

Hermiteova interpolacija na parametričnih ploskvah

Hermiteovo interpolacijo je praviloma lažje ugnati, saj interpolacijske pogoje običajno predpišemo le na robovih trikotnih krp. Parametrične sheme so zelo uporabno orodje za modeliranje zapletenih 3D oblik. Sheme imajo bistveno večje število prostih parametrov kot metode za predstavitev neparametričnih ploskev. Kako določiti parametre, da

dobimo shemo z dobrimi aproksimacijskimi lastnostmi in enostavno konstrukcijo, ostaja izziv. V veliko algoritmih najprej zgradimo mrežo robnih krivulj za trikotne krpe, nato določimo še notranje kontrolne točke [26, 35, 70]. Sheme so praviloma precej zapletene; vsebujejo dodatne korake subdivizije, dvigovanja stopnje polinomov ali tehnike postopnega prehajanja med različnimi površinami. Glavne težave pri konstrukcijah so, kako zadosti zapletenim nelinearnim pogojem geometrijske (G^1) gladkosti med krpami. V [54] so izpostavili, da večina algoritmov lahko ustvari površine neželenih oblik, s slabo porazdelitvijo ukrivljenosti ali dodatnimi izboklinami. Slabe oblike površin so večinoma posledica neprimernih robnih krivulj.

Krivulje z majhno napetostno energijo in trikotne krpe z majhno Willmorejevo energijo

Robne krivulje trikotnih krp pomembno vplivajo na končno obliko Hermiteove interpolacijske ploskve, zato je podrobna analiza konstrukcije le-teh pomemben korak. Če so krpe nižjih stopenj (npr. kubične), je vpliv krivulj še toliko večji, saj večino kontrolnih točk krpe predstavljajo robne kontrolne točke.

V disertaciji predstavimo Hermiteovo interpolacijsko shemo za krivulje, ki imajo majhno napetostno energijo. Za kriterij optimalnosti vpeljemo funkcional približne napetostne energije, ki je odvisen od danega parametra. Dobljena shema je posplošitev več do sedaj razvitih metod. Optimalne krivulje so regularne in dobro ohranjajo obliko originalnih krivulj. Območje dopustnih smeri tangentnih vektorjev in obliko krivulje študiramo v odvisnosti od danega parametra oblike.

Shemo za krivulje uporabimo pri konstrukciji kubičnih trikotnih krp z majhno Willmorejevo energijo. Krpe interpolirajo točke in pripadajoče tangente ravnine v svojih krajiščih. Robne krivulje za različne parametre oblike ω primerjamo med seboj. Pri parametru $\omega = 16$ se izkaže, da optimalne krivulje sovpadajo z robnimi krivuljami PN trikotnikov [68].

Površine, ki imajo manjše spremembe normalnih ukrivljenosti, so praviloma na pogled lepših oblik. Zato preostale parametre zleпка določimo tako, da ima površina majhno Willmorejevo energijo,

$$\mathcal{W}(\mathbf{s}) = \frac{1}{4} \int_{\mathbf{s}} (\kappa_1 - \kappa_2)^2 dA,$$

kjer sta κ_ℓ glavni ukrivljenosti ploskve \mathbf{s} in dA pripadajoči površinski element. Energija meri, koliko je dan kos površine podoben delu sfere; sfera ima energijo enako nič. Ker je analiza energije prezahtevna, vpeljemo funkcional približne Willmorejeve energije, pri katerem enoličen minimum vedno obstaja.

Interpolacijski problem za krivulje

Naj bosta $\mathbf{P}_0, \mathbf{P}_1$ robni točki in $\mathbf{d}_0, \mathbf{d}_1$ pripadajoča enotska tangentna vektorja v \mathbb{R}^3 . Označimo $\Delta\mathbf{P} := \mathbf{P}_1 - \mathbf{P}_0$. Radi bi konstruirali kubično krivuljo $\mathbf{b} : [0, 1] \rightarrow \mathbb{R}^3$, ki reši

Hermiteov interpolacijski problem

$$\begin{aligned} \mathbf{b}(0) &= \mathbf{P}_0, & \dot{\mathbf{b}}(0) &= \alpha_0 \mathbf{d}_0, \\ \mathbf{b}(1) &= \mathbf{P}_1, & \dot{\mathbf{b}}(1) &= \alpha_1 \mathbf{d}_1, \end{aligned}$$

kjer sta $\alpha_\ell \in \mathbb{R}$ pozitivna parametra.

Izmed vseh dopustnih krivulj bi radi izbrali takšno, ki ima majhno ukrivljenost κ [22, 65]. Zaradi zahtevne analize omenjene količine v praksi pogosto minimiziramo funkcional približne napetostne energije φ [69, 65, 28],

$$\int_0^1 \kappa^2(t) dt \approx \varphi(\alpha_0, \alpha_1) := \int_0^1 \|\ddot{\mathbf{b}}(t)\|^2 dt.$$

Ker je iskanje minimuma integrala v zaključeni obliki pogosto pretežko, integral ponostavimo s kvadraturnim pravilom. S ψ_ω označimo 3-točkovno kvadraturno pravilo za aproksimacijo φ , odvisno od parametra $\omega \in [0, \infty)$,

$$\psi_\omega(\boldsymbol{\alpha}) := \frac{1}{\omega + 2} \left(\|\ddot{\mathbf{b}}(0)\|^2 + \omega \left\| \ddot{\mathbf{b}}\left(\frac{1}{2}\right) \right\|^2 + \|\ddot{\mathbf{b}}(1)\|^2 \right).$$

Z $\vartheta_\ell := \angle(\Delta \mathbf{P}, \mathbf{d}_\ell) \in [0, \pi]$, $\ell = 0, 1$, in $\vartheta := \angle(\mathbf{d}_0, \mathbf{d}_1) \in [0, \pi]$ označimo kote. Izkaže se, da obstaja enolična optimalna rešitev interpolacijskega problema, če so izpolnjeni določeni geometrijski pogoji.

Izrek 6. *Funkcional ψ_ω ima enoličen minimum pri*

$$\alpha_\ell = \frac{36 [(\omega + 20)\langle \Delta \mathbf{P}, \mathbf{d}_\ell \rangle + (\omega - 16)\langle \Delta \mathbf{P}, \mathbf{d}_{1-\ell} \rangle \langle \mathbf{d}_0, \mathbf{d}_1 \rangle]}{(\omega + 20)^2 - (\omega - 16)^2 \langle \mathbf{d}_0, \mathbf{d}_1 \rangle^2}, \quad \ell = 0, 1. \quad (1)$$

Če koti ϑ_0, ϑ_1 in ϑ zadoščajo $\vartheta_0, \vartheta_1 \in [0, \pi/2)$ ter zvezi

$$0 < (\omega + 20) \cos(\vartheta_\ell) + (\omega - 16) \cos(\vartheta_{1-\ell}) \cos(\vartheta), \quad \ell = 0, 1,$$

potem sta parametra α_ℓ pozitivna in krivulja je regularna, brez zank ali osti.

Predstavljena metoda je posplošitev naslednjih obstoječih shem. Ker velja $\psi_4 = \varphi$, je krivulja, ki minimizira funkcional za $\omega = 4$, optimalna krivulja v [71]. Pri $\omega = 16$ naša shema reproducira shemo iz [44, 42], kjer funkcional φ aproksimirajo s trapeznim pravilom ter druge odvode s pomočjo prvih. Čeprav študiramo funkcional ψ_ω samo za nenegativne vrednosti ω , bi lahko naredili posplošitev tudi za nekatere negativne vrednosti. Pri $\omega = -2$ bi optimalna krivulja minimizirala funkcional deviacije ukrivljenosti $\int_0^1 \|\dot{\mathbf{b}}(t) \times \ddot{\mathbf{b}}(t)\|^2 dt$ [43].

Za večje vrednosti ω se izkaže, da so optimalne krivulje čedalje bližje linearnim krivuljam. Zato je smiselno uporabljati le manjše vrednosti parametra. Iz numeričnih primerov sklepamo, da se je smiselno omejiti na območje $\omega \in [0, 30]$. V disertaciji predstavimo tudi hevrističen postopek, kako izbrati primeren ω glede na dane interpolacijske podatke.

Posplošitev na trikotne ploskve

Za dane točke $\{\mathbf{P}_\ell\}_\ell$ v \mathbb{R}^3 in pripadajoče normalne vektorje $\{\mathbf{n}_\ell\}_\ell$ bi radi konstruirali zvezen zlepek iz trikotnik krp z majhno Willmorejevo energijo. Predpostavimo, da je vnaprej podan referenčni linearni zlepek $\mathbf{s}^\triangleright$ (tj. prostorska triangulacija), ki interpolira točke $\{\mathbf{P}_\ell\}_\ell$. Ploskev je skupek linearnih krp $\mathbf{p}_\ell^\triangleright$, $\mathbf{s}^\triangleright =: \{\mathbf{p}_\ell^\triangleright\}_\ell$.

Ker je interpolacijska shema lokalne narave, lahko brez škode za splošnost predpostavimo, da za vsak $\mathbf{p}_\ell^\triangleright$ pripadajoča kubična Bézierova ploskev

$$\mathbf{p} = \mathbf{p}_\ell = \sum_{i \in \mathcal{I}_3} \mathbf{c}_i B_i^3$$

interpolira točke $\mathbf{P}_0, \mathbf{P}_1, \mathbf{P}_2$ in pripadajoče tangentne ravnine v krajiščih krpe.

Označimo z v_ℓ , $\ell = 1, 2, 3$, baricentrične točke $(1, 0, 0)$, $(0, 1, 0)$ in $(0, 0, 1)$. Naj bo $\mathbf{n}(v)$ normala krpe \mathbf{p} v točki v . Potem se interpolacijski problem glasi

$$\begin{aligned} \mathbf{p}(v_{\ell+1}) &= \mathbf{P}_\ell, \\ \mathbf{n}(v_{\ell+1}) &= \mathbf{n}_\ell, \end{aligned} \quad \ell = 0, 1, 2.$$

Pogojem bomo zadostili s konstrukcijo primernih robnih krivulj.

Robne krivulje

Ker robne krivulje krpe niso enolično določene iz interpolacijskih pogojev, želimo, da minimizirajo funkcional ψ_ω . Če bi za robno krivuljo predpisali tangentna vektorja $\mathbf{d}_0, \mathbf{d}_1$ v krajiščih, potem bi imeli enak optimizacijski problem kot pri iskanju optimalne krivulje na začetku razdelka. Za prvo krivuljo ploskve dobimo predpis

$$\begin{aligned} \mathbf{c}_{300} &= \mathbf{P}_0, & \mathbf{c}_{210} &= \mathbf{P}_0 + \frac{1}{3} \alpha_0 \mathbf{d}_0, \\ \mathbf{c}_{030} &= \mathbf{P}_1, & \mathbf{c}_{120} &= \mathbf{P}_1 - \frac{1}{3} \alpha_1 \mathbf{d}_1, \end{aligned}$$

kjer $\mathbf{d}_0, \mathbf{d}_1$ ležita v tangentnih ravninah z normalama \mathbf{n}_0 in \mathbf{n}_1 , optimalna koeficienta $\alpha_0, \alpha_1 > 0$ pa sta določena iz (1). Podoben predpis bi dobili za preostali krivulji ploskve \mathbf{p} .

Za $\omega = 16$ lahko optimalne smeri zapišemo v zaključeni obliki – dobimo jih kot pravokotno projekcijo vektorja $\Delta \mathbf{P}$ na tangentni ravnini. Izkaže se, da so optimalne robne krivulje za ψ_{16} enake robnim krivuljam PN trikotnikov.

Izrek 7. *Naj točki $\mathbf{P}_0, \mathbf{P}_1$ in normali $\mathbf{n}_0, \mathbf{n}_1$ zadoščata $\angle(\Delta \mathbf{P}, \mathbf{n}_\ell) \in (0, \pi)$, $\ell = 1, 2$. Potem pripadajoča robna krivulja interpolacijskega PN trikotnika minimizira funkcional ψ_{16} .*

Poiskati dopustne vektorje $\mathbf{d}_0, \mathbf{d}_1$, ki minimizirajo splošen funkcional ψ_ω , $\omega \neq 16$, je težji problem. Funkcional se za optimalne koeficiente α_ℓ poenostavi v

$$\psi_\omega(\mathbf{d}_0, \mathbf{d}_1) = \frac{72}{\omega + 2} \left(\|\Delta \mathbf{P}\|^2 - \frac{18((\omega + 20)(A^2 + B^2) + 2(\omega - 16)ABC)}{(\omega + 20)^2 - (\omega - 16)^2 C^2} \right),$$

kjer vpeljemo oznake $A := \langle \Delta \mathbf{P}, \mathbf{d}_0 \rangle$, $B := \langle \Delta \mathbf{P}, \mathbf{d}_1 \rangle$ in $C := \langle \mathbf{d}_0, \mathbf{d}_1 \rangle$.

Pri iskanju minimuma funkcionala je potrebno poseči po primerni numerični metodi, npr. po gradientni metodi. Pomagamo si lahko z naslednjim homotopskim pristopom, ki temelji na sledečem premisleku. Smiselno je pričakovati, da majhna sprememba ω botruje k majhni spremembi optimalnih vektorjev \mathbf{d}_ℓ , saj je ψ_ω zvezna funkcija svojih parametrov. Najprej izračunamo optimalne smeri za $\omega = 16$. Nato v vsakem koraku iteracijskega algoritma zmerno spremenimo vrednost ω v ustrezno smer in popravimo optimalne smeri tangentnih vektorjev za novi ω . Za izračun popravkov vektorjev lahko vzamemo enostavno iterativno metodo, kot je npr. Newtonova metoda na gradientu funkcionala ψ_ω .

Numerični primeri pokažejo, da se optimalne krivulje za različne ω vidno razlikujejo, če vzamemo interpolacijske podatke iz bolj razgibane ploskve. Za manjše vrednosti ω dobimo na pogled lepše krivulje z enakomernejšo razporeditvijo ukrivljenosti.

Notranja kontrolna točka in funkcional približne Willmorejeve energije

Fiksirajmo točke $\mathbf{P}_0, \mathbf{P}_1, \mathbf{P}_2$, normale $\mathbf{n}_0, \mathbf{n}_1, \mathbf{n}_2$ in robne kontrolne točke Bézierove krpe \mathbf{p} . Določiti moramo še preostalo notranjo točko \mathbf{c}_{111} , tako da bo vrednost Willmorejeve energije za ploskev \mathbf{p} majhna. Omejimo se na primer, ko \mathbf{c}_{111} izrazimo na naslednji geometrijski način,

$$\mathbf{c}_{111}(r) := \frac{\sum_{\ell=0}^2 \mathbf{n}_\ell}{\|\sum_{\ell=0}^2 \mathbf{n}_\ell\|} r + \frac{1}{3} \sum_{\ell=0}^2 \mathbf{P}_\ell, \quad r \in \mathbb{R}.$$

Z D_{u_1}, D_{u_2} označimo operatorje smernih odvodov v smereh $u_1 = v_2 - v_1$ in $u_2 = v_3 - v_1$, zapisane v baricentričnih koordinatah. Koeficienti prve in druge fundamentalne forme ploskve \mathbf{p} so

$$\begin{aligned} E &:= \langle D_{u_1} \mathbf{p}, D_{u_1} \mathbf{p} \rangle, & L &:= \langle D_{u_1} D_{u_1} \mathbf{p}, \mathbf{n} \rangle, \\ F &:= \langle D_{u_1} \mathbf{p}, D_{u_2} \mathbf{p} \rangle, & M &:= \langle D_{u_1} D_{u_2} \mathbf{p}, \mathbf{n} \rangle, \\ G &:= \langle D_{u_2} \mathbf{p}, D_{u_2} \mathbf{p} \rangle, & N &:= \langle D_{u_2} D_{u_2} \mathbf{p}, \mathbf{n} \rangle. \end{aligned}$$

Willmorejevo energijo za krpo \mathbf{p} izračunamo kot

$$\mathcal{W}(\mathbf{p}) = \frac{1}{4} \int_{\mathbf{p}} (\kappa_1 - \kappa_2)^2 dA = \frac{1}{4} \int_D f(v) dv.$$

V izrazu na desni je $D := \{v = (\alpha, \beta, 1 - \alpha - \beta) : \alpha \in [0, 1], \beta \in [0, 1 - \alpha]\}$ trikotnik in

$$f := \frac{G^2 L^2 - 4FGLM + (4F^2 - 2EG)LN + 4EGM^2 - 4EFMN + E^2 N^2}{(EG - F^2)^{3/2}}.$$

Integrala v splošnem ne znamo izračunati analitično. Poenostavimo ga s primernim kvadraturnim pravilom, da bo minimum dobljenega funkcionala enostavno poiskati. Vpeljimo trapezno pravilo za aproksimacijo \mathcal{W} na štirih točkah. Funkcional približne Willmorejeve energije se glasi

$$\mathcal{W}_t(r) := \frac{1}{36} \sum_{\ell=1}^3 f(v_\ell; r) + \frac{1}{24} f(v_c; r), \quad (2)$$

pri čemer z $f(v; r)$ označimo izračun funkcionala f v točki v in pri parametru r ter označimo $v_c := 1/3(v_1 + v_2 + v_3)$. Interpolacijsko krpo, ki minimizira \mathcal{W}_t in ima robne krivulje, ki minimizirajo funkcional ψ_ω , označimo s HI- ω .

Funkcional f ima v izbranih štirih točkah močno poenostavljeno obliko, zato lahko dokažemo naslednji izrek.

Izrek 8. *Energijski funkcional \mathcal{W}_t ima enoličen minimum.*

Če bi želeli večjo natančnost, bi lahko študirali kvadraturno pravilo za \mathcal{W} tudi na gostejši mreži aproksimacije. V tem primeru bi lahko minimum izpeljanega funkcionala \mathcal{W}_t vzeli za začetni približek iskanega minimuma.

Namesto funkcionala v (2) bi lahko vzeli tudi splošnejšo obliko

$$\mathcal{W}_t(\mathbf{r}) := \frac{1}{36} \sum_{\ell=1}^3 f(v_\ell; \mathbf{r}) + \frac{1}{24} f(v_c; \mathbf{r}),$$

kjer je točka $\mathbf{c}_{111} =: \mathbf{r}$ poljubna v \mathbb{R}^3 . Vendar se v praksi se izkaže, da oblika krp pri minimizaciji slednjega funkcionala ne odtehta zahtevnejšega minimizacijskega problema.

Geometrijska interpolacija z dvorazsežnimi parametričnimi makro-elementi

Alternativa predstavljeni kubični shemi, kako določiti proste parametre zlepka, je pristop, da kontrolne točke konstruiramo na podoben način, kot so določene pri (neparametričnih) makro-elementih. Slednji sodijo v posebno kategorijo C^r gladkih interpolacijskih zlepkov na triangulacijah [51, 50, 1, 73, 16]. Glavne prednosti omenjenih zlepkov so: struktura, ki se izogne problemom dimenzije prostora, oblika zlepka je odvisna le od lokalnih podatkov, zlepek je zapisan v zaprti obliki in ima optimalen red aproksimacije. Zaradi omenjenih lastnosti so pomembno in uveljavljeno orodje v teoriji aproksimacije in pri reševanju parcialnih diferencialnih enačb [51].

Slabost interpolacijske sheme z majhno Willmorejevo energijo je, da se zlepki med seboj stikajo le zvezno. Za dosego višje gladkosti med krpami moramo poseči po višji stopnji polinomov ali po večjemu številu krp. Namesto študija geometrijske G^r gladkosti, se omejimo na strožje C^r pogoje [29, 28, 72, 4]. Prednost takšnega pristopa je, da so pogoji med krpami opisani z linearnimi enačbami, kontrolne točke pa so med seboj povezane z lepimi geometrijskimi predpisi. Glavna slabost je omejitev, da takšni zlepki ne morejo aproksimirati površin poljubne topologije [36]. Če bi torej želeli opisati kompleksno obliko, bi morali v določenih točkah ploskve dopustiti blažje G^r stike med krpami.

V disertaciji konstrukcijo parametričnih makro-elementov izpeljemo iz konstrukcije standardnih funkcijskih makro-elementov. Interpolacijski podatki, pravimo jim tudi vozliščna določitvena množica (angl. *nodal minimal determining set*) [51], so za funkcijske ploskve sestavljeni iz vrednosti in parcialnih ter smernih odvodov funkcije. Nadomestimo jih z geometrijskimi objekti, ki so bolj primerni za opis parametričnih ploskev.

Pri konstrukciji zlepkov se omejimo na dva posebna tipa: C^1 zlepki stopnje 5 na poljubni triangulaciji ter kubični C^1 zlepki na Clough–Tocherjevi triangulaciji. Kontrolne točke dobimo tako, da projiciramo enakomerno razporejene točke linearnega zlepka na

ustrezne interpolacijske ravnine. Da dosežemo C^1 gladkost na skupnih povezavah sosednjih krp, moramo določiti popravke točk; izračunamo jih po metodi najmanjših kvadratov. Dobljena shema je lokalna in linearne časovne zahtevnosti. Pri dovolj gosti mreži interpolacijskih podatkov je parametričen zlepek čedalje bolj podoben funkcijskemu makroelementu.

Interpolacijski problem

Naj bo Δ triangulacija območja Ω . Z \mathcal{V} in \mathcal{E} označimo pripadajočo množico vozlišč v in povezav e . S Δ_{CT} označimo Clough–Tocherjevo finejšo delitev triangulacije Δ . Prostor parametričnih zlepkov totalne stopnje $\leq d$, C^r globalne gladkosti in C^ρ , $\rho \geq r$, gladkosti v vozliščih $v \in \mathcal{V}$ označimo z

$$\mathcal{S}_d^{r,\rho}(\Delta) := \{\mathbf{s} \in C^r(\Omega) \cap C^\rho(\mathcal{V}) : \mathbf{s}|_\tau \in \mathcal{P}_d^3, \tau \in \Delta\}.$$

Tu smo s \mathcal{P}_d označili prostor polinomov totalne stopnje $\leq d$. Za $\tau \in \Delta$ zapišemo pripadajoče Bézierove krpe kot $\mathbf{s}|_\tau =: \mathbf{p}^{[\tau]} = \sum \mathbf{c}_i^{[\tau]} B_i^d$.

S $T_v \mathbf{s}$ in $C_v \mathbf{s}$ označimo tangentno ravnino in formo normalne ukrivljenosti zlepka \mathbf{s} v vozlišču v . Oglejmo si naslednja interpolacijska problema. Iščemo zlepek $\mathbf{s} \in \mathcal{S}_5^{1,2}(\Delta)$, ki reši interpolacijski/aproksimacijski problem,

$$\begin{aligned} (a) \quad & \mathbf{s}(v) = \mathbf{P}_v, \\ (b) \quad & T_v \mathbf{s} = \Pi_v, & v \in \mathcal{V}, \\ (c) \quad & C_v \mathbf{s} = \{\mathbf{u}_1^*(v), \mathbf{u}_2^*(v), \kappa_1(v), \kappa_2(v)\}, \\ (d) \quad & T_{\frac{1}{2}(v_0+v_1)} \mathbf{s} \approx \Pi_{\frac{1}{2}(v_0+v_1)}, & (v_0, v_1) = e \in \mathcal{E}, \end{aligned}$$

ter zlepek $\mathbf{s} \in \mathcal{S}_3^{1,1}(\Delta_{CT})$, ki reši problem

$$\begin{aligned} (a) \quad & \mathbf{s}(v) = \mathbf{P}_v, & v \in \mathcal{V}, \\ (b) \quad & T_v \mathbf{s} = \Pi_v, \\ (d) \quad & T_{\frac{1}{2}(v_0+v_1)} \mathbf{s} \approx \Pi_{\frac{1}{2}(v_0+v_1)}, & (v_0, v_1) = e \in \mathcal{E}. \end{aligned}$$

Točke $v \in \mathcal{V}$ in povezave $e \in \mathcal{E}$ so vezane na originalno triangulacijo Δ . Pogoji (a), (b) in (c) predstavljajo predpise za interpolacijo točk, tangentnih ravnin in form normalnih ukrivljenosti v vozliščih triangulacije. Pogoji so nadomestek za vrednosti ter prve in druge odvode neparametrične funkcije. Formo ukrivljenosti ploskve opišemo kot množico glavnih smeri \mathbf{u}_ℓ^* s pripadajočimi ukrivljenostmi κ_ℓ . Ker se izkaže, da na sredini povezav ni dovolj prostih parametrov za interpolacijo tangentne ravnine, predpišemo le njeno aproksimacijo (pogoj (d)). Pogoj nadomesti interpolacijo smernega odvoda funkcije na povezavi v neparametričnem okolju.

Pogojem interpolacije bomo zadostili v vrstnem redu, kot so naštet. Pogoju (a) pri konstrukciji zlepka $\mathbf{s} \in \mathcal{S}_5^{1,2}(\Delta)$ zadostimo tako, da konstruiramo linearni zlepek \mathbf{s}^\flat polinomske stopnje pet nad triangulacijo Δ , ki interpolira točke \mathbf{P}_v . Vsako krpo linearnega zlepka zapišemo kot $\sum \mathbf{c}_i^\flat B_i^d$, kjer točke \mathbf{c}_i^\flat ležijo na isti ravnini in so na trikotniku enakomerno razporejene. Pri konstrukciji zlepka $\mathbf{s} \in \mathcal{S}_3^{1,1}(\Delta_{CT})$, linearni zlepek \mathbf{s}^\flat stopnje

tri zgradimo nad triangulacijo Δ_{CT} . Slednji v težišču vsakega originalnega trikotnika dodatno interpolira povprečno vrednost točk v ogliščih trikotnika.

Preostalim trem interpolacijskim pogojem (b), (c), (d) bomo zadostili tako, da bomo projicirali enakomerno razporejene kontrolne točke linearnega zlepka $\mathbf{s}^\triangleright$ na ustrezne ravnine v prostoru.

Interpolacijski pogoji in minimizirajoče celice

V razdelku si bomo pogledali, kako določimo kontrolne točke interpolacijskega zlepka \mathbf{s} , ki pripadajo trem interpolacijskim omejitvam. Ker geometrijski interpolacijski pogoji ne bodo določili kontrolnih točk \mathbf{c}_i na enoličen način, bomo preostale parametre svobode uporabili za aproksimacijo enakomerne razporeditve kontrolnih točk linearnega zlepka $\mathbf{s}^\triangleright$ polinomske stopnje d . Enakomernejšo razporeditev točk si želimo doseči zato, ker slednja praviloma botruje k enakomernejši razporeditvi ukrivljenosti površine.

Kontrole točke polinomskega zlepka morajo zadoščati tudi pogojem gladkosti prostora, zato bomo konstrukcijo točk razdelili na dva glavna koraka. Najprej bomo kontrolne točke linearnega zlepka projicirali na interpolacijske ravnine s poševno projekcijo. Ker dobljene točke ne bodo zadoščale pogojem gladkosti, bomo izračunali popravke točk kot rešitev po metodi najmanjših kvadratov.

Z $\mathcal{D}_m(v)$ označimo množico vseh kontrolnih točk zlepka, ki so kvečjemu za m indeksov stran od kontrolne točke, ki pripada vozlišču v . Natančneje, za krpo $\mathbf{p} = \sum \mathbf{c}_i B_i^d$ na trikotniku $\tau = (v_0, v_1, v_2)$ definiramo disk s centrom v in radijem m ,

$$\mathcal{D}_m(v_0, \mathbf{p}) := \{\mathbf{c}_i : |\mathbf{i}| = d, i \geq d - m\}.$$

Podobno definiramo diska za preostali vozlišči. Skupek vseh diskov s centrom v označimo z

$$\mathcal{D}_m(v) := \bigcup_{\tau \in \Delta} \left\{ \mathbf{c}_i^{[\tau]} : \mathbf{c}_i^{[\tau]} \in \mathcal{D}_m(v, \mathbf{p}^{[\tau]}) \right\}.$$

Kolobar s centrom v in radijem m definiramo kot

$$\mathcal{R}_m(v) := \mathcal{D}_m(v) \setminus \mathcal{D}_{m-1}(v).$$

Interpolacija tangentne ravnine

V vsaki točki $v \in \mathcal{V}$ želimo interpolirati točko \mathbf{P} in pripadajočo tangentno ravnino Π , ki ima normalni vektor \mathbf{n} . Prvemu pogojju enostavno zadostimo z $\mathcal{D}_0(v) = \{\mathbf{P}\}$. Da je izpolnjen drugi pogoj, mora veljati

$$\langle \mathbf{c}_i - \mathbf{P}, \mathbf{n} \rangle = 0, \quad \mathbf{c}_i \in \mathcal{R}_1(v). \quad (3)$$

Točke \mathbf{d}_i dobimo tako, da projiciramo pripadajoče točke $\mathbf{c}_i^\triangleright$ linearnega zlepka na ravnino Π . Smer poševne projekcije zadošča pogojju $(\mathbf{c}_i^\triangleright - \mathbf{P}) \perp (\mathbf{d}_i - \mathbf{c}_i^\triangleright)$. Točke \mathbf{d}_i izpolnjujejo pogoje (3), vendar ne zadoščajo pogojem gladkosti prostora. Iskane kontrolne točke $\mathbf{c}_i \in \mathcal{R}_1(v)$ dobimo kot popravke točk \mathbf{d}_i . Dobimo jih z minimizacijo funkcionala φ , ki meri relativne razdalje med množicama točk,

$$\varphi = \sum \frac{\|\mathbf{c}_i - \mathbf{d}_i\|^2}{\|\mathbf{d}_i - \mathbf{P}\|^2}. \quad (4)$$

Pri tem so točke \mathbf{c}_i med seboj povezane s C^1 pogoji gladkosti. Optimalni množici točk pravimo minimizirajoča celica (angl. *minimising cell*).

Interpolacija forme normalne ukrivljenosti

Predpostavimo, da je množica $\mathcal{D}_1(v)$, $v \in \mathcal{V}$, že določena. Množico $\mathcal{D}_2(v)$ želimo določiti tako, da bo zlepek \mathbf{s} interpoliral formo normalne ukrivljenosti v točki v . Zaradi konsistentnosti določitve ukrivljenosti za vse krpe, ki se stikajo v v , predpostavimo, da velja $\mathbf{s} \in C^2(v)$.

Iskane točke $\mathbf{c}_i \in \mathcal{R}_2(v)$ dobimo tako, da projiciramo pripadajoče točke $\mathbf{c}_i^\triangleright$ s poševno projekcijo na ustrezne interpolacijske ravnine. Za razliko od interpolacije tangentne ravnine, tu vsaka projicirana točka \mathbf{d}_i leži na različni interpolacijski ravnini, katera je enolično določena iz normalne ukrivljenosti v izbrani smeri.

Podobno kot prej, popravke točk \mathbf{d}_i dobimo z minimizacijo funkcionala φ v (4). Pri tem so točke \mathbf{c}_i so med seboj povezane s C^2 pogoji gladkosti.

Aproksimacija tangentne ravnine v središču povezave

Naj bosta $\mathbf{p}^{[\tau_1]}$ in $\mathbf{p}^{[\tau_2]}$ sosednji krpi, ki sta definirani na trikotnikih $\tau_1 = (v_0, v_1, v_2)$ in $\tau_2 = (v_0, v_2, v_3)$ s skupno povezavo $e := (v_0, v_2)$. Z \mathcal{D}_e označimo pripadajoči kontrolni točki povezave e ,

$$\mathcal{D}_e := \left\{ \mathbf{c}_{(d-1)/2,1,(d-1)/2}^{[t_1]}, \mathbf{c}_{(d-1)/2,(d-1)/2,1}^{[t_2]} \right\}.$$

Predpostavimo, da so kontrolne točke

$$\{\mathbf{c}_i^{[\tau_1]} : \mathbf{i} \in \mathcal{I}_d, j = 0, 1\} \cup \{\mathbf{c}_i^{[\tau_2]} : \mathbf{i} \in \mathcal{I}_d, k = 0, 1\} \setminus \mathcal{D}_e \quad (5)$$

že določene. Množico \mathcal{D}_e , $e \in \mathcal{E}$, moramo določiti tako, da bo zlepek \mathbf{s} v točki $v =: 1/2(v_0 + v_2)$ aproksimiral dano tangentno ravnino Π .

Ker je robna krivulja zlepka na povezavi e enolično določena s kontrolnimi točkami v (5), v točki v ne moremo interpolirati poljubne tangentne ravnine Π . Interpolacijski pogoj zamenjamo tako, da namesto Π v točki v interpoliramo dopustno ravnino, ki se najbolj prilega Π .

Od tu naprej je postopek podoben kot v prejšnjih dveh algoritmih. Pripadajoči kontrolni točki linearnega zlepka projiciramo na tangentne ravnine in izračunamo popravke točk, da zadostimo C^1 pogojem gladkosti na povezavi e .

Predstavljene tri postopke za izračun kontrolnih točk na koncu združimo v enoten algoritem za določitev parametričnega makro-elementa. Z določitvijo množic $\mathcal{D}_2(v)$ za $v \in \mathcal{V}$ ter \mathcal{D}_e za $e \in \mathcal{E}$ so vse kontrolne točke zlepka $\mathbf{s} \in \mathcal{S}_5^{1,2}(\Delta)$ enolično določene. Pri zlepku $\mathbf{s} \in \mathcal{S}_3^{1,1}(\Delta_{CT})$ interpolacijski podatki ($\mathcal{D}_1(v)$ za $v \in \mathcal{V}$ ter \mathcal{D}_e za $e \in \mathcal{E}$) ne določajo neposredno vseh kontrolnih točk. Preostale točke so enolično določene iz C^1 pogojev na povezavah Clough–Tocherjeve delitve.

Zaključek

Rezultati o pozitivnosti glavnih minorjev Bézierovih kolokacijskih matrik predstavljajo pomembno teoretično podlago za reševanje z omejitvami pogojene Lagrangeeve interpolacije na trikotniku. Rešitev slednjega problema predstavlja pomemben korak pri konstrukciji Lagrangeevega interpolacijskega zlepka nad triangulacijo. Kljub temu, da osnovne domneve o korektnosti problema za enakomerno razporejene interpolacijske točke ne dokažemo za poljubno stopnjo polinomov, je rezultat pomemben za praktično uporabo, kjer polinomov visokih stopenj ni priporočljivo uporabljati. V disertaciji študiramo le korektnost interpolacijskega problema. Optimalna lega točk ostaja odprt problem za nadaljnje delo. Možnost nadaljnjega raziskovanja je tudi razširitev Lagrangeevega interpolacijskega problema na parametrične ploskve.

Za reševanje Hermiteovega interpolacijskega problema predstavimo dve novi shemi. Robne krivulje Bézierovih krp pomembno vplivajo na obliko zlepka. Pri konstrukciji kubičnih trikotnik krp z majhno Willmorejevo energijo je zato poudarek na konstrukciji primernih robnih krivulj, ki minimizirajo funkcional približne napetostne energije.

Druga shema je posplošitev standardne interpolacijske sheme za makro-elemente v parametričen okvir. Hermiteove interpolacijske podatke za funkcijski primer zamenjamo z geometrijskimi podatki, ki so primerni za opisovanje parametričnih ploskev. Za opis površin poljubne topologije bi morali v določenih točkah interpolacijskega zlepka ublažiti stroge pogoje C^r gladkosti. Študij geometrijskih G^r stikov ali približne gladkosti ostaja odprt problem za prihodnje delo.

Iz numeričnih zgledov sklepamo, da sta razviti shemi primerljivi ostalim uveljavljenim metodam. V večini primerov se najboljše izkažejo makro-elementi, saj interpolirajo tudi večje število podatkov. Kubični zlepki z majhno Willmorejevo energijo so primerna izbira, če želimo enostavnejšo strukturo z manjšim številom kontrolnih točk. Predstavljeni shemi lahko uporabimo pri reševanju različnih problemov, kot sta rekonstrukcija površin iz točk in polnjenje lukenj. Shemi imata tudi pomembno lastnost, da lahko obliko dobljenih interpolacijskih zlepkov enostavno lokalno popravimo, če zaznamo nezaželeno obliko površine.